8. SITE 754[1]

Shipboard Scientific Party[2]

Hole 754A

Date occupied: 13 May 1988

Date departed: 15 May 1988

Time on hole: 1 day, 10 hr, 45 min

Position: 30°56.439′S, 93°33.991′E

Bottom felt (rig floor; m; drill-pipe measurement): 1074.6

Distance between rig floor and sea level (m): 11.0

Water depth (drill-pipe measurement; corrected m): 1063.6

Total depth (rig floor; corrected m): 1246.7

Penetration (m): 172.1

Number of cores: 23

Total length of cored section (m): 170.0

Total core recovered (m): 128.27

Core recovery (%): 75

Oldest sediment cored:
Depth sub-bottom (m): 172.1
Nature: chalk and chert
Earliest age: Maestrichtian
Measured velocity (km/s): 3.1

Hole 754B

Date occupied: 15 May 1988

Date departed: 18 May 1988

Time on hole: 3 days, 4 hr

Position: 30°56.439′S, 93°33.954′E

Bottom felt (rig floor; m; drill-pipe measurement): 1076.4

Distance between rig floor and sea level (m): 10.9

Water depth (drill-pipe measurement; corrected m): 1065.5

Total depth (rig floor; corrected m): 1431.1

Penetration (m): 354.7

Number of cores: 25

Total length of cored section (m): 232.0

Total core recovered (m): 91.85

Core recovery (%): 39

Oldest sediment cored:
Depth sub-bottom (m): 354.7
Nature: limestone and chert
Earliest age: early Maestrichtian or older
Measured velocity (km/s): 3.1

Principal results: Ocean Drilling Program (ODP) Site 754 (proposed Site BR-3) was positioned to penetrate the maximum thickness—0.175 s two-way traveltime (TWT) below seafloor (bsf)—of the subhorizontal pelagic sequence that caps the erosional unconformity at Broken Ridge. The site was selected at shotpoint 1040 on line 20 of the single-channel seismic survey conducted in 1986 by *Robert D. Conrad* Cruise 2708 (RC2708). The site location is near the center of the crest of Broken Ridge, about 15 km north of the main south-facing escarpment.

The principal objectives at Site 754 were (1) to sample the oldest material deposited on the truncation surface, in order to compare its age, lithology, and water depth with the youngest material clearly below the unconformity drilled at Site 753, and (2) to penetrate and sample a prominent seismic reflector at about 0.3 s TWT bsf which represents a surface of onlap in the truncated, northward-dipping sedimentary section at Broken Ridge. Unfortunately, the second objective was not met because the rotary bit failed in a lower Maestrichtian chert/chalk sequence at a depth of 355 m below seafloor (mbsf) in Hole 754B, still above the target reflector.

Hole 754A was cored using the advanced hydraulic piston corer (APC), extended core barrel (XCB), and Navidrill (NCB) to a depth of 172 mbsf. In following this coring sequence, Site 754 became the first ODP drill site to make true operational use of the Navidrill in sediments. Although core recovery was good with the NCB (73%), the penetration rate proved slow in the Maestrichtian chert/chalk sequence, and Hole 754A was terminated after drilling 12.3 m with the NCB. Hole 754B was spudded nearby, and after washing down 123 m, the hole was RCB cored to a total depth of 354.7 mbsf, at which point the bit failed. The bit was then released, the drill string pulled to 160 mbsf (to cover a potentially unstable zone above the unconformity), and two logging runs were made. The first run, with the geochemical string, proceeded without incident, but after a successful run with a modified seismic stratigraphic string, the drill string was found to be stuck, and logging was terminated so that the pipe could be freed.

Two lithologic units are recognized at Site 754:

Unit I (0–132 mbsf): Pleistocene to upper Eocene foraminifer nannofossil ooze in which foraminifers become less abundant and micrite becomes more abundant with depth.

Unit II (151–355 mbsf): upper to lower Maestrichtian (Campanian?) chalks and limestones with chert and volcanic ash.

The angular unconformity observed in seismic profiles over Broken Ridge coincides with the top of Unit II (151 mbsf). At Site 754, the depositional hiatus across this truncation surface spans late Maestrichtian to late Eocene time. As at Site 752, a second hiatus (late Eocene to late Oligocene) occurs in the subhorizontally layered Unit I sediments deposited above the truncation surface. Whereas the angular unconformity is probably related to the uplift of Broken Ridge during rifting and subsequent subaerial erosion of its exposed crest, the origin of the younger hiatus remains speculative. The younger hiatus is possibly related either to the middle Oligocene eustatic sea-level fall or to enhanced current activity at that time.

The physical properties of the sediments are dramatically different above and below the angular unconformity. As the unconformity is crossed from above, bulk density increases from about 1.8 to 2.4 g/cm^3, although the grain density remains roughly constant and the porosity decreases from 60% to 30%. Similarly, the percent calcium carbonate in the recovered cores decreases from an approximately constant level of 96% in lithologic Unit I to a mean level of about 70% in the upper Maestrichtian, further declining to about 60% in the lower Maestrichtian.

A surprise result of the drilling at Broken Ridge was the amount of ash encountered in the section, particularly because the corresponding Upper Cretaceous–Paleogene section on the Kerguelen Plateau appears, from Leg 119 and 120 drilling, to contain much less ash. Because these ashes are mainly basaltic in composition, mag-

[1] Peirce, J., Weissel, J., et al., 1989. *Proc. ODP, Init. Repts.*, 121: College Station, TX (Ocean Drilling Program).

[2] Shipboard Scientific Party is as given in the list of Participants preceding the contents.

netic susceptibility data from core samples provide a rapid, qualitative measure of the variation with depth of volcanic ash in the section. Preliminary calculations show that the ash-accumulation rates increase downsection and that the relative proportion of ash in the sediment similarly increases. We note the possibility of using the ash content in the stratigraphic section at Broken Ridge as a long-term record of eruptive activity of the Kerguelen/Ninetyeast hot spot.

Paleomagnetic data, biostratigraphy, and synthetic seismograms (determined from both downhole logging and sample properties) indicate that the sediments at the base of Hole 752B overlap stratigraphically with the upper Maestrichtian chalks encountered immediately below the truncation surface at Site 754. The exact amount of overlap is debated, but it is probably in the range of 20–40 m. Thus, Sites 752 and 754 provide about 500 m of composite, but continuous, section of the lower Maestrichtian to lower Eocene part of the truncated, northward-dipping sediments at Broken Ridge.

BACKGROUND AND OBJECTIVES

Overview

Detailed discussions of the background and objectives for drilling at Broken Ridge during ODP Leg 121 are found in the "Leg 121 Background and Objectives" chapter and the "Background and Objectives" section of the "Site 752" chapter (this volume). The reader is referred there for general information. The particular drilling objectives for Site 754 (Fig. 1) are described in this section.

Drilling Objectives for Site 754

Site 754 (proposed Site BR-3) is 14 km north of the south-facing escarpment of Broken Ridge on a north-south transect of drill sites across the crest of the ridge (proposed Sites BR-1 through BR-4; Fig. 2). This transect of drill sites was intended to sample the entire dipping and truncated sedimentary sequence at Broken Ridge in single-bit holes, with each site located to ensure some overlap of section between sites.

Site 754 was positioned for drilling through the maximum thickness (~160 m) of the subhorizontally layered sedimentary sequence above the angular unconformity (Fig. 2). The primary objective for drilling at Site 754 was to obtain the age, lithology, and depositional depth of the stratigraphically lowest sediments in the subhorizontal capping sequence at Broken Ridge. The age difference between those sediments and the stratigraphically highest sediments in the dipping and truncated sedimentary sequence at Broken Ridge sampled at Site 753 (proposed Site BR-1 in Fig. 2) provides a maximum estimate for the duration of the Broken Ridge–Kerguelen Plateau rifting event, if the latter sediments are shown to be a pre-rift sequence. Moreover, if the lowermost sediments above the unconformity at Site 754 contain a significant fraction of middle to upper Eocene detrital material (like at Deep Sea Drilling Project [DSDP] Site 255), then we can demonstrate that Broken Ridge was uplifted and exposed to wave-base erosion prior to that time. We note that rifting had ended at Broken Ridge by late Eocene time because seafloor spreading between Broken Ridge and Kerguelen Plateau had begun by the time of anomaly 18 (~42 Ma).

We planned at least 450 m of penetration at Site 754 in order to drill through a particularly prominent seismic reflector that constitutes a seismic sequence boundary within the dipping and truncated sediments at Broken Ridge (see "Broken Ridge Underway Geophysics" chapter, this volume). The target reflector lies at 0.3 s TWT bsf at the location of Site 754 (Fig. 2). A second drilling objective at Site 754 was to determine whether the northward-dipping sediments that onlap the prominent seismic reflector constitute an upward-fining, shallow-water clastic unit. If this was found to be the case, the seismic reflector might correspond to the onset of rifting at Broken Ridge.

A third drilling objective at Site 754 was to understand why seismic-refraction velocities in the dipping and truncated sequence increase rapidly downsection from about 2 to more than 4 km/s over a depth interval of less than 200 m (see "Broken Ridge Underway Geophysics" chapter and Driscoll et al., this volume). Therefore, the drill site was located to sample this critical depth interval below the unconformity. Explanations under consideration for this rapid increase in seismic velocity include changes in lithology, diagenetic effects, or both of these factors.

Drilling terminated at Site 754 after drilling Holes 754A and 754B to a total depth of 354.7 mbsf when the RCB bit failed in Hole 754B. This premature termination of drilling left us above the target seismic reflector (the surface of onlap). Nevertheless, all of our other drilling objectives at Site 754 were met even with the reduced penetration. Before abandoning Hole 754B, two downhole logging runs were completed. The first run featured the standard geochemical tools and the second consisted of a modified seismic stratigraphic string.

OPERATIONS

Site 754

While the post mortem of the flapper and hinge pin was conducted following Site 753 operations, the ship was offset 6 nmi in dynamic positioning (DP) mode to Site 754. As at Site 753, the vessel hove to over the site in DP mode during a Global Positioning System satellite window and was able to make an accurate beacon drop at 1830 hr (local time), 13 May.

Hole 754A

The standard bottom-hole assembly (BHA) used for APC/XCB coring was assembled with the enhancement of a latch sub required for operating the Navidrill coring system, which was planned for use if appropriate in this hole. After running the drill pipe to the seafloor, piston coring began with a successful mud-line core establishing the operating water depth at 1074.6 m below rig floor at 2222 hr. Routine APC cores were taken until Core 121-754A-12H, which penetrated the base of the now-familiar Neogene ooze cap and required 35,000-lb overpull to extract. We then changed to the XCB coring system for the next six cores. Recovery during the XCB sequence was quite poor because of the presence of loose beach-type gravel followed by chalk with chert nodules and stringers (Table 1).

With diminishing returns beginning to dominate XCB operations, the NCB system was deployed for what was to be its first true operational use. Five NCB cores were taken with mixed success. The coring tool functioned perfectly from a mechanical point of view. Four different diamond "core bits" (cutting shoes) were employed to find the optimum combination for the chert/chalk formation. Only Core 121-754A-20N achieved the full 4.5-m stroke. The soft, white chalk interbedded with hard chert was a good test for the device, and the results were encouraging, but the net penetration rate after five cores was only about 1 m/hr, counting turn-around time on deck. This time requirement was not adequate to justify the continuation of NCB coring, despite significant interest in the possibilities offered by the NCB coring approach. Thus, Hole 754A was terminated at 172.1 mbsf, and the drill string was pulled in order to change over to the RCB coring system to pursue the 450-mbsf scientific target in the most time-effective manner. The bit cleared the seafloor at 0150 hr on 15 May, officially ending Hole 754A.

Hole 754B

A rotary coring system BHA with a hydraulic bit release was made up and run to the seafloor. The hole was spudded and quickly washed to 122.7 mbsf, where coring resumed in an attempt to get more recovery from the presumed loose gravel zone at about 135 to 155 mbsf. Like the previous attempts with the XCB, the RCB system was also unable to capture any more than traces of the elusive gravel from Cores 121-754B-2R through

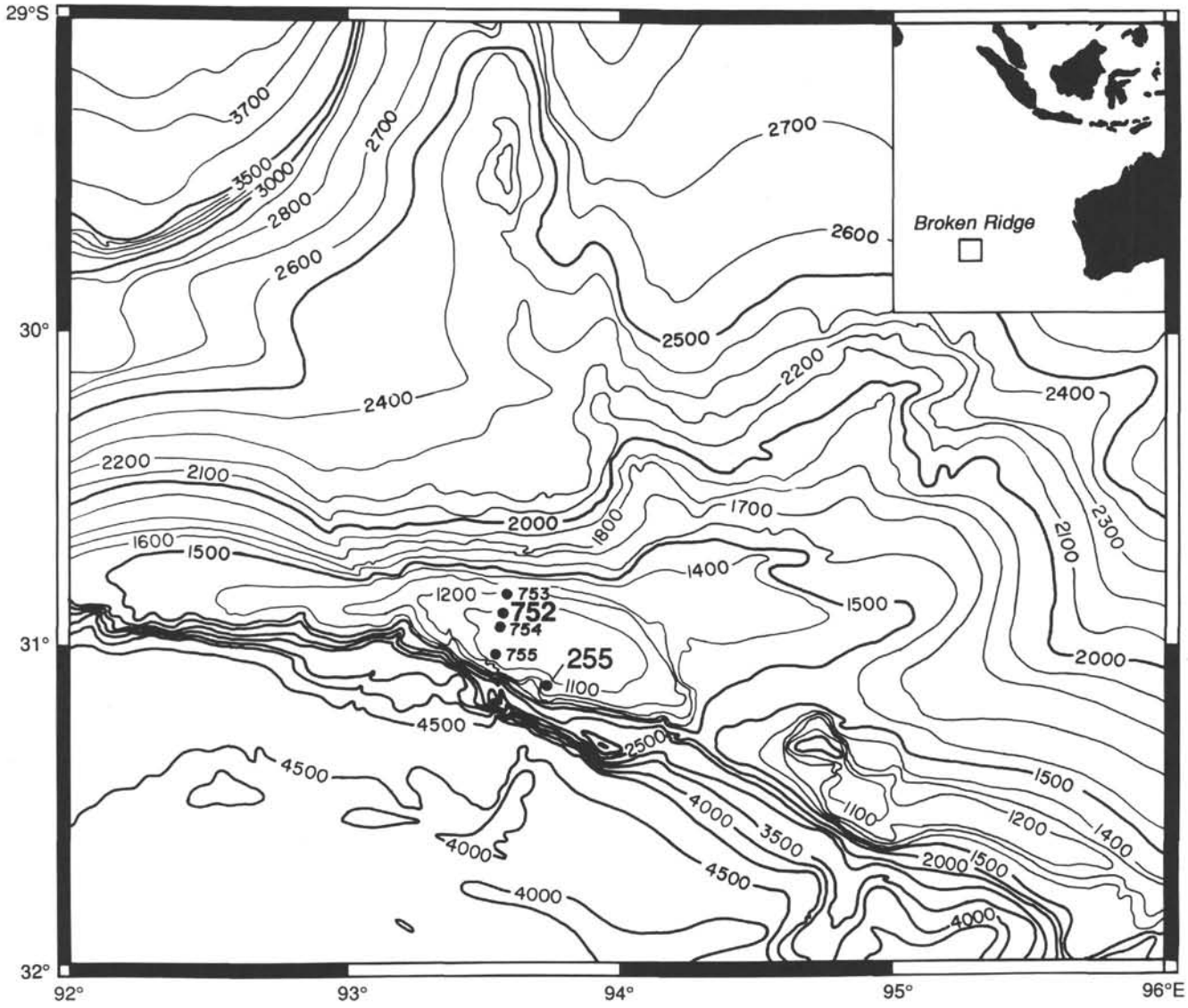

Figure 1. Bathymetric map showing locations of ODP Site 754, DSDP Site 255, and other Leg 121 sites at Broken Ridge. The bathymetry is based mainly on RC2708 echo-sounder data and is contoured at 100-m intervals except along the south-facing escarpment, where contours are omitted for clarity.

121-754B-4R (Table 1). Chert and chalk were encountered in Core 121-754B-5R at 155 mbsf, as in Hole 754A. A great deal of interbedded chert was drilled in the next 20 cores, yet recovery was at times extremely good. In a few chert-free zones of limestone, the cores were at or near 100% recovery and remarkably undisturbed. Our good fortune began to fade after Core 121-754B-15R (257.9 mbsf), because chert began to predominate below this depth. Chert was soon controlling the drilling parameters to the point that it was no longer possible to obtain recovery in the softer layers between chert stringers. The core bit began to show signs of penetration difficulty during Cores 121-754B-24R and 121-754B-25R and would not make any hole when we attempted Core 121-754B-26R. A bit deplugger was pumped into place but did not remedy the situation. The bit was declared dead at a total depth of 354.7 mbsf, and coring was terminated.

A full wiper trip was run in preparation for downhole logging. With the bit back at the bottom, the hole was swept with 45 bbl of polymer mud, flushed for 35 min with seawater, and displaced with mud to which potassium chloride had been added. The bit was then released and the pipe was pulled to the initial logging depth of 160 mbsf. This allowed the drill collars to bridge the unstable gravel zone that extended from about 120 to 155 mbsf.

The first logging run was the geochemical suite (GST-ACT-CNT-NGT-GPIT). The hole was logged successfully from bottom to the mud line, with the upper 160 m logged through the pipe twice. The second logging run was the seismic stratigraphic combination with resistivity added (DIT-E–LSS–CAL–CNL–NGT). This tool string was 35.5 m long and just fit between the blocks and the stool when fully rigged up. Running this string in a heavy sea would be difficult. This suite of tools was lowered through nearly the entire hole, but found 33 m of fill at the bottom of the hole. Successful logs were recorded from this level as the tool was run from bottom to the end of the pipe. We planned to raise the pipe one stand while pumping a slug of gel mud to expose the gravel zone to the logging tools, thereby enabling safe recording of a log for this interval when the tool reentered the drill pipe. The pipe was found to be stuck at this point, however, and could not be freed in 20 min of pulling and circu-

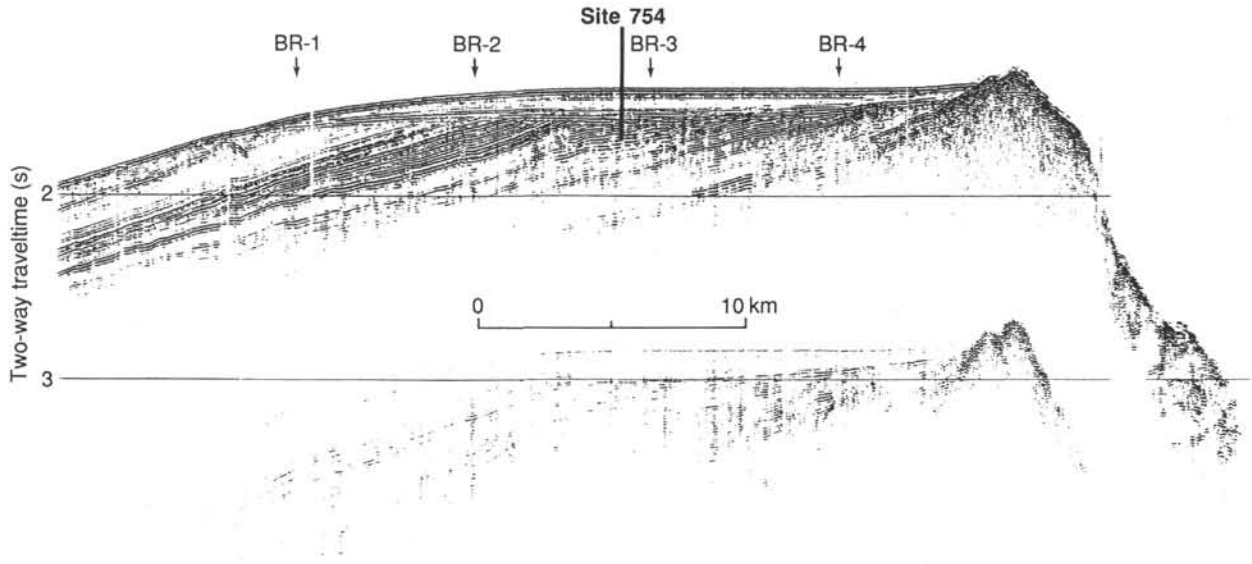

Figure 2. RC2708 single-channel seismic-reflection profile line 20 across Broken Ridge.

lating. The logging tools were then pulled to the deck to avoid getting them stuck as well. Higher flow than was possible with the packoff of the logging line used to wash away the cuttings jamming the pipe. Working the pipe with 300,000-lb overpull plus a high circulation rate was sufficient to free the pipe. Further plans to log the then-unstable hole were abandoned, and the pipe was pulled. The end of the pipe was on deck at 0915 hr, 18 May, while under way in DP mode back to Site 752.

LITHOSTRATIGRAPHY AND SEDIMENTOLOGY

Sediments of Pleistocene through Cretaceous age were recovered from two holes at Site 754 before drilling was terminated in lower Maestrichtian limestone in Hole 754B. Two lithologic units are recognized (Fig. 3 and Table 2): Unit I, 132 m of foraminifer nannofossil ooze of Pleistocene to late Eocene age, and Unit II, a 204-m-thick sequence of Maestrichtian calcareous chalk, limestone, and chert.

Unit I includes Cores 121-754A-1H to 121-754A-14X (0–131.7 mbsf) and 121-754B-2R (122.7–132.3 mbsf). The unit is dominated by a foraminifer nannofossil ooze, with foraminifers becoming less abundant and micrite more abundant downcore. Two subunits are identified (Fig. 3 and Table 2): Subunit IA is a foraminifer nannofossil ooze and Subunit IB is a nannofossil ooze with foraminifers and micrite.

The Pleistocene to lower Miocene foraminifer nannofossil ooze subunit is strongly mottled and white (10YR 8/2) to light brownish gray (10YR 6/2) in the first two cores. The remainder of the subunit is stark white (whiter than 10YR 8/1) to white (10YR 8/2) and homogeneous. The sediment is strongly mottled in the upper 15 m and homogeneous over the remainder of Subunit IA. Faint planar pale brown (10YR 8/3) laminae are found in Cores 121-754A-4H and 121-754A-5H. A 15-cm-thick pale yellow layer, with a sharp basal contact and a gradational upper contact, containing 2% volcanic ash occurs in Core 121-754A-8H.

Sediments in Subunit IB are similar in composition to those in Subunit IA but contain fewer foraminifers and more micrite. These lower Miocene to upper Eocene homogeneous nannofossil oozes grade in color from stark white (whiter than 10YR 8/1) at the top of Subunit IB through white (10YR 8/2) to yellow (10Y 7/8) and yellowish brown (10YR 5/8) downsection. Foraminifers constitute only 10%–15% of the sediment whereas micrite increases in abundance to 10%–20%. Thin ash layers and ash pockets are found in Cores 121-754A-10H, 121-754A-12H, and 121-754A-14X. Shell fragments, about 1 cm in size, are scattered throughout Core 121-754-14X. A layer of gravel and sand occurs at the base of this subunit in Core 121-754B-2R. The layer consists of quartz sand and pebbles and cobbles of limestone, chert, and shell fragments.

Grain-size data were collected on the bulk sediments of Unit I above the sand and pebble layer. A description of the analytical procedure and equipment can be found in the "Explanatory Notes" chapter (this volume). The data from Unit I in Hole 754A (Fig. 4 and Table 3) show a fining-upward sequence that begins immediately above the pebble layer at 122 mbsf (upper Oligocene) and extends to 60 mbsf (middle Miocene). From this depth, the grain size of the bulk sediment coarsens upward to 25 mbsf (upper Miocene/lower Pliocene), which is followed by a decrease within the Pliocene. Superimposed on these general trends are grain-size maxima in the lower Miocene at 80 mbsf and in the Pleistocene at 2 mbsf.

Unit II is dominated by Maestrichtian calcareous chalk, limestone, and chert (Table 2 and Fig. 3). The unit includes Cores 121-754A-17X to 121-754A-23N (151.0–172.1 mbsf) and 121-754B-5R to 121-754B-25R (151.7–354.7 mbsf). Three subunits are identified (Table 2): Subunit IIA is a hard calcareous chalk, Subunit IIB is a laminated limestone, and Subunit IIC is an alternating limestone/chert sequence.

The calcareous chalk of Subunit IIA alternates between greenish gray (5G 7/1, 5GY 5/1, 5G 5/1, and 5G 6/1) and lighter shades of gray and white (5Y 8/1, 5Y 7/1, and 5GY 7/1). Millimeter-scale planar and cross-bedded laminae are common; some have sharp basal contacts and graded bedding. Mottling is common throughout the sequence, with pyrite and chert filling many burrows. The darker greenish gray intervals contain up to 10% ash. Ash layers with up to 50% ash are found in Cores 121-754B-7R and 121-754A-23N. Many ash-bearing intervals have sharp basal contacts and grade upward. Chert pebbles occur in Cores 121-754A-17X through 121-754A-19N and 121-754B-6R. Chert layers several centimeters thick are in Cores 121-754A-21N, 121-754A-22N, 121-754B-7R, and 121-754B-8R. *Inoceramus* fragments were found in Section 121-754B-8R-CC.

Subunit IIB consists of strongly mottled limestone (Table 2 and Fig. 3). The limestone is dark greenish gray (5G 4/1) to light greenish gray (5G 7/1), with distinct wavy to subhorizontal 1–5-mm-thick laminae in the upper half of the subunit and fainter

Table 1. Coring summary, Site 754.

Core no.	Date (May 1988)	Time (local)	Depth top (mbsf)	Depth bottom (mbsf)	Length cored (m)	Length recovered (m)	Recovery (%)
121-754A-							
1H	13	2230	0.0	6.1	6.1	6.14	100.0
2H	13	2255	6.1	15.7	9.6	9.20	95.8
3H	13	2320	15.7	25.3	9.6	9.32	97.1
4H	13	2350	25.3	34.9	9.6	9.51	99.0
5H	14	0025	34.9	44.5	9.6	9.73	101.0
6H	14	0055	44.5	54.1	9.6	9.42	98.1
7H	14	0125	54.1	63.8	9.7	9.48	97.7
8H	14	0150	63.8	73.5	9.7	10.05	103.6
9H	14	0220	73.5	83.2	9.7	9.08	93.6
10H	14	0310	83.2	92.9	9.7	8.87	91.4
11H	14	0340	92.9	102.6	9.7	9.37	96.6
12H	14	0430	102.6	112.3	9.7	9.67	99.7
13X	14	0540	112.3	122.0	9.7	4.97	51.2
14X	14	0620	122.0	131.7	9.7	5.59	57.6
15X	14	0705	131.7	141.4	9.7	0.00	0.0
16X	14	0750	141.4	151.0	9.6	0.00	0.0
17X	14	0905	151.0	156.7	5.7	0.23	4.0
18X	14	1110	156.7	159.8	3.1	0.19	6.1
19N	14	1530	159.8	160.5	0.7	0.74	100.0
20N	14	1820	162.6	167.1	4.5	3.37	74.9
21N	14	2020	167.1	170.1	3.0	1.79	59.6
22N	14	2200	170.1	171.1	1.0	0.59	59.0
23N	14	2345	171.1	172.1	1.0	0.96	96.0
					170.0	128.27	75.5
121-754B-							
1W	15	1135	0.0	122.7	122.7	0.00	(wash core)
2R	15	1205	122.7	132.3	9.6	0.36	3.8
3R	15	1245	132.3	142.0	9.7	0.00	0.0
4R	15	1320	142.0	151.7	9.7	0.00	0.0
5R	15	1440	151.7	161.3	9.6	5.14	53.5
6R	15	1620	161.3	171.0	9.7	4.55	46.9
7R	15	1800	171.0	180.6	9.6	9.05	94.3
8R	15	1945	180.6	190.3	9.7	2.38	24.5
9R	15	2125	190.3	200.0	9.7	8.96	92.4
10R	15	2305	200.0	209.6	9.6	6.61	68.8
11R	16	0125	209.6	219.2	9.6	3.46	36.0
12R	16	0315	219.2	228.9	9.7	2.05	21.1
13R	16	0435	228.9	238.5	9.6	8.14	84.8
14R	16	0615	238.5	248.2	9.7	10.07	103.8
15R	16	0805	248.2	257.9	9.7	9.15	94.3
16R	16	1030	257.9	267.6	9.7	4.81	49.6
17R	16	1235	267.6	277.3	9.7	3.14	32.4
18R	16	1450	277.3	287.0	9.7	2.13	21.9
19R	16	1630	287.0	296.7	9.7	1.62	16.7
20R	16	1820	296.7	306.3	9.6	2.55	26.5
21R	16	2010	306.3	316.0	9.7	2.36	24.3
22R	16	2135	316.0	325.6	9.6	2.09	21.8
23R	16	2320	325.6	335.3	9.7	0.58	6.0
24R	17	0110	335.3	345.0	9.7	2.04	21.0
25R	17	0300	345.0	354.7	9.7	0.61	6.3
	Coring				232.0	91.85	39.6
	Washing				122.7	0.00	
					354.7		

laminae in the lower half. This subunit is marked by the formation of incipient stylolite seams and microfractures in the limestone. Pyrite blebs and *Inoceramus* shell fragments occur throughout Subunit IIB. Volcanic ash layers, some with ash contents up to 75%, are common in most of the cores and noticeably darken the host sediment to bluish gray and dark bluish gray (5B 5/1 and 5B 4/1) (Fig. 5). Chert fragments were found in Cores 121-754B-9R and 121-754B-11R, and several chert layers are in Core 121-754B-16R.

Subunit IIC is a lower Maestrichtian sequence of alternating limestone and chert (Table 2 and Fig. 3). The limestone is gray (5Y 5/1) to olive (5Y 4/3) in color and is weakly laminated and mottled. *Inoceramus* shell fragments, microfaults, fractures, and calcite- and silica-filled fractures are common. Chert, generally black (5Y 2.5/1 and 5Y 2.5/2), occurs in discrete layers up to 20 cm thick and as fragments up to 5 cm in diameter (Fig. 6). Chalcedony veinlets are common, and rare vugs are lined with white or black quartz microcrystals. About one-third of the olive limestones in Core 121-754B-22R have been replaced by dolomite in the form of millimeter-scale rhombs.

BIOSTRATIGRAPHY

The primary objectives of drilling Site 754 on Broken Ridge were to (1) recover and date the sedimentary cap above the unconformity; (2) determine the age of the unconformity; (3) determine the age, facies, and depth of deposition of the dipping and truncated units beneath the unconformity; and (4) penetrate and recover as much sediment as possible to a target total depth of 450 mbsf, with emphasis on determining the age and nature of the lowermost seismic sequence boundary at 0.3 TWT bsf.

Two holes were drilled at Site 754 before drilling was abandoned in Hole 754B in lower Maestrichtian limestones. Nevertheless, a generally complete Neogene sequence of foraminifer nannofossil ooze was recovered from Core 121-754A-1H to Section 121-754A-11H-CC. The foraminifer nannofossil ooze directly overlying the unconformity, in Samples 121-754A-12H-CC to 121-754A-14X-1, 145–146 cm, is dated as late Oligocene and placed in calcareous nannofossil Zone CN19a. The unconformity consists of a layer of gravel and sand in which limestone, chert pebbles, and shell fragments were found. Within this "hardground," up to 50% of the planktonic foraminifers and nannofossils are reworked, moderately preserved, late Eocene age forms. The brown nannofossil ooze recovered in Core 121-754A-14X is dated as late Eocene (nannofossil Zone CP15b). Although there was no recovery in Cores 121-754A-15X and 121-754A-16X, recovery from Cores 121-754A-17X to 121-754A-23N was excellent. The sediments are dominated by calcareous chalks, limestones, and cherts and assigned to the late/middle Maestrichtian nannofossil Zone CC24.

Hole 754B was washed down through the entire Neogene and RCB drilled in sediments below the unconformity. Sediments in Cores 121-754B-1W and 121-754B-2R are assigned to late Eocene age nannofossil Zone CP15b. There was no recovery from Cores 121-754B-3R to 121-754B-5R. Cores 121-754B-6R to 121-754B-25R contain a late/middle to early Maestrichtian age (nannofossil Zones CC24–23b) assemblage of nannofossils and planktonic foraminifers. The hole was terminated at 354.7 mbsf because of RCB bit failure.

Calcareous nannofossils are abundant in all of the cores. Throughout the Pliocene and Miocene sediments, nannofossil preservation is generally good. Strong overgrowth of the discoasters, in combination with the lack of zonal markers resulting from latitudinal effects, made zonal assignments of the lower and middle Miocene sections more difficult. In the Maestrichtian and late Campanian(?), however, preservation is poor. Datum levels used for the calcareous nannofossils are shown in Table 4.

Neogene planktonic foraminifers are abundant and well preserved, with assemblages showing Southern Ocean, high-latitude affinities. The Eocene, Paleocene, and Maestrichtian planktonic foraminifer assemblages are also of a temperate nature. The absence, therefore, of low-latitude marker species makes it impossible to apply known tropical zonation schemes. Datum levels used for planktonic foraminifers are shown in Table 4. The age-depth curve for Site 754, based on nannofossil and planktonic foraminifer datums (Fig. 7), is not extended beyond the unconformity owing to insufficient datum levels in the Eocene and Cretaceous.

The planktonic foraminifer zonation matches well with the calcareous nannofossil zonation. The biostratigraphic subdivisions of Holes 754A and 754B are summarized in Figures 8 and 9, respectively.

Well-preserved benthic foraminifer assemblages were found throughout the Cenozoic.

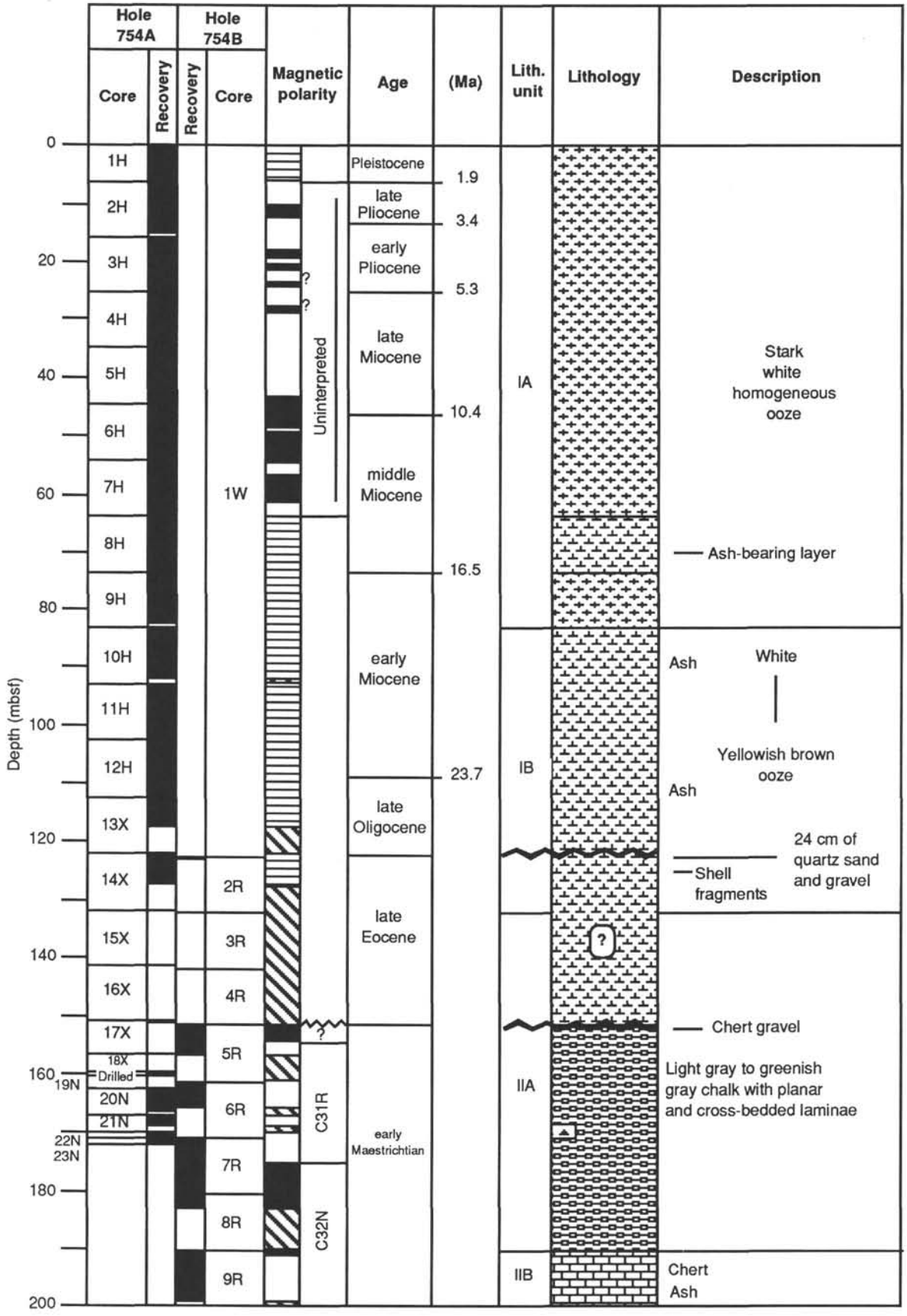

Figure 3. Site 754 summary diagram.

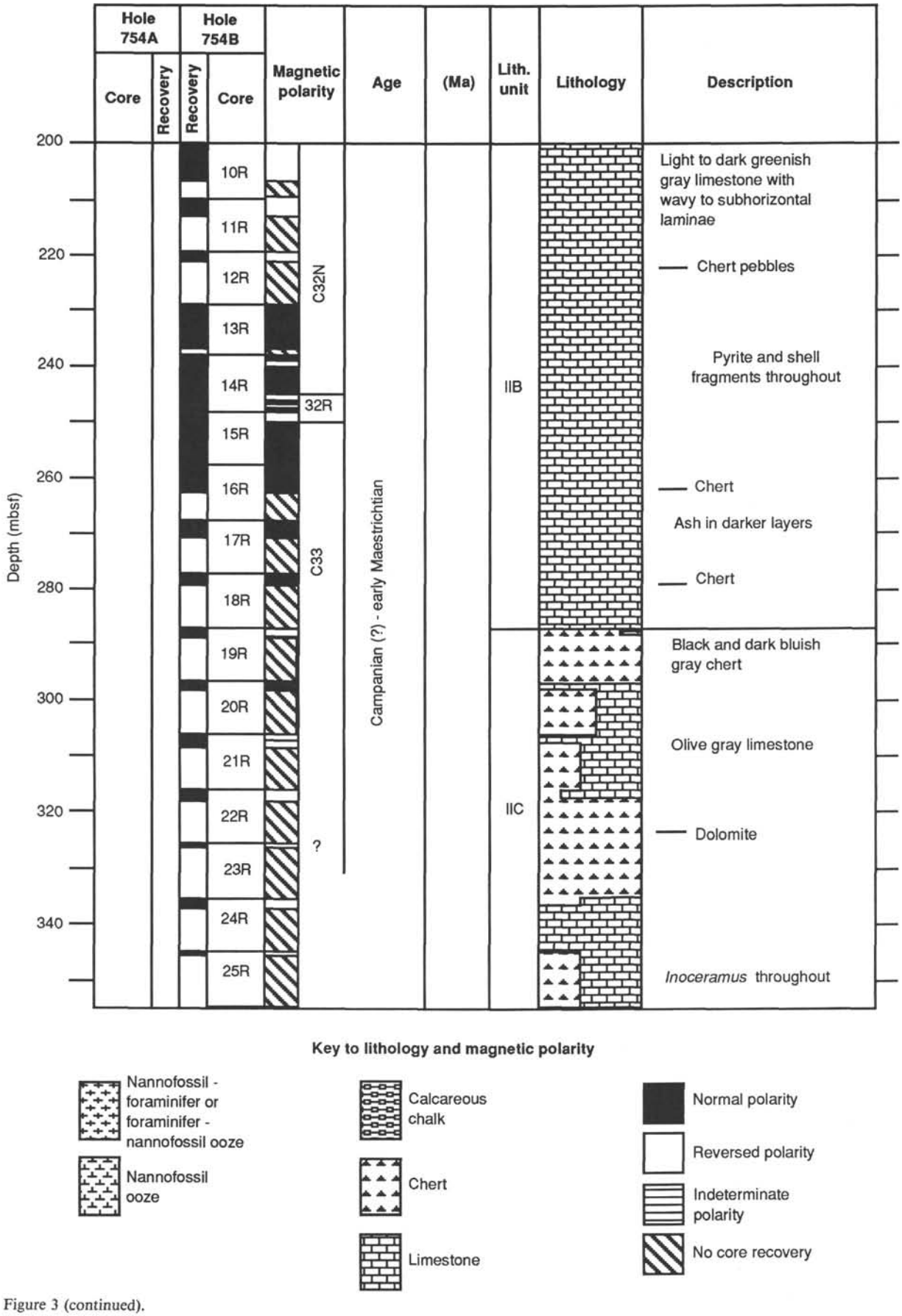

Figure 3 (continued).

Table 2. Lithostratigraphic summary for Site 754.

Unit	Core interval	Depth (mbsf)	Age	Lithostratigraphy
IA	754A-1H to -9H	0–83.2	Pleistocene–early Miocene	Foraminifer–nannofossil ooze
IB	754A-10H to -14X 754B-2R	83.2–131.7	early Miocene–late Eocene	Nannofossil ooze with foraminifers and micrite
IIA	754A-17X to -23N	151.0–172.1	late Maestrichtian	Calcareous chalk
	754B-5R to -8R	151.7–190.3		
IIB	754B-9R to -18R	190.3–287.0	Maestrichtian	Limestone
IIC	754B-19R to -25R	287.0–354.7	early Maestrichtian	Limestone and chert

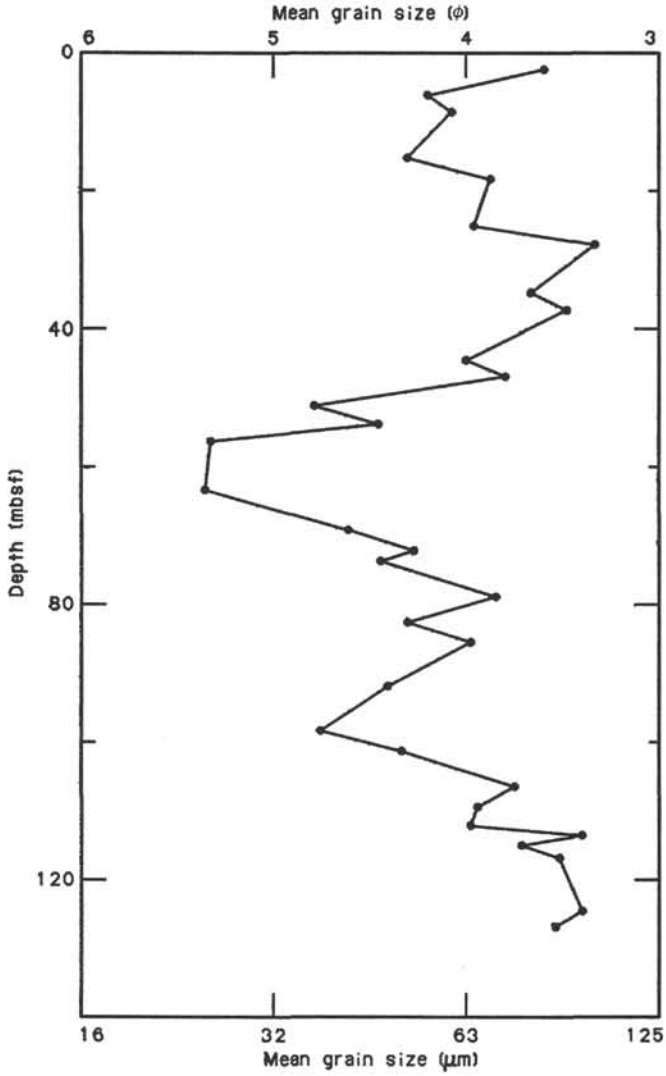

Figure 4. Grain size of the bulk sediment of lithologic Unit I, Hole 754A.

Table 3. Grain-size data, Hole 754A.

Core, section, interval (cm)	Depth (mbsf)	Grain size (μm)	Grain size (φ)
1H-2, 80	2.30	81.80	3.61
1H-CC, 1	6.01	54.00	4.21
2H-2, 85	8.45	59.00	4.08
2H-CC, 1	15.11	50.00	4.32
3H-2, 85	18.05	67.90	3.88
3H-7, 25	24.95	64.00	3.97
4H-2, 85	27.65	98.60	3.34
4H-CC, 1	34.64	78.30	3.67
5H-2, 85	37.25	89.60	3.48
5H-CC, 1	44.39	62.00	4.01
6H-2, 85	46.85	72.00	3.80
6R-5, 55	51.05	36.00	4.80
6H-CC, 1	53.73	45.50	4.46
7H-2, 85	56.45	24.90	5.33
7H-CC, 1	63.41	24.40	5.36
8H-4, 85	69.15	40.70	4.62
8H-6, 85	72.15	51.40	4.28
8H-CC, 1	73.66	45.60	4.45
9H-4, 85	78.85	69.50	3.85
9H-6, 150	82.50	50.40	4.31
10H-2, 80	85.50	63.20	3.98
10H-CC, 1	91.91	47.20	4.41
11H-4, 85	98.25	36.90	4.76
11H-6, 80	101.20	49.40	4.34
12H-3, 80	106.40	74.40	3.75
12H-5, 80	109.40	64.70	3.95
12H-CC, 1	112.13	63.50	3.98
13X-1, 120	113.50	95.00	3.40
13X-2, 120	115.00	76.50	3.71
13X-CC, 1	116.97	87.00	3.52
14X-2, 90	124.40	95.00	3.40
14X-4, 20	126.70	86.10	3.54

Rare specimens of diatoms are present only at a few levels, in the Neogene in Hole 754A and in the Cretaceous in Hole 754B. Unfortunately, these few specimens could not be assigned to any particular diatom zonation scheme because they are too poorly preserved. Radiolarians, silicoflagellates, and sponge spicules are also present in particular samples.

Calcareous Nannofossils

Calcareous nannofossils were found to be abundant in all cores taken from Hole 754A. Preservation is good in the Pliocene and Pleistocene sections and moderate to poor in the upper Maestrichtian to Miocene sequences. Strong overgrowth of the Miocene discoasters impeded quick and accurate identification. Miocene nannofossil biostratigraphy was also hindered by the absence of low-latitude marker species which made it necessary to combine several of the zones of Okada and Bukry (1980). The presence of abundant reticulofenestrids in the Broken Ridge sediments and the general lack of delicate forms from the discoaster group in the upper Oligocene to middle Miocene sections are indicative of cooler waters and may reflect the effects of the late Oligocene establishment of the Antarctic Circumpolar Current reported by Kennett and Burns (1972). A diversity increase is noted in the uppermost Miocene and Pliocene sections, with an increasing abundance of discoasters, ceratoliths, and especially scyphospheres. This same assemblage increase was also noted in Indian Ocean sediments by Müller (1977) and was attributed to a productivity increase during that time. It may also be indicative of a slight late Miocene warming trend.

Neogene

Pleistocene to Pliocene

Pleistocene sediments were recovered in Core 121-754A-1H. The last occurrence of *Discoaster brouweri* in Sample 121-

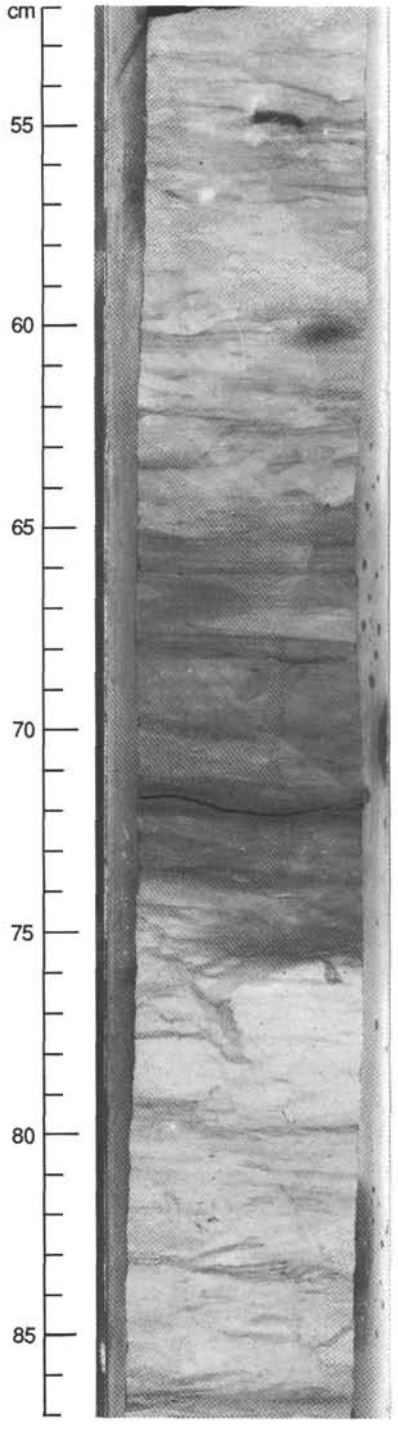

Figure 5. A typical ash-bearing interval within the limestone of lithologic Subunit IIB (Section 121-754B-10R-1, 52–87 cm).

754A-2H-1, 45–46 cm (6.60 mbsf), is used to approximate the Pliocene/Pleistocene boundary. Cores 121-754A-3H and 121-754A-2H (CN10–12) contain a condensed but apparently complete Pliocene sequence. *D. brouweri, Discoaster pentaradiatus, Discoaster surculus*, and *Discoaster tamalis* are present, along with common amauroliths, ceratoliths, and scyphospheres. The first occurrence of *Ceratolithus acutus* in Sample 121-754A-3H-6, 45–46 cm (22.7 mbsf), is used to denote the Miocene/Pliocene boundary. Nannofossils are abundant and preservation is generally good through this interval.

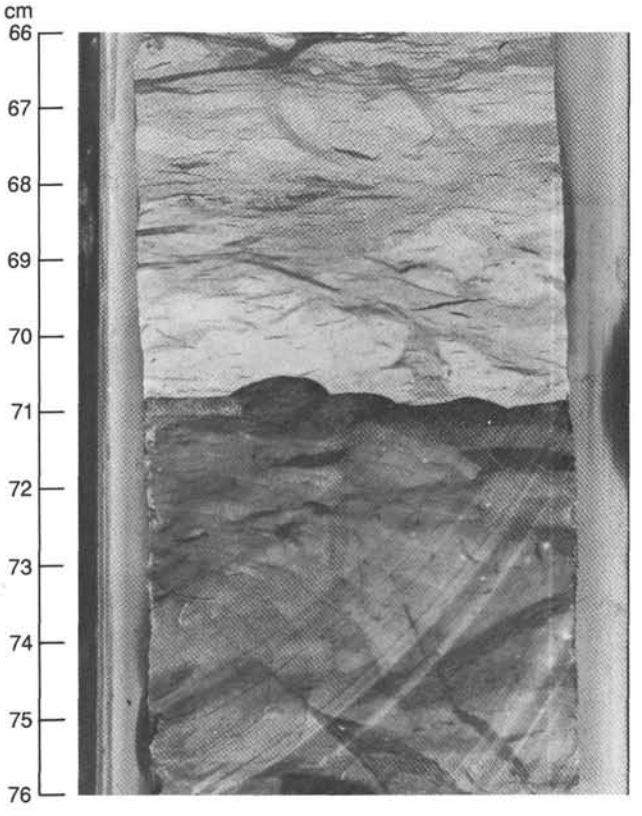

Figure 6. Sharp contact between a lighter-colored limestone and underlying darker chert in lithologic Subunit IIB (Section 121-754B-16R-3, 66–76 cm).

Miocene

Miocene sediments are in Cores 121-754A-4H to 121-754A-12H. Core 121-754A-4H is assigned the combined Zones CN9b–10a (late Miocene age), based on the presence of *Amaurolithus primus* and the absence of *C. acutus* or other species of the genus *Ceratolithus*. The interval from Samples 121-754A-4H-5, 45–46 cm, to 121-754A-6H-2, 45–46 cm, (21.8–46.5 mbsf) is assigned to the combined Zones CN7–9a (late Miocene age). The preservation of discoasters is poor throughout this interval, and the species used to delineate these zones have not been noted yet. The combined zones are based on the first occurrence of few to common *D. pentaradiatus*, along with *D. brouweri, Discoaster variabilis*, and *Reticulofenestra pseudoumbilica*. The interval from Samples 121-754A-6H-2, 45–46 cm, to 121-754A-9H-3, 45–46 cm, (46.5–77.0 mbsf) is assigned to the combined Zones CN5–6 (middle Miocene), based on the presence of *Discoaster exilis* and *D. variabilis*, the lack of *D. pentaradiatus* and *Sphenolithus heteromorphus*, and the general upsection decrease in abundance of *Cyclicargolithus floridanus* and *Discoaster deflandrei*.

The interval encompassing the last occurrence of *S. heteromorphus* (Sample 121-754A-9H-3, 45–46 cm; 77.0 mbsf) and the first occurrence of *D. variabilis* and *D. exilis* (Sample 121-754A-9H-5, 45–46 cm; 80.0 mbsf) is assigned to Zone CN4 (early Miocene age). *S. heteromorphus* and *C. floridanus* are common through this interval, along with *Sphenolithus conicus* and *Calcidiscus macintyrei*. The remaining sections of Core 121-754A-9H to the first occurrence of *S. heteromorphus* (Sample 121-754A-10H-3, 45–46 cm; 86.7 mbsf) are placed in Zone CN3. The first occurrence of *Sphenolithus belemnos* is used to mark the CN1/2 zonal boundary in Sample 121-754A-10H-5, 45–46 cm (89.7 mbsf). The interval from Core 121-754A-11H to

Table 4. Datum levels used at Site 754.

Species[a]	Age (Ma)	Depth (mbsf)
Calcareous nannofossils		
Hole 754A		
LO *Discoaster brouweri*	1.9	6.6–6.1
LO *Discoaster pentaradiatus*	2.2	8.1–6.6
LO *Discoaster tamalis*	2.6	11.1–9.6
LO *Reticulofenestra pseudoumbilica*	3.5	16.2–15.7
FO *Discoaster tamalis*	3.8	17.7–19.2
FO *Ceratolithus acutus*	5.0	22.7–25.3
FO *Amaurolithus primus*	6.5	31.8–34.9
FO *Discoaster pentaradiatus*	12.0	46.5–48.5
LO *Sphenolithus heteromorphus*	14.4	77.0–73.5
FO *Discoaster variabilis* or *Discoaster exilis*	15.4	80.0–83.2
FO *Sphenolithus heteromorphus*	17.1	86.7–89.7
FO *Sphenolithus belemnos*	21.5	89.7–92.9
LO *Reticulofenestra bisecta* or *Zygrhablithus bijugatus*	23.7	108.6–107.1
LO *Ceratolithus altus*	28.2	116.8–113.8
CP15b/19a boundary	37.7–28.2	122.05–122.0
Hole 754B		
LO *Tranolithus phacelosus*	74.0	228.9–219.2
LO *Reinhardtites anthophorus*	75.0	267.6–257.9
Planktonic foraminifers		
Hole 754A		
FO *Globorotalia truncatulinoides*	1.66	6.1–9.2
FO *Globorotalia crassaformis*	4.11	5.7–25.3
FO *Globorotalia puncticulata*	4.4	25.3–34.9
LO *Globorotalia conomiozea*	6.1	34.9–44.5
LO *Globorotalia mayeri*	10.4	44.5–59.0
LO *Globorotalia peripheroacuta*	14.9	54.1–63.8
FO *Orbulina* spp.	15.2	63.8–73.5
FO *Praeorbulina glomerosa curva*	16.5	73.5–80.2
FO *Praeorbulina sicana*	16.6	73.5–80.2
LO *Catapsydrax dissimilis*	17.6	80.2–83.2
FO *Globigerinoides*	23.3	83.2–92.9
LO *Chiloguembelina cubensis*	30.0	113.8–116.8

[a]FO = first occurrence; LO = last occurrence.

the Oligocene/Miocene boundary marked in Sample 121-754A-12H-5, 45–46 cm (108.6 mbsf), is placed in Zone CN1 (early Miocene age), based on the absence of *Reticulofenestra bisecta, Zygrhablithus bijugatus*, and *S. belemnos* and the presence of abundant *D. deflandrei*.

Paleogene

Oligocene to Eocene

Upper Oligocene sediments (Zone CP19) are present in the interval from Samples 121-754A-12H-5, 45–46 cm, to 121-754A-13X-CC (108.6–122.0 mbsf). *Chiasmolithus altus* is present in the lower sections of Core 121-754A-13X, along with common to abundant *R. bisecta* and *Z. bijugatus*. A disconformity (missing CP16–18) separating upper Oligocene and upper Eocene sediments is placed between Samples 121-754A-13X-CC and 121-754A-14X-1, 5 cm (122.0–122.05 mbsf). The latter sample, plus the remaining sediments of Core 121-754A-14X, were examined and found to contain a rich upper Eocene (CP15b) assemblage consisting of common *Isthmolithus recurvus, Reticulofenestra umbilica, Coccolithus formosa, Chiasmolithus oamaruensis*, and few *Discoaster saipanensis*. Also present are rare braarudosphaerids and highly overgrown specimens of *Lanternithus minutus*, which are considered shallow-water forms.

After washing down to 122.7 mbsf at Hole 754B, RCB coring produced one core (121-754B-2R) containing upper Eocene (CP15) sands and gravels. Sediments of this core contain two distinct nannofossil assemblages. The presence of *C. oamaruensis, Ericsonia subdisticha*, and possible *I. recurvus* indicates a late Eocene age (CP15b). The second assemblage consists of the middle Eocene forms *Neococcolithus dubius, Chiasmolithus expansus, Coccolithus solitus*, and *Reticulofenestra reticulata*. This assemblage is indicative of Zone CP14 and appears to be entirely reworked.

Cretaceous

There was no recovery in Cores 121-754A-15X and 121-754A-16X. Cores 121-754A-17X to 121-754A-23N (150.0–171.1 mbsf) are assigned to Zone CC24. The assemblage lacks both *Nephrolithus frequens* and *Tranolithus phacelosus* and contains common *Reinhardtites levis, Arkhangelskiella cymbiformis*, and *Kamptnerius magnificus*.

Good Maestrichtian sections from the Southern Ocean are rare. Unfortunately, the preservation through this interval is poor for the most part, but detailed study of this material should add to the slowly increasing knowledge of austral, high-latitude Maestrichtian biostratigraphy.

In Hole 754B, after two cores with no recovery (121-754B-3R and 121-754B-4R), 18 cores in the interval from 151.7 to 325.6 mbsf were recovered containing Campanian(?)-Maestrichtian chalks and limestones. The limestones are well indurated, and the nannofossils, although common to abundant in some sections, are poorly preserved and, at times, were difficult to separate from the rest of the material. A special technique using the ultrasonic bath and 1% Calgon solution proved to be the only way to effectively produce slides worthy of examination.

Nannofossil assemblages are characterized by intervals of low diversity, with overgrown specimens of *Micula decussata* as the most abundant form, and intervals where diversity is somewhat greater. The more diverse assemblages consist of common *R. levis, A. cymbiformis, K. magnificus, Zygodiscus compactus*, and *Eiffellithus turriseiffeli*. The presence of common *Biscutum magnum* and rare specimens of *Biscutum coronum, Biscutum dissimilis, Nephrolithus corystus*, and *Monomarginatus quaternarius* indicates the austral nature of this assemblage.

Cores 121-754B-5R to 121-754B-12R (151.7–228.9 mbsf) are assigned to the combined Zones CC25 and CC26. Rare specimens of the marker *N. frequens* may be present in Core 121-754B-5R, but because of the poor preservation of the intervals examined, positive identification could not be made. The presence of *N. frequens* would facilitate better agreement with foraminiferal paleontologists on the age assignment for this core. The rare presence of *N. corystus* along with *N. frequens* was noted in sediments from Hole 752B. This situation is indicative of the lower part of Zone CC25 and should be present in Core 121-754B-5R if *N. frequens* is positively identified.

Cores 121-754B-13R to 121-754B-16R (228.9–257.9 mbsf) contain *T. phacelosus* without *Reinhardtites anthophorus* and are assigned to Zone CC23 (late Campanian/Maestrichtian age). Cores 121-754B-17R to 121-754B-25R (257.9–354.7 mbsf) contain *R. anthophorus* and *R. levis* and are assigned to Zones CC22/23. The upper Campanian marker species *Aspidolithus parcus constrictus* and *Eiffellithus eximius* were not found in the samples examined, suggesting that Campanian sediments were not reached. The possibility of ecological exclusion cannot be ruled out, but the relatively diverse assemblage in Sample 121-754B-25R-CC would suggest that this is not the case. In addition, although the presence of *R. anthophorus*, according to the zonation scheme of Sissingh (1977), indicates an age of Campanian, *R.* aff. *R. anthophorus* is reported to range slightly higher in the same scheme. Specimens examined from Hole 754B are probably more closely related to *R.* aff. *R. anthophorus*. It is clear that only additional detailed taxonomic work can resolve this problem.

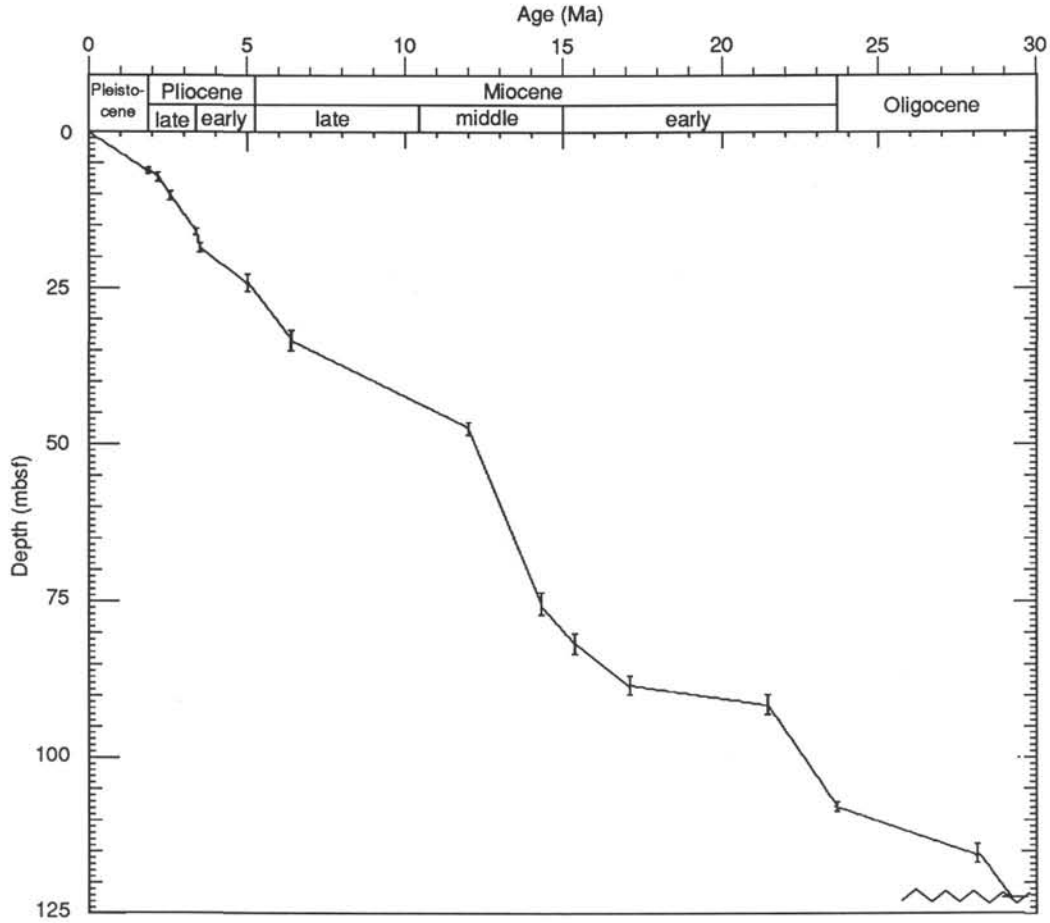

Figure 7. Age vs. depth plot for Site 754.

Planktonic Foraminifers

Neogene

A well-preserved Neogene assemblage of planktonic foraminifers was recovered in Hole 754A, down to 101.2 mbsf. In contrast, the assemblages above and within the upper Eocene to upper Oligocene hardground are moderately preserved and show signs of dissolution.

Dominating the Neogene assemblages are typical, middle- to high-latitude, temperate faunas and other more cosmopolitan species. Difficulties, therefore, arose in trying to recognize the zonal boundaries of Blow (1969), Banner and Blow (1965), or Bolli and Saunders (1985) owing to the lack of nominate marker species. This is probably the result of latitudinal control on the distribution of the taxa, rather than selective dissolution. The recovered planktonic foraminiferal assemblages have an affinity with other high-latitude, Neogene faunas of the Southern Hemisphere, such as those in southeast Australia (Jenkins, 1960), New Zealand (Jenkins, 1967), the South Atlantic (Jenkins, 1978), and the South Pacific (Kennett, 1973). Because of this apparent low-latitude taxon discrimination, the temperate, zonal schemes of Srinivasan and Kennett (1981) and Kennett (1973) were applied.

Pleistocene

Pleistocene sediments were recovered only from Sample 121-754A-1H-CC. The planktonic foraminifer assemblage is dominated by *Globorotalia inflata, Globorotalia crassaformis*, and *Globigerina bulloides*. The dominance of *G. inflata*, a species that is characteristic of a temperate water mass, is typical of other midlatitude sites in the Indian Ocean (Vincent, 1977). This is in marked contrast to Indian Ocean low- and high-latitude sites, which are dominated by *Globorotalia menardii* (and other tropical species) and *Globorotalia pachyderma*, respectively. Of equal importance is the abundance of *G. bulloides*, which is restricted presently to transitional and cooler waters (Bé and Tolderlund, 1971). Few tropical forms are present in this sample. Pink *Globigerinoides ruber* are present in small numbers, below the core top. According to Vincent (1977) these may have a stratigraphic importance, or they may be merely reworked. The presence of *Globorotalia tosaensis* with *Globorotalia truncatulinoides* assigns this sample to the lowermost Pleistocene.

Pliocene

The Pliocene/Pleistocene boundary was placed at the first occurrence of *G. truncatulinoides*. Although this datum is reported to be unreliable, the extinction of *Discoaster brouweri* at the same level suggests otherwise.

A nearly complete Pliocene sequence was recovered from Samples 121-754A-2H-3, 120–122 cm, to 121-754A-3H-CC. Only the upper Pliocene *G. inflata* Zone is not recognized. This is probably due the size of the sampling interval. The dominant components of the planktonic foraminifer assemblage in the Pliocene are *G. bulloides, Globigerina woodi, Globigerina falconensis, G. crassaformis*, and species of the *Globorotalia conoidea–G. inflata* lineage, the first occurrences of which are used to zone the Pliocene. With the exception of rare occurrences of *Globigerinoides sacculifer*, none of the warm to tropical forms, such as *Globorotalia tumida, Globorotalia tumida flexuosa,*

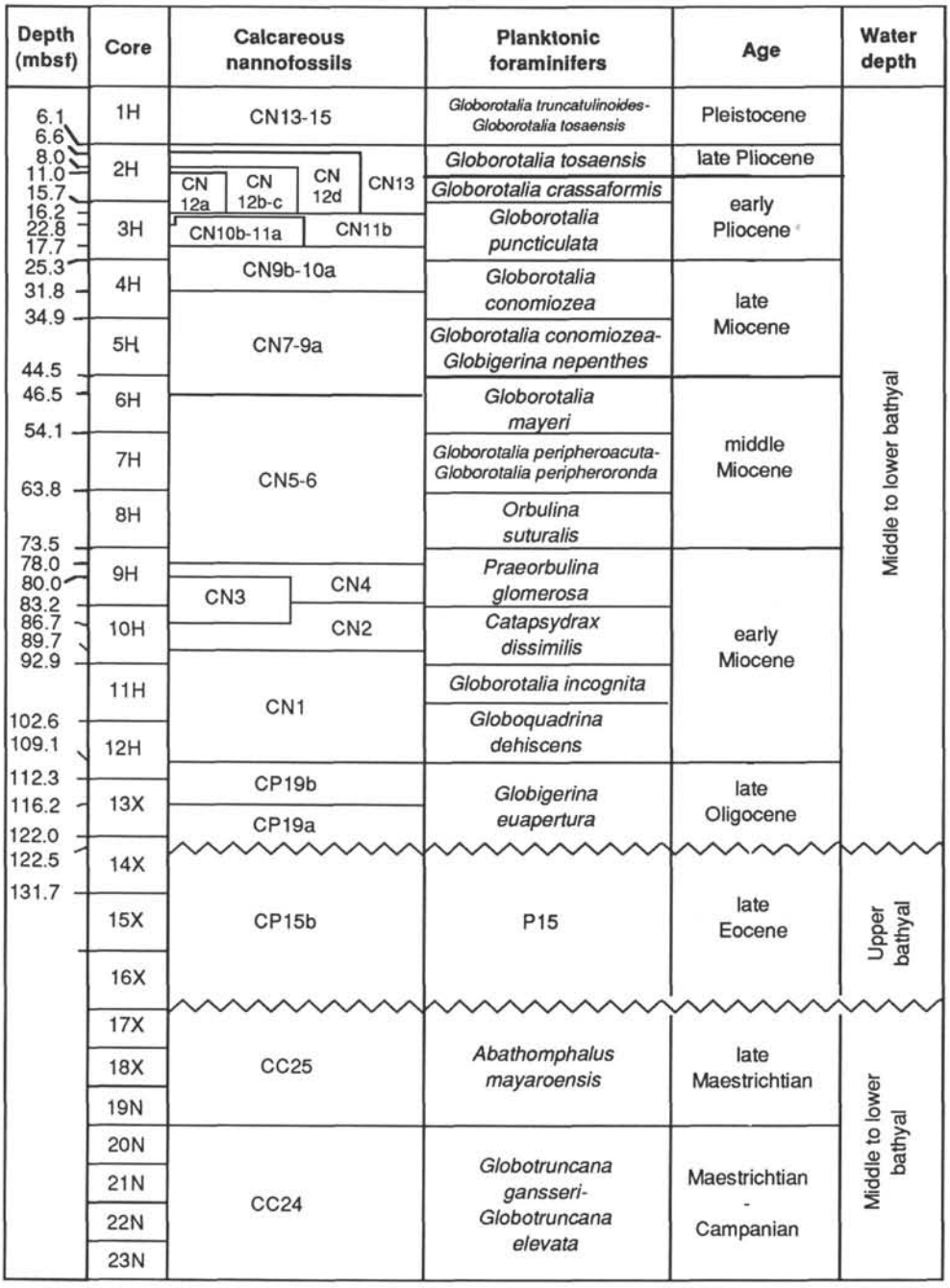

Figure 8. Biostratigraphic results of Hole 754A.

Sphaeroidinella dehiscens, Pulleniatina obliquiloculata, Neogloboquadrina dutertrei, and *Neogloboquadrina humerosa*, are present. Preservation throughout this interval is excellent.

Miocene

The Miocene/Pliocene boundary is tentatively placed at the first appearance of *Globorotalia puncticulata* and *Globorotalia margaritae* in Sample 121-754A-3H-CC. The first occurrence of the calcareous nannofossil *Ceratolithus acutus* in this sample helps with recognition of the boundary. The last occurrence of *Globoquadrina dehiscens*, which approximates the boundary (Berggren, 1973), is paleoceanographically controlled (Vincent, 1977) and is therefore not used in this study. The last occurrence of *G. dehiscens* in Hole 754A is in Sample 121-754A-5H-CC.

The upper Miocene planktonic foraminifer assemblages are dominated by *Globigerina nepenthes, G. conoidea, Globorotalia miozea, Globorotalia panda, G. bulloides, G. falconensis*, and *G. dehiscens. G. menardii* is present in small numbers.

The base of the middle Miocene is delineated by the first appearance of *Orbulina suturalis* from *Praeorbulina glomerosa curva* (the *Orbulina* datum) in Sample 121-754A-8H-CC. All of the temperate planktonic foraminiferal zones in the middle Miocene are discerned. The absence of the low-latitude marker species *Globorotalia praefohsi, Globorotalia fohsi, Globorotalia fohsi lobata*, and *Globorotalia fohsi robusta* testifies to the higher latitudinal position of Broken Ridge at that time. Only the more temperate to subtropical earlier forms of the *G. fohsi* evolutionary lineage, *Globorotalia peripheroronda* and *Globo-*

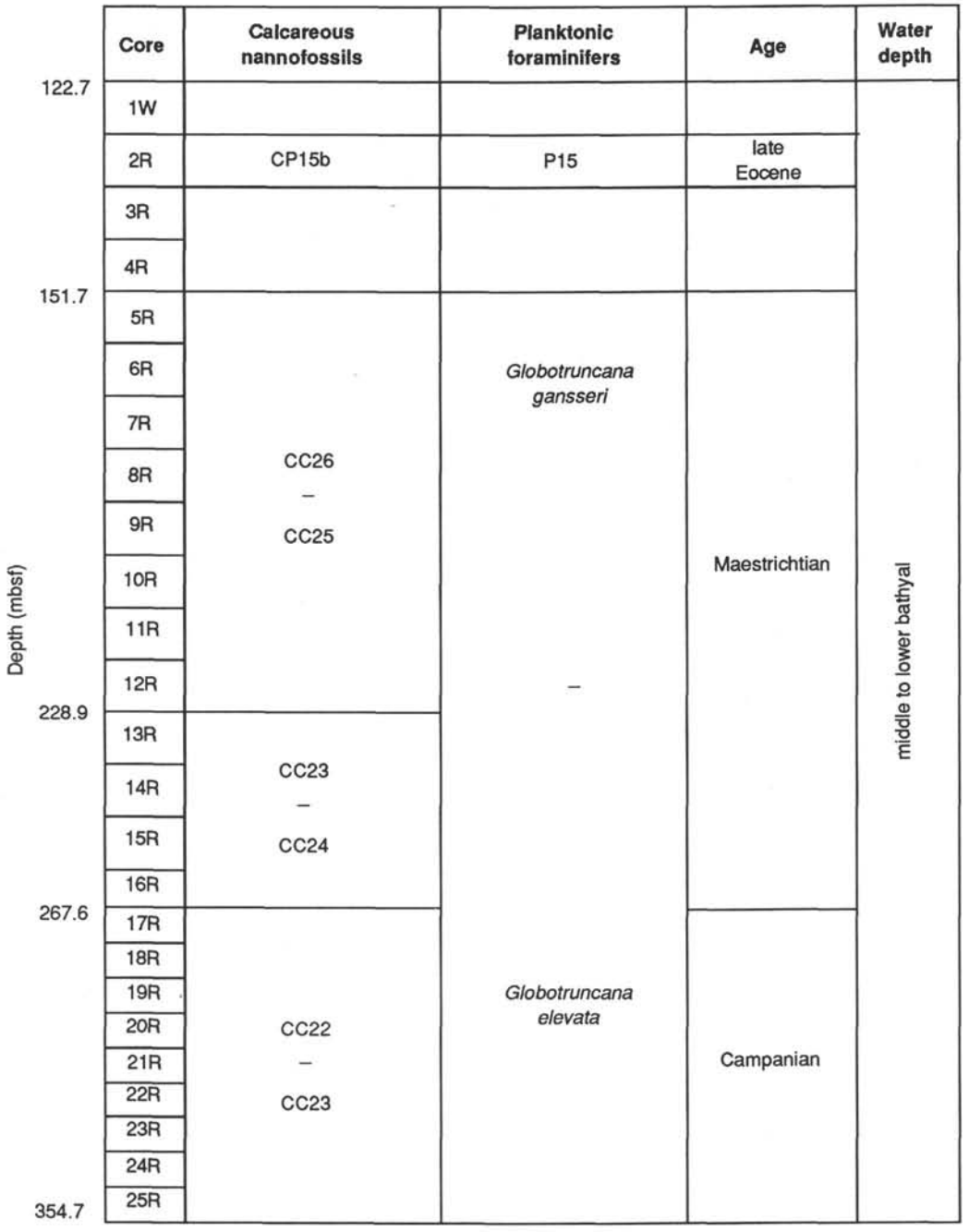

Figure 9. Biostratigraphic results of Hole 754B.

rotalia peripheroacuta, are present. The co-occurrence of these two forms in Sample 121-754A-7H-CC delineates the *Globorotalia peripheroronda–Globorotalia peripheroacuta* Zone of the middle Miocene.

The top of the lower Miocene, the *Praeorbulina glomerosa* Zone, is represented in Sample 121-754A-9H-CC. Within this sample, the ancestral forms of *Orbulina* sp.—*Praeorbulina sicana, P. glomerosa curva, Praeorbulina glomerosa glomerosa*, and *Praeorbulina glomerosa circularis*—are present.

Below this interval down to Sample 121-754A-11H-CC, the sediments are of early Miocene age, as characterized by *G. dehiscens, Globigerinoides trilobus, Catapsydrax dissimilis, G. bulloides, Globorotalia incognita*, and *Globorotalia zealandica*.

Paleogene

Oligocene

The Miocene/Oligocene boundary is placed between Samples 121-754A-11H-CC and 121-754A-12H-6, 100–105 cm, based on the first appearance of *G. dehiscens*. Other boundary markers such as *Globigerinoides primordius* and *Globorotalia kugleri* are absent. Within both samples the ancestor to *G. dehiscens, Globoquadrina praedehiscens*, is present. The planktonic foraminifer fauna in Sample 121-754A-13X-3, 100–105 cm, is assigned a late Oligocene age based on the co-occurrence of *Globigerina angulisuturalis* and *Chiloguembelina cubensis*, along with the absence of *Globigerina angiporoides* and *G. dehiscens*.

The interval from Samples 121-754A-12H-6, 100–105 cm, to 121-754A-13X-CC contains an assemblage of planktonic foraminifers of late Oligocene age, based on the presence of *G. praedehiscens* and rare occurrences of *C. cubensis* and *G. angulisuturalis*. Up to 25% of the assemblages within these samples are composed of reworked, early Oligocene and late Eocene age forms such as *Globigerinatheka* sp., *G. angiporoides*, and *Pseudohastigerina* sp.

Eocene

Middle to late Eocene age *Globigerinatheka index* and *Gt. index* were found in Sample 121-754A-13X-CC, above the upper hardground. They are stained green and mixed with latest Eocene or Oligocene age faunas represented by *Globigerina ampliapertura* and *Catapsydrax* aff. *dissimilis*. Sample 121-754A-14X-CC contains a planktonic foraminiferal fauna, fragments of corals, bryozoans, brachiopods, bivalves, and crinoids, and large amounts of chert containing Cretaceous foraminifers such as *Globigerinelloides* sp. The fauna, which is probably indigenous, contains a temperate fauna with *G. index, Acarinina* aff. *primitiva*, and *Acarinina bullbrooki*. The high abundance of acarininids is indicative of the middle Eocene in temperate/austral areas, according to Jenkins (1985). According to Toumarkine and Luterbacher (1985) the overlap of *G. index* and *A. bullbrooki* occurs in Zones P13–14 (preferably P14), which may represent the oldest post-rift sediment.

Cretaceous

The uppermost Maestrichtian is represented by its index fossil *Abathomphalus mayaroensis* in Sample 121-754B-5R-CC, although the few specimens found are not advanced forms, as evidenced by the weakly developed double keel on the last chamber. *Abathomphalus intermedius*, without *A. mayaroensis*, is found in Sample 121-754B-6R-CC. The middle Maestrichtian, found in Sample 121-754B-7R-CC, is represented by *Globotruncanella citae*, without *A. mayaroensis* and *A. intermedius*. The evolutionary sequence *G. citae–A. intermedius–A. mayaroensis* is biostratigraphically important because the same transition is found at the base of Hole 752B. *A. intermedius* without *A. mayaroensis* is found in Sample 121-752B-19R-CC, and *A. mayaroensis* is found in Samples 121-752B-17R-CC through 121-752B-14R-CC. Thus, the biostratigraphically important datum of the first occurrence of *A. mayaroensis* is placed between Sections 121-752B-17R-CC and 121-752B-19R-CC and between Sections 121-754B-5R-CC and 121-754B-6R-CC.

The abundance and preservation of planktonic foraminifers decreases downhole. Because washed residues were impossible to obtain, slabs of rocks stained with methylene blue were commonly used to assess foraminiferal content. Faunas are mainly composed of *Rugoglobigerina rugosa, Rugoglobigerina* sp., *Globigerinelloides* sp., *Globigerinelloides aspera, Globigerinelloides ehrenbergi*, and *Hedbergella* sp., an assemblage typical of the austral/boreal temperate provinces (Caron, 1985; Herb, 1974). The continued presence of *Rugoglobigerina* sp. normally would be indicative of a Campanian-Maestrichtian age for Samples 121-754B-7R-CC to 121-754B-25R-CC (180.6–325 mbsf). It is not clear whether the specimens seen on the slab surface are larger archaeoglobigerinid species, in which case an age as old as Santonian cannot be excluded.

Benthic Foraminifers

All core-catcher samples from Holes 754A and 754B were examined for >125-μm benthic foraminifers. Benthic foraminifers are well preserved but rare in the Pleistocene to lower Miocene sediments. Samples 121-754A-17X-CC to 121-754A-23N-CC contain Maestrichtian moderately preserved benthic foraminifers. Poorly to moderately preserved faunas were found in the Cretaceous recovery of Hole 754B. Sample 121-754B-22R-CC did not yield any benthic forms.

Neogene

Pleistocene

The fauna in Sample 121-754A-1H-CC is characterized by the dominance of *Globocassidulina crassa* and is also marked by low species diversity. Common species in this fauna are *Planulina wuellerstorfi* and *Cibicidoides kullenbergi. Pleurostomella, Bulimina*, and *Stilostomella* are uncommon.

Pliocene

Pliocene faunas are recognized in Samples 121-754A-2H-CC and 121-754A-3H-CC. The main elements of these faunas are represented by *Globocassidulina subglobosa, Uvigerina proboscidea*, and *P. wuellerstorfi*. Moreover, *Cibicidoides, Stilostomella*, and *Orthomorphina* are common and include many diversified forms. The Holocene distribution of these main elements associates the Pliocene faunas mainly with Indian Deep Water (Peterson, 1984) and subsequently, Indian Bottom Water (Corliss, 1979).

Miocene

Typical Miocene faunas cannot be determined without further quantitative analyses. However, three faunal associations are recognized in the core-catcher samples.

Samples 121-754A-4H-CC and 121-754A-5H-CC contain common *U. proboscidea* and *G. subglobosa* in association with *Gyroidina orbicularis* and *Pullenia bulloides*. Also included are species of *Orthomorphina, Stilostomella*, and *Pleurostomella*. Smaller size globocassidulinids are common throughout. These faunas are similar to those of the Pliocene, suggesting no drastic oceanographic changes from late Miocene to Pliocene.

In Samples 121-754A-6H-CC and 121-754A-7H-CC the faunas are characterized by a low diversity. The species *P. wuellerstorfi, Oridorsalis umbonatus*, and *Cibicidoides* spp. are dominant.

In Samples 121-754A-8H-CC to 121-754A-11H-CC the faunas are characterized by globocassidulinids and *Burseolina pacifica. B. pacifica*, however, may fall within the range of variation of *Cassidulina cuneata* depicted by Boltovskoy (1978), who noted *C. cuneata* as the dominant taxon in the upper Oligocene to lower Miocene. Common elements in these faunas include *O. umbonatus, G. orbicularis, Gyroidina soldani, P. wuellerstorfi, P. bulloides, Pullenia subcarinata, Cibicidoides* spp., *Lenticulina* spp., *Stilostomella lepidula*, and *Orthomorphina*. Agglutinated forms such as *Martinottiella scabra* and *Vulvulina* spp. are found in Samples 121-754A-9H-CC and 121-754A-10H-CC.

Uvigerinids are common only in the upper Miocene. Usually, uvigerinids in the Pacific are related to low-oxygen episodes (Woodruff, 1985).

Paleogene

Oligocene

The Oligocene faunas in Samples 121-754A-12H-CC and 121-754A-13X-CC are similar to those in the Miocene, with common occurrences of *Cibicidoides* spp., *Globocassidulina* spp., *Planulina* spp., and *P. bulloides*.

Eocene

Sample 121-754A-14X-CC yields poorly preserved benthic foraminifers. Somewhat better preserved forms are of deep-water elements such as *Hanzawaia cushmani, Osangularia mexicana, O. umbonatus, Bulimina tuxpomensis, Cibicidoides* spp., and *Nuttalides truempyi*, which are Eocene species. Along with

these taxa, typical shallow-water taxon *Amphistegina* and bryozoan fragments were also found. However, they are badly preserved, indicating the transportation. In addition to the aforementioned fauna, upper bathyal species *Cibicidina walli* was found in Sample 121-754B-2R-1, 24–26 cm. Based on the depth association of these taxa, an upper bathyal depth (200–600 m) is inferred for the late Eocene. The shallower elements of the assemblage are considered to have been transported.

Cretaceous (Maestrichtian)

In the interval from Samples 121-754A-17X-CC to 121-754A-23N-CC and 121-754B-5R-CC to 121-754B-25R-CC, Maestrichtian faunas consist of *Stensioina beccariiformis, Cibicidoides velascoensis, Gyroidinoides globosus, Bolivinoides draco, Coryphostoma incrassatus*, and *Gyroidina girardana*, along with *Lenticulina* spp., *Anomalinoides* spp., *Pullenia* spp., *Cibicidoides* spp., *Bulimina* spp., *Praebulimina* spp., *Gyroidina* spp., *Osangularia* spp., and *Ellipsoidella* spp. Among these, *S. beccariiformis* is dominant.

For the characteristic species examined, these faunas generally represent upper bathyal to abyssal depths (van Morkhoven et al., 1986). However, they are obtained from bioturbated as well as laminated sediments, suggesting a middle to lower bathyal environment. The low planktonic/benthic ratios (30/70–40/60) and a diversified benthic fauna without deep-water agglutinated forms support this interpretation.

Diatoms

All core-catcher samples from Holes 754A and 754B were examined. Diatoms and other siliceous microfossils (radiolarians, sponge spicules, silicoflagellates) are present at very few levels. In addition, these occurrences consist of rare and poorly preserved specimens.

Neogene

Rare Neogene specimens of *Thalassiothrix longissima, Actinocyclus ingens, Azpeitia tabularis*, and *Coscinodiscus* sp. were observed in Samples 121-754A-7H-CC and 121-754A-8H-CC.

Paleogene

No diatoms were observed in core-catcher samples of Paleogene sediments.

Cretaceous

Of the core-catcher samples examined, diatoms are only present in Sample 121-754B-25R-CC (Upper Cretaceous). Specimens belonging to the genera *Triceratium* and *Trinacria* were recognized. They are too poorly preserved to be identified at a specific level. Radiolarians, silicoflagellates, and sponge spicules are also present.

Samples 121-754B-14R-CC and 121-754A-19N-CC (Upper Cretaceous) contain rare radiolarian and sponge spicule fragments.

Environmental Interpretation

The calcareous nannofossil and planktonic foraminifer assemblages recovered from the samples of Holes 754A and 754B have an affinity with high-latitude, Southern Ocean faunas.

Within the Cretaceous, low planktonic/benthic ratios (30/70–40/60) and a diversified benthic fauna without deep-water agglutinated forms indicate deposition in the upper bathyal to abyssal range.

Within the middle Eocene, the dominance of *Stensioina beccariiformis, Cibicidoides velascoensis, Cibicidoides* spp., *Pullenia* spp., and *Osangularia* spp. indicates that deposition continued at upper bathyal to abyssal depths. Section 121-754B-2R-1, consisting of 36 cm of sands and gravels that testify to the depositional environment, is the only recovery of late Eocene age. (The upward-grading sequence in Core 121-754B-2R is only an artifact of settling in the core.)

Sample 121-754B-2R-1, 0–2 cm, is a fine-grained "sand" composed of 90% planktonic and <1% benthic foraminifers. Almost half of the planktonic foraminifer assemblage is reworked and represents Zone P14. The remainder of the assemblage contains fresh late Eocene age (P15 and P16) forms that show few signs of abrasion, thereby establishing the age of latest reworking. The absence of Oligocene and Neogene forms further indicates that reworking occurred during the Eocene. The high percentage of planktonic foraminifers relative to benthic foraminifers indicates hemipelagic/pelagic deposition. The benthic foraminifers are typically upper bathyal faunas. The faunas are moderately preserved, indicating little transportation. The nonforaminiferal 10% of the sand is composed of fine, equigranular, angular quartz fragments.

Sample 121-754B-2R-1, 24–26 cm, is a medium- to coarse-grained sand, composed predominantly of angular quartz fragments, 1–4 mm in diameter. Shell and bryozoan fragments and a small amount of microfossils, such as shallow-water benthic foraminifers (e.g., *Amphistegina*) and ostracodes, comprise 5% of the assemblage. All of the fossils, however, show a high degree of abrasion resulting from reworking or transportation. Within this sample are large (10–15-mm), fine-grained clasts that contain a completely reworked planktonic foraminifer assemblage of latest middle Eocene (P14) age, indicative of the youngest age of the unconformity.

The lowermost sands (gravels) in Sample 121-754B-2R-1, 36–38 cm, contain well-sorted, angular grains of chert/quartz from 3 to 10 mm in diameter. Both microfossils and macrofossils are absent.

This sequence of sediments indicates that the site remained below sea level, at upper bathyal depths or deeper, throughout the latest Eocene. The high percentage of reworked, fragmented material suggests that the sands are transported. The presence of late Eocene age high planktonic/benthic ratios infers that deposition took place in an open-ocean, pelagic environment. Evidence from the benthic foraminifer assemblages suggests this was probably at upper bathyal depths. The presence of poorly preserved corals, bryozoans, and typical shallow-water benthic foraminifers indicates transportation from shallower, calmer waters, presumably from the higher flanks to the south. The size of the coarsest grains suggests sediment transport in a high-energy regime. (The angularity of the fragments suggests little transportation from their source.) Therefore, this deposit was transported and deposited in an open-ocean environment. The age of the unconformity is placed at latest middle Eocene (Zone P14). The age of the youngest strata below the unconformity is middle Eocene (Zones P11 or CP13c). Uplift of the sediments below the unconformity took place between the time of Zones P11 and P14 (i.e., 3.5 to 7.5 m.y.). Sufficient energy to truncate the underlying dipping sequence was probably provided by the uplift of Broken Ridge to within wave base. There is no evidence to suggest that Broken Ridge at Site 754 was subaerially exposed during the Eocene.

Within the middle Oligocene to middle Miocene, the nature of the benthic foraminifer assemblages suggests that the sediments were deposited at bathyal depths. The lack of diversity among the discoasters also shows that cooler waters were prevalent at that time.

Within the upper Miocene and Pliocene, the high diversity of both plankton groups is attributed to productivity increases (Müller, 1977) or a period of warming.

PALEOMAGNETICS

Paleomagnetic analyses of sediments from Holes 754A and 754B include whole-core susceptibility and remanence measure-

ments and discrete sample demagnetization studies of key intervals. Susceptibilities were generally measured at a 10-cm spacing; however, volcanic ash-rich levels of the Maestrichtian sequence from Hole 754B (210–257 mbsf in lithologic Subunit IIB) were measured at a 5-cm spacing to facilitate study of possible cyclic patterns in the ash layers. In addition to alternating field (AF) treatment, 10 samples from Hole 754B were subjected to stepwise thermal demagnetization. Measurements were halted after the 500°C step because color changes and increased viscous behavior suggested significant alteration during heating.

Zijderveld diagrams indicate that the samples were commonly only partially demagnetized at peak fields of 20 to 40 mT or peak temperatures of 500°C. Demagnetization in higher peak alternating fields and at higher temperatures will be necessary to completely determine the magnetization pattern. The magnetostratigraphic interpretation, therefore, is preliminary and may be revised following more rigorous shorebased studies under more controlled conditions.

Susceptibility

The bulk susceptibility of the Pleistocene to upper Eocene oozes (lithologic Subunits IA and IB; Cores 121-754A-1H to 121-754A-14X) down to 80 mbsf is approximately 10^{-6} cgs units. A large part of this value is probably either paramagnetic or diamagnetic in origin (Fig. 10A). From 80 to about 110 mbsf the susceptibility values are higher (around 2×10^{-6} cgs units, with spikes up to 2×10^{-5} cgs units). The sandy ooze sequence at the level of the Oligocene/Eocene unconformity (Core 121-754A-14X; 124 mbsf) is clearly visible in the susceptibility log (Fig. 10A) as a sustained peak about 10^{-4} cgs units.

The susceptibility of the Maestrichtian sequence (lithologic Unit II) varies markedly with the lithology (Fig. 10B). The upper chalk sequence (Subunit IIA; 151.7–190.3 mbsf) shows a susceptibility base level of about 5×10^{-6} to 20×10^{-6} cgs units, with peaks up to 200×10^{-6} cgs units. Single measurement peaks at the tops of cores may be due to rust contamination. The ash-rich pelagic limestone sequence (upper part of Subunit IIB; 190–255 mbsf) shows a susceptibility base level of about 20×10^{-6} cgs units in the upper part of the sequence (Cores 121-754B-9R to 121-754B-12R; 190.3–228.9 mbsf) that increases to 200×10^{-6} cgs units in the lower part of the sequence (Core 121-754B-13R to the top of Core 121-754B-15R; 228.9–248.2 mbsf). Susceptibility spikes as high as 800×10^{-6} cgs units are clearly correlatable with the ash-rich layers. Further discussion of the susceptibility data and their implications for the history of Kerguelen hot-spot volcanism is in the "Tephra" and "Paleomagnetics" sections of the "Broken Ridge Summary" chapter (this volume).

A sudden drop in susceptibility to a base level of 10^{-6} to 5×10^{-6} cgs units at 254.7 mbsf correlates with the abrupt disappearance of ash layers and the appearance of chert fragments in the basal part of the lower Maestrichtian pelagic limestone sequence (basal part of Subunit IIB; 255–287 mbsf). Higher susceptibility base levels in the lower part of this sequence and a sporadic susceptibility peak as high as 30×10^{-6} to 140×10^{-6} cgs units suggest that sporadic and limited influx of ash preceded the major influx at 254.7 mbsf. This interpretation is supported by the presence of a pumice layer in Section 121-754B-17R-2 (270 mbsf), which correlates with a susceptibility peak of 140×10^{-6} cgs units.

The lowermost pelagic limestone/chert sequence (Subunit IIC; 287–354.7 mbsf) is characterized by low to very low susceptibility values (less than 3×10^{-6} cgs units) in the limestone and unmeasurable to negative susceptibility values for the cherts.

Remanence

Values of initial remanence of the Pleistocene to upper Eocene ooze sequence (Subunits IA and IB; 0–132 mbsf) generally ranged from 0.1 to 5 mA/m (Fig. 11). The basal part of the Oligocene sequence and the Oligocene/Eocene unconformity sequence of Subunit IB (112–132 mbsf) show an increase in the intensity of natural remanent magnetization (NRM) from 1 to about 10 mA/m.

NRM intensities of the upper Maestrichtian chalk sequence and the upper part of the pelagic limestone sequence (Subunit IIA and the top of Subunit IIB; 151.7–220 mbsf) range from 10^{-2} to 10 mA/m (Fig. 11B). The lower values of this range are associated with chert horizons. The middle part of the pelagic limestone sequence (lower part of Subunit IIB; 229–254.7 mbsf) shows a two order of magnitude increase in NRM intensity to values of 10 to 100 mA/m, which is followed by a sudden drop at 254.7 mbsf to 0.1 to 1.0 mA/m (Fig. 11B). This sharp drop in intensity (both in NRM and after 9-mT demagnetization) parallels the abrupt decrease in susceptibility values described previously. Both parameters record the abrupt disappearance of ash layers. The lower part of the pelagic limestone sequence (Subunit IIB; 255–287 mbsf) and the chert/pelagic limestone sequence (Subunit IIC; 287–354.7 mbsf) show low NRM intensities in the range 0.1 to 10 mA/m.

Magnetostratigraphy

The interpretation of magnetic polarity for the Pleistocene to upper Eocene sequence (Unit I; 0–131.7 mbsf) is at present limited to the uppermost 65 m. Below this depth, the polarity of the whole-core data is indeterminate. Systematic inclination variations within sections and discontinuities that coincide with section boundaries suggest that the magnetization was disturbed by the mechanical effects of core sectioning and splitting (Fig. 12). Although the remanent intensities are well above the noise level of the cryogenic magnetometer, this disturbance has obscured the polarity sufficiently to prohibit interpretation. It is unclear why this effect is not more pronounced in the more recent, fluid-rich sediments.

The polarity pattern for the upper 65-m sequence (to the top of Core 121-754A-8H) is based exclusively on whole-core demagnetization behavior and must therefore be considered speculative. Comparison of the polarity pattern in the upper 30 m with nannofossil datum levels ("Biostratigraphy" section, this chapter) suggests a correlation with the lowermost Matuyama Chron through Chron 5 (Berggren et al., 1985). In view of the lack of discrete sample confirmation and the poor correlation elsewhere between the inferred polarity of Hole 754A and the geomagnetic reversal time scale (GRTS), correlation to the GRTS is not warranted at this stage.

Whole-core and discrete sample measurements provide a reasonably complete magnetostratigraphic section for the sediments of Unit II (151.0–354.7 mbsf). Correlation of this reversal sequence with the GRTS, however, is uncertain for a number of reasons. Biostratigraphic ages for the section are diverse and provide only a limited basis for correlation. The basic polarity sequence inferred from whole-core measurements was confirmed by demagnetization of about 35 discrete samples (Fig. 13). However, the presence of several short polarity intervals (commonly at the tops and bottoms of cores) suggests that significant magnetic overprints or acquired remanent magnetization imparted during demagnetization may render parts of the sequence incorrect. Shorebased measurements at higher demagnetization levels may reveal such discrepancies, but for the present discussion we have assumed that the basic polarity pattern is correct.

Previous seismic, magnetic, and biostratigraphic results from Site 752 provide some age constraints for Site 754. In particular, seismic correlations ("Seismic Stratigraphy" section, this chapter) suggest that more than 40 m of overlap between Holes 752B and 754B is not probable. Biostratigraphic age assignments for the two holes are consistent with a significant overlap ("Biostra-

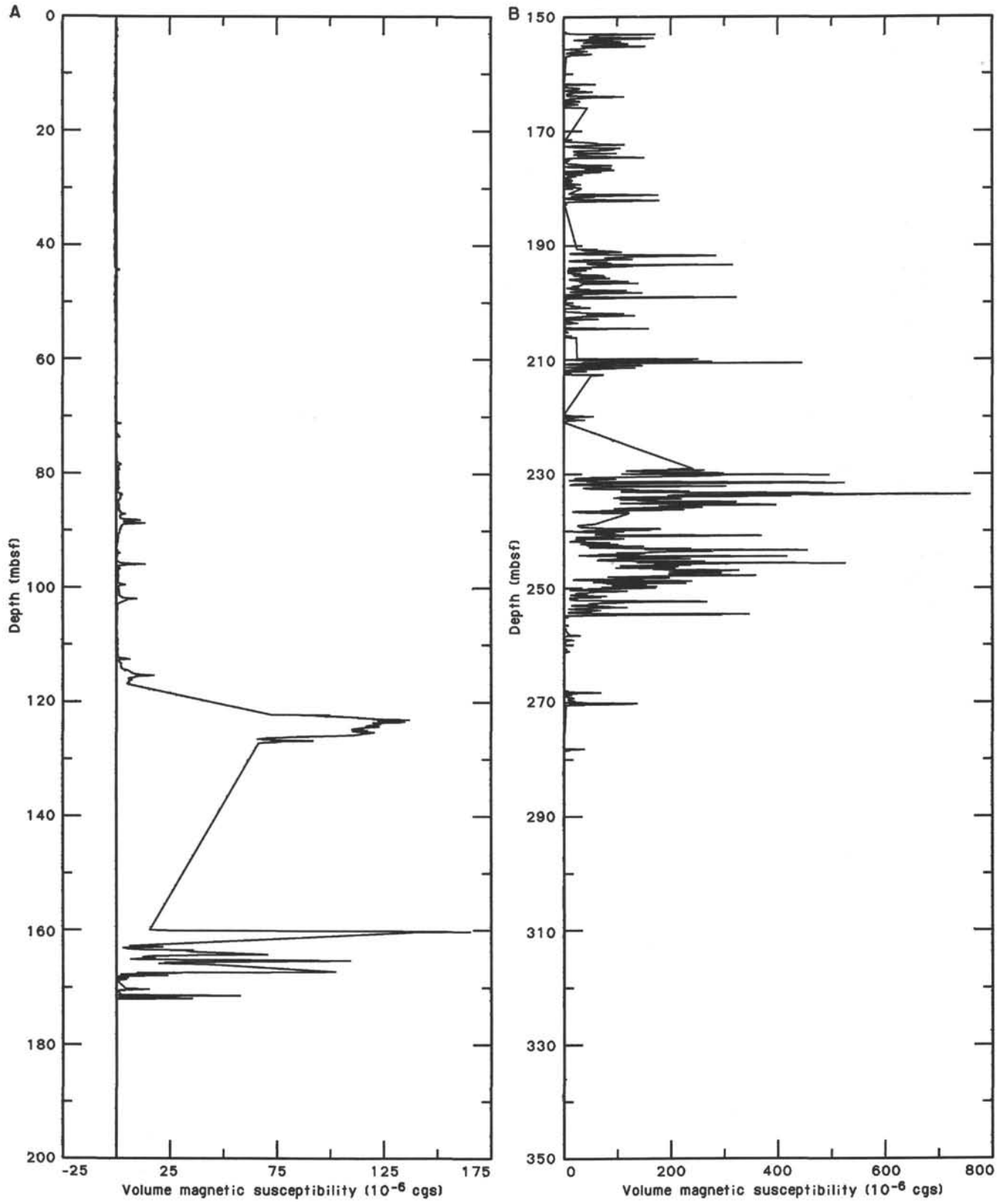

Figure 10. Volume magnetic susceptibility plots. **A.** Hole 754A. **B.** Hole 754B.

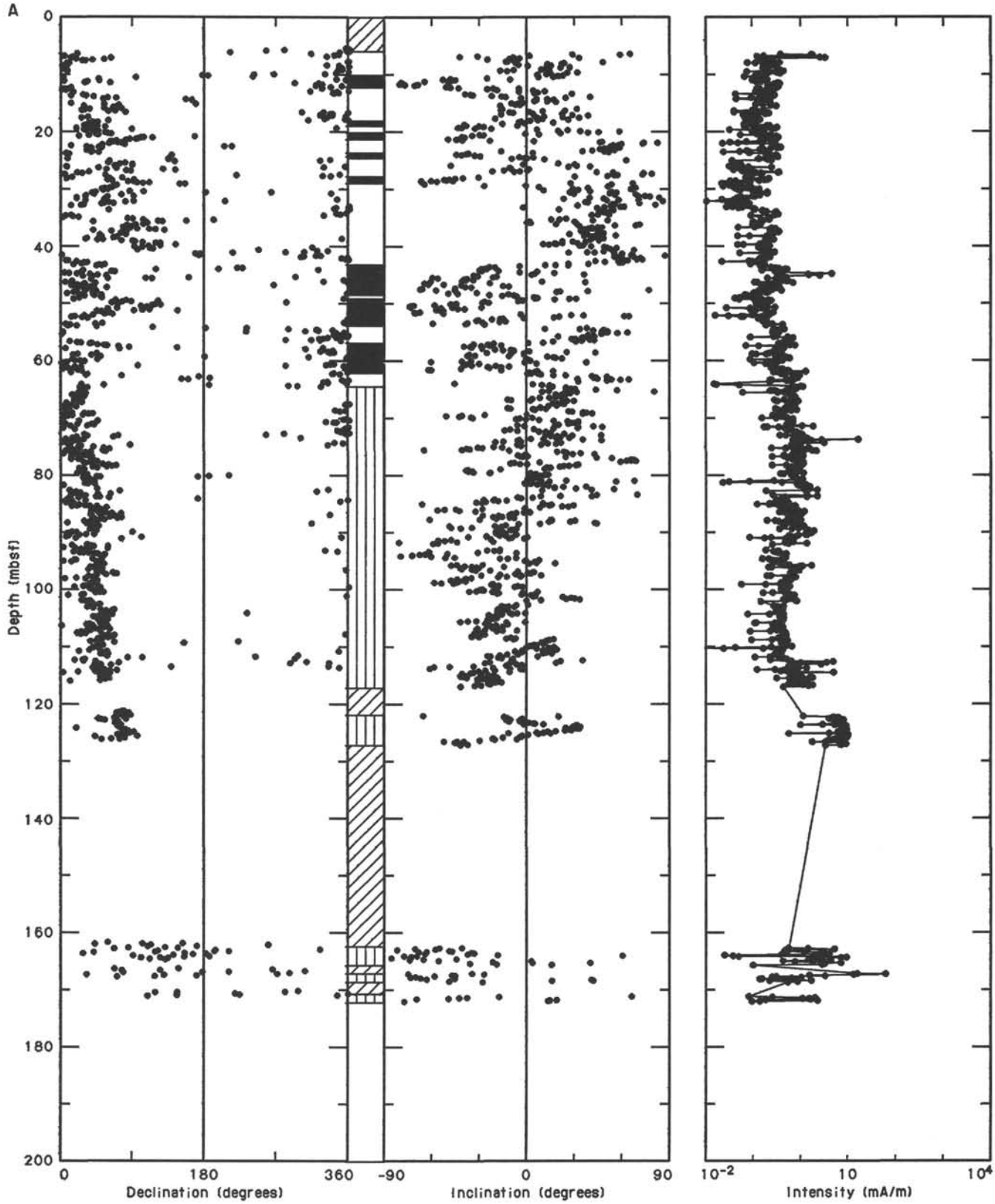

Figure 11. Declination, inclination, intensity, and interpretive polarity data for Holes 754A (A) and 754B (B) after AF demagnetization at 9 mT. Black (white) corresponds to normal (reversed) polarity. Diagonal (vertical) ruled pattern indicates no recovery (indeterminate polarity).

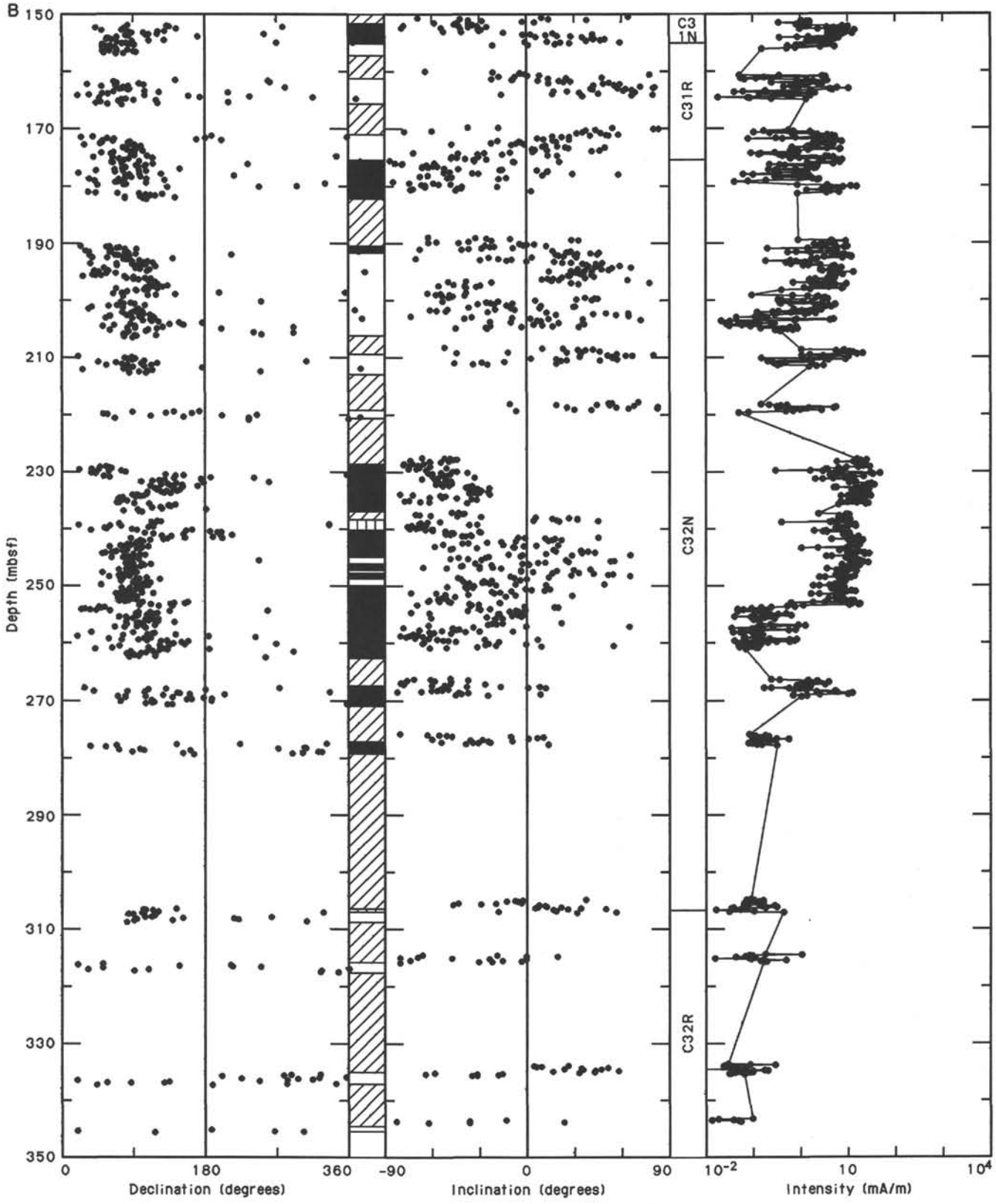

Figure 11 (continued).

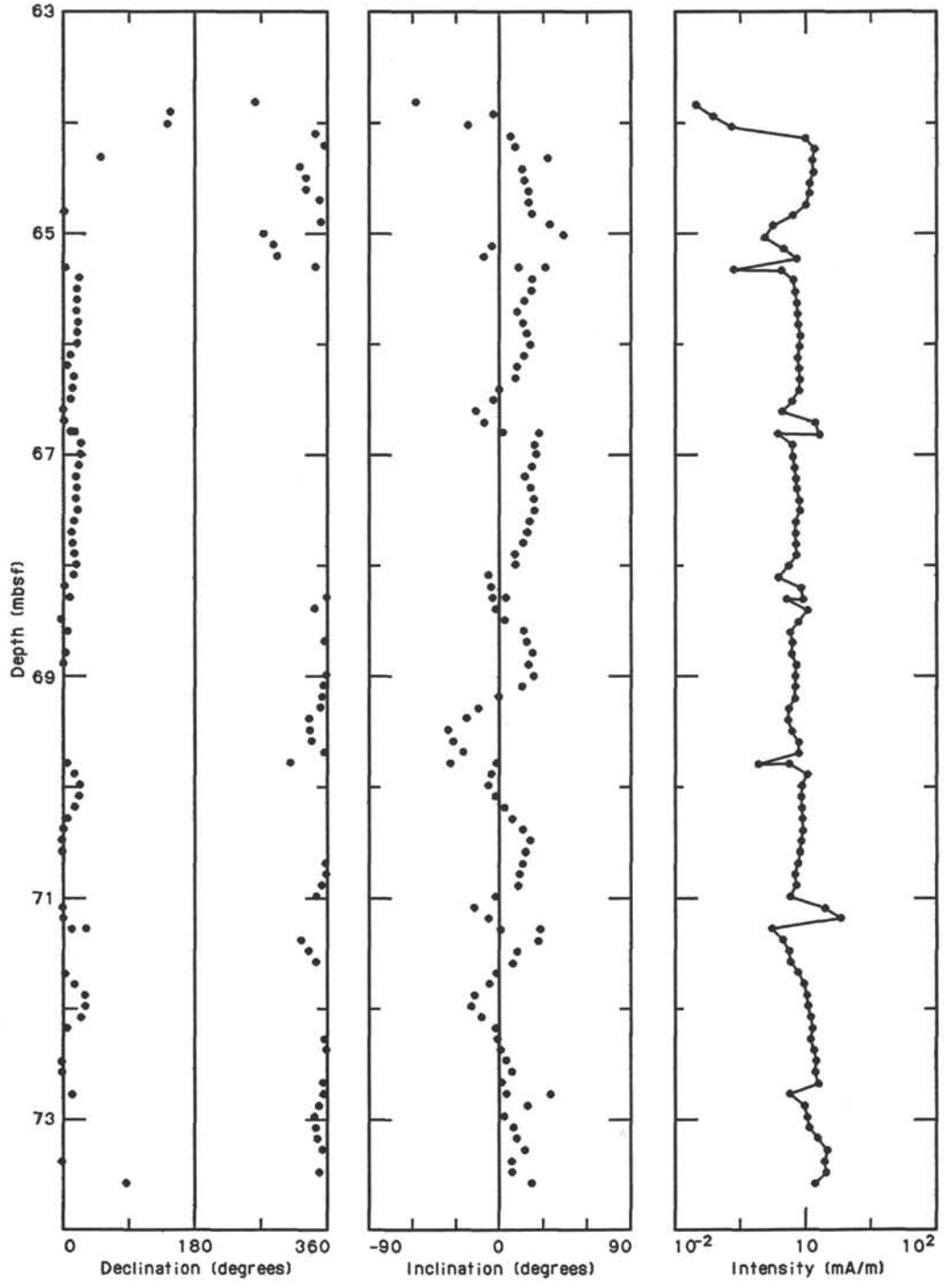

Figure 12. Declination, inclination, and intensity plot for Core 121-754A-8H. The systematic relationship between inclination variation and discontinuities at section breaks (low zones in the intensity data) indicates that the magnetization was affected by the mechanical disturbance of splitting and sectioning.

tigraphy" section). The *Abathomphalus mayaroensis* Zone occurs at the base of Hole 752B (Cores 121-752B-14R to 121-752B-19R) and in the top part of Hole 754B (Cores 121-754B-5R to 121-754B-7R). Calcareous nannofossil Zone CC26 is found in the lower section of Hole 752B and the uppermost part of Hole 754B. The base of Hole 754B is thought to lie within calcareous nannofossil Zone CC23, constraining the age to late Campanian or younger.

The biostratigraphic correlations between the two holes suggest a tentative correlation to the GRTS (Fig. 11B). The reversed to normal transition in Core 121-754B-5R (155 mbsf) is tied to the Chron C31R/C31N transition in Core 121-752B-15R (400 mbsf). The identification of Chron C31R at the base of Hole 752B is relatively well established, based on the position of the Cretaceous/Tertiary boundary within Chron C29R. Correlation of the remainder of the polarity sequence is constrained by the late Campanian age fauna at the base of Hole 754B. This correlation requires an overlap of approximately 40 m between the two holes. Variations in sedimentation rate from about 10 m/m.y. during Chron C31R to 127 m/m.y. during Chron

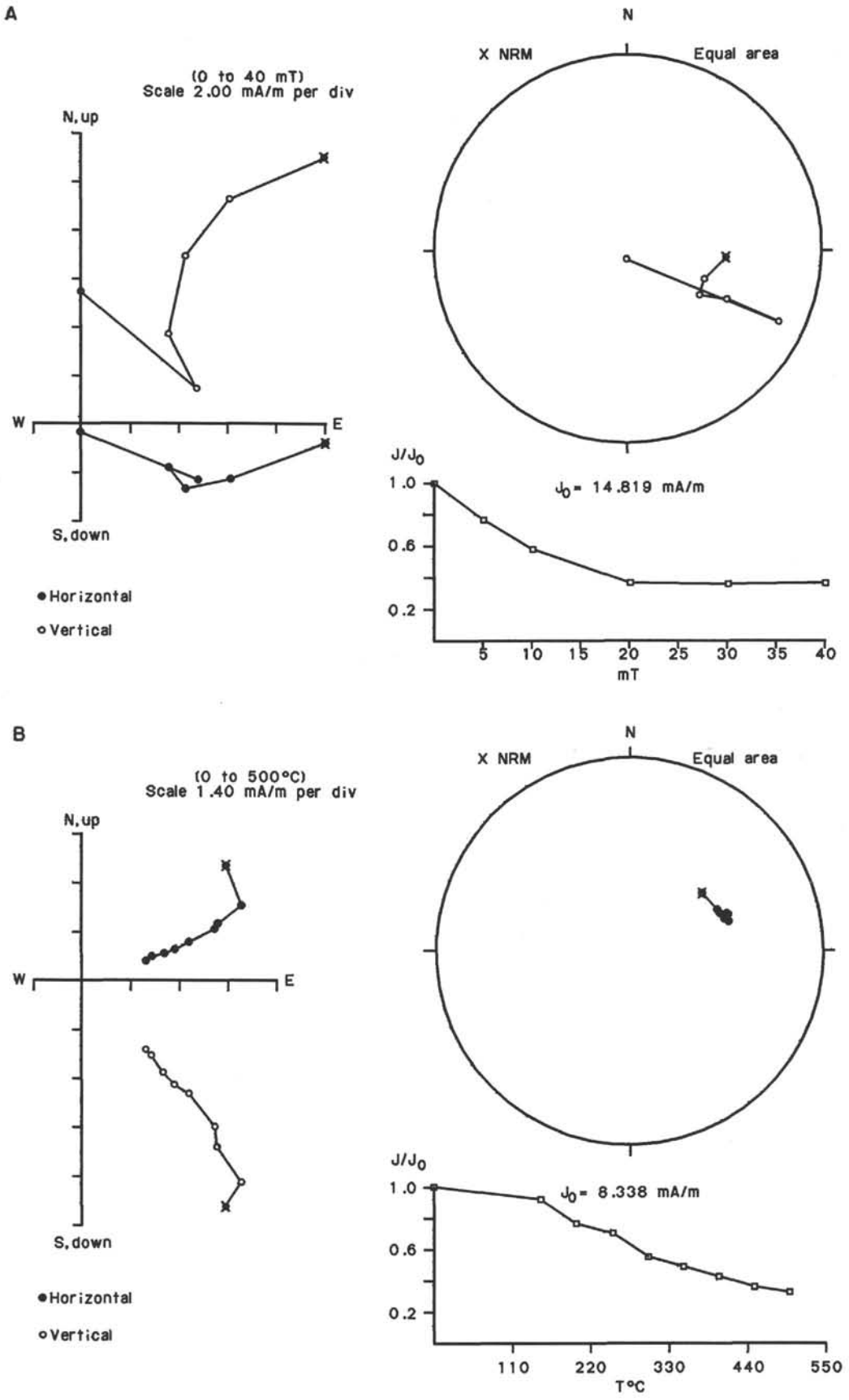

Figure 13. Zijderveld diagrams, equal-area stereographic projections, and intensity decay curves. **A.** Sediment showing significant anhysteretic remanent magnetization (ARM) acquisition during AF demagnetization above 20.0 mT (Sample 121-754B-5R-2, 18 cm). **B.** Sediment subjected to stepwise thermal demagnetization (Sample 121-754B-9R-4, 102 cm).

C32N-1r are also implied, with an overall sedimentation rate of approximately 60 m/m.y. during Chron C32.

Other schemes devised to satisfy the available data involve either large time gaps between the two holes or basal ages older than those suggested by the biostratigraphic zonations. Further clarification of the correlation between biostratigraphy and magnetostratigraphy at Site 754 is dependent on a more detailed biozonation.

INORGANIC GEOCHEMISTRY

The objectives of the inorganic geochemistry studies for Leg 121 are given in the "Inorganic Geochemistry" section of the "Site 752" chapter. A summary of the overall results for the Broken Ridge section of Leg 121 is in the "Broken Ridge Summary" chapter.

Results

The pore-water chemistry for Site 754 exhibits distinct differences from that of Sites 752 and 753 (see Table 5 and Fig. 14). The calcium and magnesium ion concentrations and alkalinity exhibit only slight changes with depth. The chloride ion concentration increases with depth, with the largest increase in the deepest sample. The sulfate ion concentration shows only slight change with depth except for a distinct decrease in the deepest sample.

Discussion

The large increase in calcium concentration with depth encountered at Sites 752 and 753 was not observed at Site 754. Although "ash" horizons are abundant in the sediments below the Eocene unconformity (see "Lithostratigraphy and Sedimentology" section, this chapter), no unaltered glass shards were observed. The ash in the carbonate sediment apparently has been completely altered to smectitic clays and possibly heulandite (Fig. 15 and Table 6), which could mean that ash alteration was essentially complete before the sediments above the unconformity were deposited. Therefore, no calcium signal would be generated by the underlying sediments. In addition, the degree to which the induration of the underlying sediments inhibits diffusion and other chemical reactions may be of greater importance in controlling the pore-water chemistry.

The chemical changes exhibited in the pore waters from the deepest sample interval at Site 754 are suspect. The double-charged ionic species decrease while chloride increases. A pressure in excess of 35,000 lb was used to get just 2 mL of sample from this 15-cm core section. Because the double-charged ions are more likely to be adsorbed than chloride, the observed changes might have been induced by the squeezing process.

ORGANIC GEOCHEMISTRY

Samples from Holes 754A and 754B were routinely studied to determine the amount and composition of hydrocarbon gases as well as carbonate carbon and total carbon contents. Rock-Eval analyses were performed to quantitatively and qualitatively study hydrocarbons and CO_2 released from the organic matter in the rocks upon combustion.

Samples for the analysis of headspace gas were taken from every third core at Site 754 (see "Organic Geochemistry" section, "Site 752" chapter). Carbonate carbon measurements were made of all physical-properties samples and a few organic geochemistry and headspace samples. Total carbon analyses were performed on most of the physical-properties samples and on the organic geochemistry and headspace samples also used for carbonate carbon analyses.

Gas Analyses

The amount of headspace methane in all of the samples did not significantly exceed the concentration in the laboratory air (i.e., 5 ppm). Other hydrocarbon gases were not detected. Thus, the total concentration of hydrocarbon gases is extremely low, like at the other Broken Ridge sites studied prior to drilling Site 754.

Organic Carbon

Total amounts of organic carbon are low in the sedimentary sequence drilled at Site 754 (Table 7). Most of the Neogene samples (0–107 mbsf) contain no organic matter. There are, however, a few samples with up to 0.4% organic carbon. Organic carbon values at Site 752 have a similar distribution.

At Site 754, the highest percentage of organic carbon was found at 126 mbsf, where carbonate percentages are lower than in the overlying Tertiary sediments (Table 7 and Fig. 16). A negative correlation of organic carbon with carbonate carbon amounts was observed on previous ODP legs (see "Organic Geochemistry" section, "Site 722" chapter; Shipboard Scientific Party, 1989). This negative correlation may be explained by an admixture of terrestrial organic and silicious debris with the predominant marine calcitic material. The marine organic matter (e.g., organic parts of foraminifers or nannoplankton) is chemically highly labile and, therefore, rarely preserved in the sediments.

Sediments of the upper Maestrichtian (150–220 mbsf) and upper part of the lower Maestrichtian (220–290 mbsf) are similar to those of the Neogene in that they contain practically no organic matter. The lowermost Maestrichtian (290–350 mbsf; Fig. 16) consistently contains some organic material, but the percentages do not significantly exceed 0.4%.

Quality of Organic Matter

By measuring and recording the release of hydrocarbons and CO_2 during anaerobic heating (pyrolysis), hydrogen and oxygen contents of the organic matter can be calculated. Thus, pyrolysis experiments give an indication of the bulk composition of organic materials. Factors such as the composition of the mineral matrix, however, also effect the results of pyrolysis analyses

Table 5. Interstitial-water geochemistry data, Site 754.

Core, section, interval (cm)	Depth (mbsf)	Volume (mL)	pH	Alkalinity (mmol/L)	Salinity (g/kg)	Magnesium (mmol/L)	Calcium (mmol/L)	Chloride (mmol/L)	Sulfate (mmol/L)	Mg^{2+}/Ca^{2+}
121-754A-										
1H-3, 145–150	4.45	35	7.60	2.730	35.5	52.80	11.40	545.00	29.60	4.63
3H-4, 145–150	21.65	35	7.60	2.670	36.0	51.90	13.50	546.00	29.20	3.84
6H-5, 145–150	51.95	28	7.60	2.300	35.5	50.80	14.00	540.00	28.70	3.63
9H-5, 145–150	80.95	37	7.50	2.350	35.5	51.20	13.80	549.00	28.80	3.71
12H-5, 145–150	110.05	45	7.70	2.390	35.5	51.50	13.80	544.00	29.20	3.73
121-754B-										
5R-2, 140–150	154.60	2			36.0	45.50	12.10	576.00	27.40	3.76

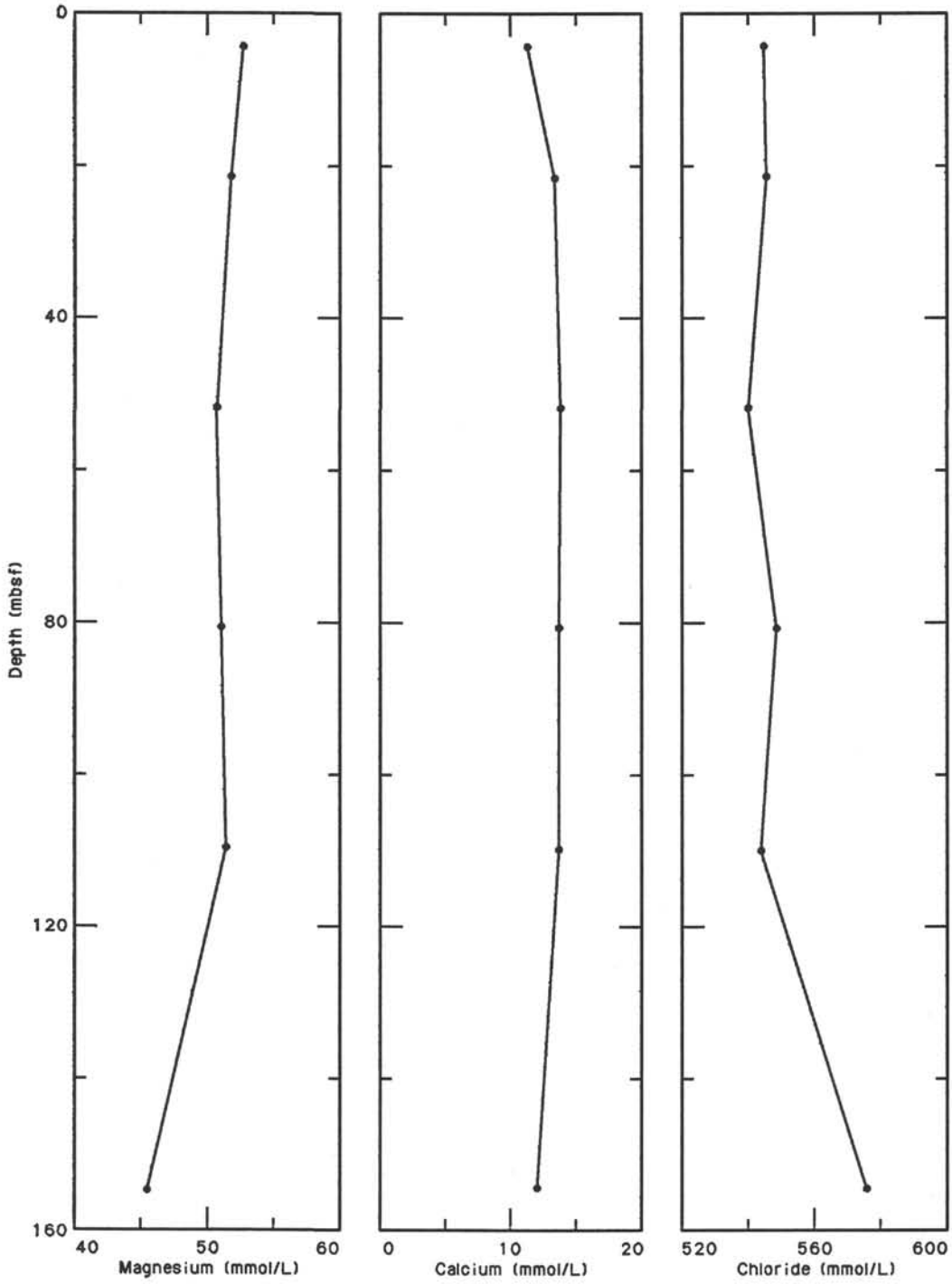

Figure 14. Magnesium, calcium, and chloride interstitial-water concentrations, Site 754.

(e.g., Katz, 1982). Experiments revealed that smectite may have a catalytic effect on the production of hydrocarbons. On the other hand, minerals can also cohesively bind a certain amount of the generated hydrocarbons that will not be recorded at the detector. The latter effect is of great importance if organic carbon and hydrocarbon concentrations in the samples are low. Because of the small quantity of organic material in the sediments from Site 754, the following data on the release of hydrocarbons from the organic matter (Table 8 and Figs. 17 and 18) are regarded as rough estimates.

The Neogene samples from Site 754 possess no hydrocarbon generation potential at all, and the sporadic occurrences of organic matter must be interpreted as inert relics of strongly degraded organic material. This supports our observations on the poor quality of the organic matter in the Neogene samples from Site 752.

The combined organic geochemical and interstitial-water data indicate that degradation of organic matter occurred in the oxic, uppermost part of the sedimentary column sometime in the past. Organic matter degradation in the sulfate-reduction

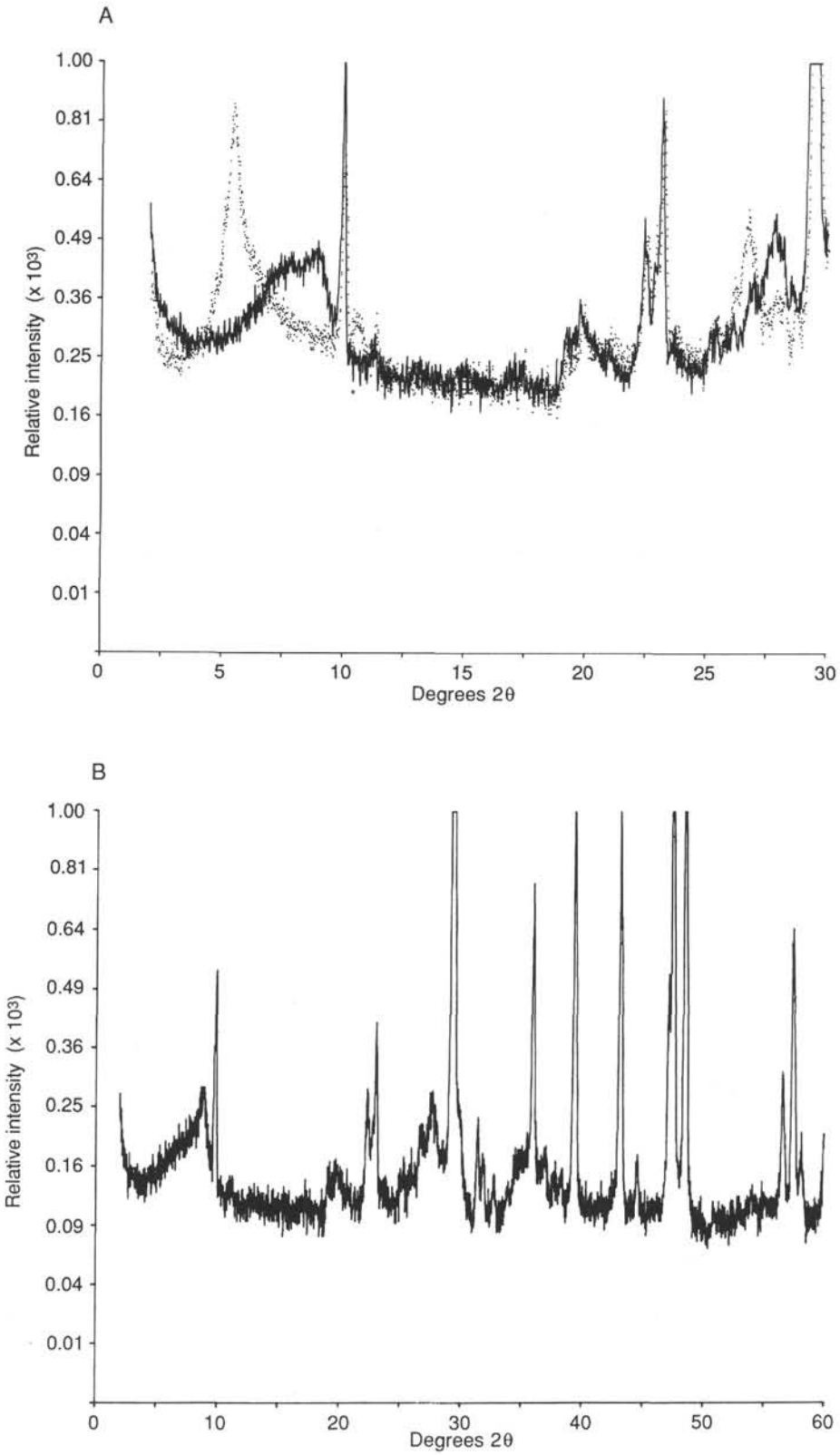

Figure 15. X-ray-diffraction patterns of Sample 121-754A-21N-1, 79–82 cm. **A.** Bulk-sediment (solid line) and glycolated (dots) plots. **B.** Bulk-sediment scan of 0° to 60° 2θ.

Table 6. Site 754 X-ray-diffraction patterns.

Core, section, interval (cm)	Shipboard database file number	Minerals identified
121-754A-		
21N-1, 79–81	008UBN.RD 016UBG.RD 040UBN.RD	Calcite, smectite, heulandite
121-754B-		
15R-3, 96–98	007UBN.RD 015UBG.RD	Smectite, calcite, heulandite

zone would have led to a decrease in percent sulfate with depth in the interstitial waters (see Lawrence, 1973), which was not observed at Site 754 (see "Inorganic Geochemistry" section, this chapter). Furthermore, fermentation processes that usually destroy organic material below the sulfate-reduction zone would have increased the concentration of methane. At Site 754, methane concentrations are, however, so low that methane generation by fermentation was probably insignificant.

The organic matter in samples from the lower part of the lowermost Maestrichtian has a fairly good hydrocarbon generation potential. We cannot exclude the preservation of at least some marine organic matter in these sediments. Advanced methods (i.e., incident light fluorescence microscopy and gas chromatography–mass spectrometry) are necessary to obtain better indications as to the amounts of terrestrial and marine organic material in these sediments.

Carbonate Carbon

According to the sedimentologic description from the smear slides, the bulk of the carbonate in the sediments from Broken Ridge is derived from either planktonic or benthic marine fauna and flora. Therefore, the carbonate percentages (Table 7) are a good measure of the calcitic fossil accumulation in these sediments. Neogene sediments at Site 754 consist almost entirely of calcite (Fig. 16), with calcite percentages at about 96%.

Only a few carbonate values were measured in the Oligocene to upper Eocene interval from 120 to 130 mbsf (Table 7 and Fig. 16) because of the poor core recovery. The carbonate values are lower than in the Neogene and decrease with depth. A more detailed sampling of this interval is necessary to explain the significance of this observation. A better data set for the older Tertiary section was obtained at Site 752 (see "Organic Geochemistry" section, "Site 752" chapter).

In the Cretaceous sediments, carbonate concentrations vary between 0% and 90% (Table 7 and Fig. 16). Mean values are about 70% in the upper Maestrichtian and about 60% in the lower Maestrichtian. Because the amount of recognizable siliceous fossils (diatoms, radiolarians, etc.) is low in the Cretaceous, these values are probably representative of biogenic sedimentary material.

The release of carbonate carbon by reaction with hydrochloric acid was unusually slow in some samples from the lowermost Maestrichtian. X-ray-diffraction measurements prove that a small part of the carbonate in samples from this interval is composed of dolomite. Thus, the calculated weight percentages of carbonate are actually slightly lower in the lowermost Maestrichtian (usually by less than 1%). Dolomite constitutes about 40% of the total carbonate in one sample from Core 121-754B-22R. In this sample we have to assume a value 2.5% lower than that presented in Table 7 (i.e., about 60%, instead of 62.7%).

Table 7. Percentages of total carbon, inorganic (carbonate) carbon, organic carbon, and calcium carbonate in samples from Holes 754A and 754B.

Core, section, interval (cm)	Depth (mbsf)	Total carbon (%)	Inorganic carbon (%)	Organic carbon (%)	Calcium carbonate (%)
121-754A-					
1H-2, 80–82	2.30	11.40	11.47	0.00	95.6
1H-4, 80–82	5.30	11.71	11.32	0.39	94.3
2H-2, 80–85	8.40		11.55		96.2
2H-4, 80–85	11.40	11.63	11.64	0.00	97.0
2H-6, 80–85	14.40		11.53		96.0
3H-2, 85–87	18.05		11.63		96.9
3H-4, 85–87	21.05	11.55	11.49	0.06	95.7
3H-6, 85–87	24.05		11.66		97.1
4H-2, 85–87	27.65		11.54		96.1
4H-4, 85–87	30.65	11.52	11.53	0.00	96.0
4H-6, 85–87	33.65		11.55		96.2
5H-2, 85–86	37.25		11.59		96.5
5H-4, 85–86	40.25	11.29	11.38	0.00	94.8
5H-6, 85–86	43.25		11.56		96.3
6H-2, 85–87	46.85		11.74		97.8
6H-4, 85–87	49.85	11.70	11.67	0.03	97.2
6H-6, 85–87	52.85		11.59		96.5
7H-2, 85–87	56.45				
7H-4, 85–87	59.45	11.74	11.54	0.20	96.1
7H-6, 85–87	62.45		11.62		96.8
8H-2, 85–87	66.15		11.61		96.7
8H-4, 85–87	69.15	11.39	11.39	0.00	94.9
8H-6, 85–87	72.15	11.61	11.60	0.01	96.6
9H-2, 85–87	75.85		11.36		94.6
9H-4, 85–87	78.85		11.40		95.0
9H-6, 85–87	81.85		11.58		96.5
10H-2, 80–82	85.50	11.30	11.43	0.00	95.2
10H-4, 80–82	88.50		11.15		92.9
10H-6, 80–82	91.50		11.57		96.4
11H-2, 80–82	95.20		11.52		96.0
11H-4, 85–87	98.25	11.49	11.55	0.00	96.2
11H-6, 80–82	101.20		11.50		95.8
12H-3, 80–82	106.40	11.58	11.54	0.04	96.1
12H-5, 80–82	109.40		11.55		96.2
13X-1, 120–122	113.50		11.28		94.0
13X-2, 120–122	115.00	11.18	11.20	0.00	93.3
13X-CC, 25	117.21		10.64		88.6
14X-1, 90–92	122.90		9.16		76.3
14X-2, 90–92	124.40	8.57	8.49	0.08	70.7
14X-4, 20–22	126.70	8.24	7.70	0.54	64.1
19N-1, 17–19	159.97	10.16	10.05	0.11	83.7
19N-1, 54–55	160.34	7.93	7.78	0.15	64.8
19N-CC, 0–1	160.35	9.28	9.07	0.21	75.6
20N-1, 82–84	163.42		11.01		91.7
20N-2, 89–91	164.99	9.80	9.79	0.01	81.6
20N-2, 120–122	165.30		3.37		28.1
21N-1, 21–23	167.31	10.19	10.14	0.05	84.5
21N-1, 79–81	167.89		6.18		51.5
21N-1, 133–135	168.43		11.23		93.6
22N-1, 7–9	170.17	10.98	10.93	0.05	91.1
23N-1, 64–65	171.74	0.13	0.06	0.07	0.5
23N-1, 70–72	171.80		3.00		25.0
121-754B-					
5R-1, 65–67	152.35	9.92	9.90	0.02	82.5
5R-2, 12–14	153.32	5.14	5.34	0.00	44.5
5R-3, 66–68	155.36	11.12	11.07	0.05	92.2
6R-2, 85–87	163.65	7.97	7.99	0.00	66.6
6R-3, 38–40	164.68		11.22		93.5
6R-CC, 1–2	165.70	1.69	1.68	0.01	14.0
[a]7R-1, 81–84	171.81	0.28	0.21	0.07	1.8
7R-3, 29–31	174.29		7.11		59.2
7R-5, 25–27	177.25		10.87		90.6
8R-1, 137–138	181.97	5.81	5.70	0.11	47.5
9R-2, 81–82	192.61		6.16		51.3
9R-4, 81–83	195.61	9.50	9.54	0.00	79.5
9R-6, 82–84	198.62		5.32		44.3
10R-2, 82–83	202.32	9.62	9.51	0.11	79.2
10R-4, 82–83	205.32		9.58		79.8
11R-2, 81–83	211.91	10.43	10.42	0.01	86.8
12R-1, 4–6	219.24	11.03	11.05	0.00	92.1

Table 7. (continued).

Core, section, interval (cm)	Depth (mbsf)	Total carbon (%)	Inorganic carbon (%)	Organic carbon (%)	Calcium carbonate (%)
121-754B- (Cont.)					
13R-2, 92–94	230.28		7.67		63.9
13R-4, 26–28	232.62		7.94		66.1
13R-6, 61–63	235.97	7.73	7.72	0.01	64.3
14R-3, 79–81	242.19	8.39	8.25	0.14	68.7
14R-4, 38–40	243.28	4.15	4.08	0.07	34.0
14R-6, 87–89	246.77		5.24		43.7
15R-2, 92–94	250.62	9.33	9.29	0.04	77.4
15R-4, 87–89	253.57	3.61	3.39	0.22	28.2
15R-6, 113–115	256.83		10.10		84.1
16R-1, 110–112	259.00	8.88	8.88	0.00	74.0
16R-2, 59–61	259.99		8.63		71.9
17R-2, 76–77	269.86	4.74	4.72	0.02	39.3
18R-1, 62–63	277.92	8.46	8.45	0.01	70.4
19R-1, 92–93	287.92	7.04	7.05	0.00	58.7
20R-1, 44–46	297.14	4.12	3.84	0.28	32.0
21R-1, 76–77	307.06	3.13	3.00	0.13	25.0
22R-1, 21–22	316.21	7.83	7.53	0.30	62.7
22R-1, 133–134	317.33	11.27	11.33	0.00	94.4
24R-2, 11–13	336.91	9.11	8.69	0.42	72.4
25R-1, 18–20	345.18	9.80	9.59	0.21	79.9

[a] Part of a chert layer.

PHYSICAL PROPERTIES

Site 754 consists of Holes 754A and 754B. Hole 754A was cored using the APC to 112.3 mbsf, XCB to 159.8 mbsf, and NCB to 172.1 mbsf. Hole 754B was cored using the RCB from 122.7 to 354.7 mbsf. Hole 754A was the first hole where the Navidrill technique was routinely applied to core sediments. Cores 121-754A-19N to 121-754A-23N were successfully obtained by the Navidrill, with a recovery of 77.9%. These five cores were less disturbed than those recovered with the RCB.

The lithology of Site 754 changes from soft calcareous ooze (Unit I) to consolidated sedimentary rocks of chalk, limestone, and chert intercalated with ash layers (Unit II), with an unconformity between the two lithologic units (see "Lithostratigraphy and Sedimentology" section). The age of Unit I is Pleistocene to late Eocene, and that of Unit II is late to early Maestrichtian (?Campanian). It is unfortunate that the section immediately above the upper Eocene/upper Maestrichtian unconformity (128–150 mbsf) was poorly sampled, because the unconformity is a zone of drastic change for most of the physical-properties parameters.

Methods

Samples from this site were measured for index properties, compressional-wave velocity, vane shear strength, electrical re-

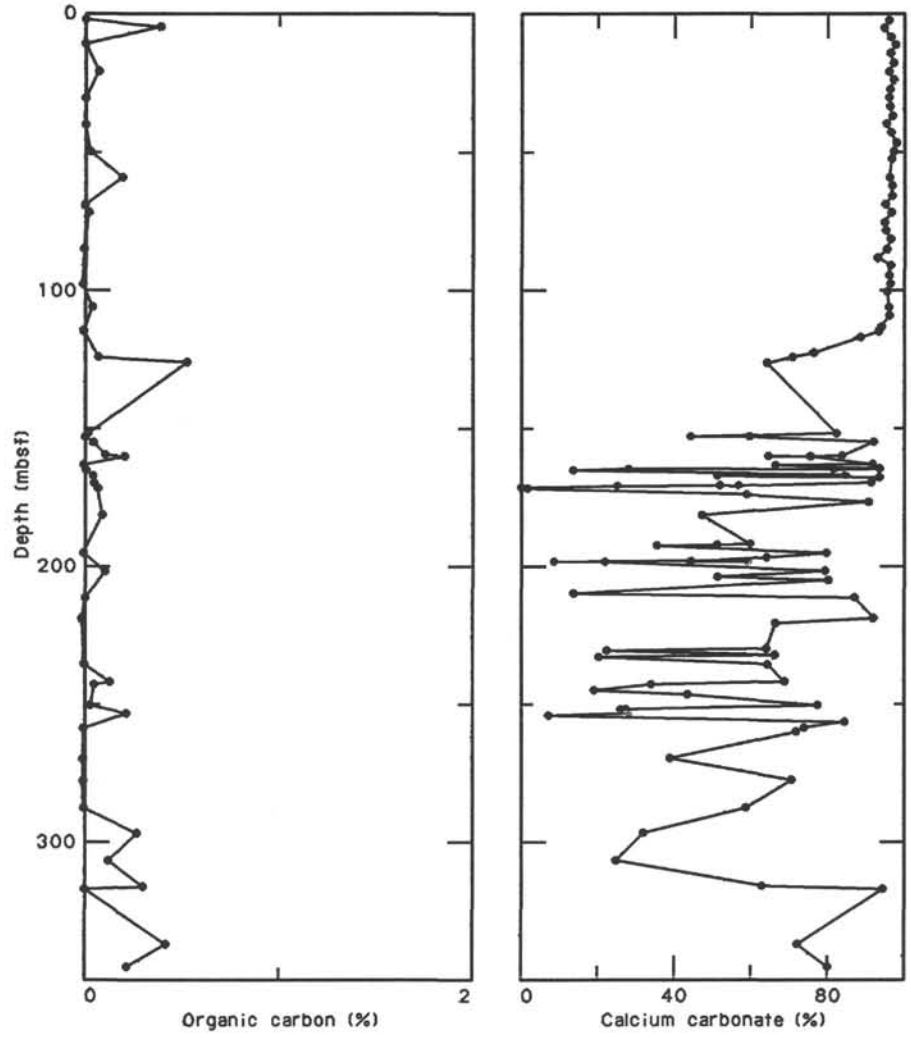

Figure 16. Organic carbon and calcium carbonate content of samples from Site 754.

Table 8. Results of Rock-Eval pyrolysis of samples from Site 754.

Core, section, interval (cm)	Depth (mbsf)	Weight (mg)	T_{max} (°C)	S1 (mg HC/g rock)	S2 (mg HC/g rock)	S3 (mg CO_2/g rock)	Productivity index	S2/S3	Pyrolysized carbon (0.083 [S1 + S2])	Total organic carbon (wt%)	Hydrogen index (mg HC/g C_{org})
121-754A-											
1H-4, 80–82	5.30	105.5	428	0.14	0.00	0.54	1.00	0.00	0.01	0.39	0
10H-4, 80–82	88.50	102.1	329	0.08	0.07	0.48	0.57	0.14	0.01	0.54	12
121-754B-											
22R-1, 21–22	316.21	103.4	434	0.14	0.73	0.47	0.16	1.55	0.07	0.30	243
24R-2, 11–13	336.91	99.5	420	0.25	0.78	0.69	0.25	1.13	0.08	0.42	185
25R-1, 18–20	345.18	108.5	414	0.11	0.36	0.28	0.24	1.28	0.03	0.21	171

sistivity, and thermal conductivity. The description of these methods is found in the "Explanatory Notes" chapter.

We began three-dimensional measurements of compressional-wave sonic velocity on laboratory samples at Hole 754B. Many of the cubic samples for paleomagnetic objectives, as well as the original samples for index properties, were used for three-dimensional velocity measurements. Special thanks are due to the paleomagnetists for allowing the measurements of sonic velocity in advance of their paleomagnetic measurements.

Results

Index Properties

Water content (expressed as water weight relative to wet sample weight), porosity, bulk density, dry-bulk density, and grain (or matrix) density of the samples from Holes 754A and 754B are listed in Table 9 and plotted relative to depth in Figure 19. GRAPE bulk densities show quite good coincidence with the wet-bulk densities of the index properties measured from the laboratory samples.

Three units are identified in terms of physical properties: units A (0–132 mbsf), B (152–196 mbsf), and C (196–345 mbsf). The boundary between units A and B is within a sampling gap resulting from poor recovery, and it coincides with the Eocene/Maestrichtian unconformity zone. A drastic change in bulk density, water content, porosity, and dry-bulk density is observed across the interval containing the unconformity (132–152 mbsf), whereas the grain density does not show appreciable change. Bulk density increases from about 1.8 to 2.4 g/cm^3 and water content decreases from about 40% to 20% at this boundary. The boundary between units B and C is recognized by the downhole decrease of water content, from 20% to 10% at 196 mbsf. A drastic increase of bulk density in the lowermost part of unit C is probably caused by intercalated chert layers. If the high values of the cherts are neglected, the values of bulk density above and below the unit B/unit C boundary are similar.

The lack of change in grain density across the unconformity horizon, regardless of the change of the other index properties, suggests that the differences between units A and B reflect degrees of lithification instead of major differences in the sediment constituents.

Unit A shows only slight variation in index-property values. Water content decreases from about 45% at the shallowest part to about 40% at 125 mbsf, just above the unconformity, and porosity decreases from 70% to 60%. Bulk density increases from 1.5 to 1.8 g/cm^3 over the same depth range, and dry-bulk density increases from 0.8 to 1.2 g/cm^3. Unit A, however, can be divided into four subunits based on slight variations in the index properties; these are labeled subunits A1, A2, A3, and A4 in order of increasing depth. Subunit A1, the upper 10 m of the section, is characterized by lower density, higher water content, and a rather high gradient of each physical-property parameter. Subunit A1 constitutes a boundary layer between the water column and the sediments below. Subunits A2 and A3 extend from 10 to 50 and 50 to 92 mbsf, respectively. Although both subunits are characterized by constant values of index properties, subunit A2 has lower bulk density (< 1.70 g/cm^3) and higher water content (> 40%), and subunit A3 has higher bulk density (> 1.70 g/cm^3) and lower water content (< 40%). Subunit A4, the lowermost part of unit A (92–124 mbsf), is characterized by marked gradients with depth as the bulk density increases and water content decreases. This subunit can also be considered a boundary layer between soft and hard lithologies.

The index properties of unit B show more variation than those of unit A. The bulk density clearly decreases with depth from about 2.5 g/cm^3 at 150 mbsf to 2.1 g/cm^3 at 315 mbsf. The rate of decrease of bulk density with depth is 0.24 ± 0.05 g/cm^3 per 100 m. Because the porosity does not show a corresponding increase with depth and the grain density also decreases with depth, this variation may be due to a compositional change of the matrix material. Variation in the amount of volcanic ash with depth may influence both the bulk and grain densities.

Compressional-Wave Velocity

Velocity data obtained from laboratory samples are listed in Table 10 and displayed in Figure 19 with the *P*-wave-logger data. Compressional-wave velocity anisotropy was examined by measuring velocities in three directions of propagation. These results are listed in Table 11 and displayed in Figure 20. Only velocity A, corresponding to the vertical direction, measured in the unit B sediments, is displayed in Figure 19. The acoustic impedance log in Figure 19 is computed from GRAPE and *P*-wave-logger data for unit A and from bulk-density and compressional-wave velocity data (velocity A) for units B and C.

P-wave-logger velocities range between 1500 and 1600 m/s and are quite constant throughout subunits A2, A3, and A4. Compressional-wave velocities of subunit A1 fluctuate from 1500 to 1600 m/s. Velocities increase abruptly from 1600 to about 2800 m/s across the unconformity separating units A and B, but velocities do not show much difference between units B and C. The mean velocity of unit B is 2800 ± 420 m/s, and that of unit C is 2860 ± 610 m/s. The velocity variations in units B and C (Fig. 19) and the large standard deviation of the value suggest some intercalated nature for the lithology. The laminated bedding character of sediments in units B and C may cause the variation of the velocity in the units. Regression analysis, however, shows a slight increase of the velocity with depth, with a gradient of 116 m/s/100 m through units B and C. The presence of ash in the sediments below 210 mbsf is largely responsible for relatively slower velocities. Similar responses are observed in the logging results (see "Geophysical Well Logging" section, this chapter, and the "Broken Ridge Summary" chapter).

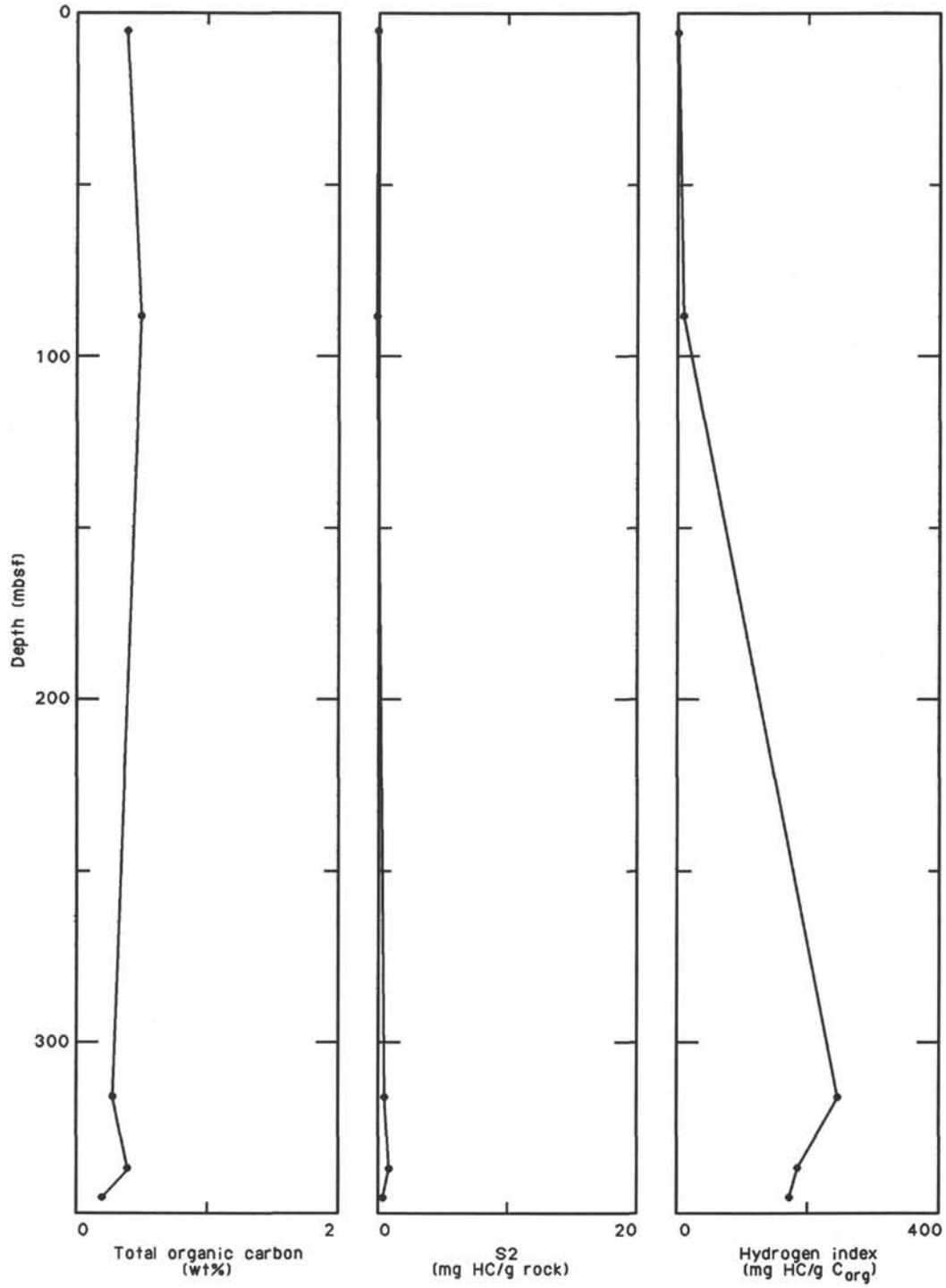

Figure 17. Total organic carbon content, S2, and hydrogen index values of selected samples from Site 754.

There is significant velocity anisotropy between the velocity of vertical propagation (velocity A) and that of horizontal propagation (velocities B and C). Velocity A is slower than either velocity B or C, in general, by about 9% (Table 11). The type of anisotropy suggests that refraction velocities obtained from sonobuoy refraction seismics may be higher than the vertical velocity used for seismic reflection. This anisotropy should be considered in estimating the sediment thickness from seismic-reflection records at Broken Ridge.

The anisotropy between horizontal velocities B and C in units B and C is 3% for the average of absolute values, which falls within the error range of the measurements. Careful measurements within a short sampling interval to avoid unmatched orientation of samples is necessary in the analysis of horizontal velocity anisotropy.

The acoustic impedance log matches the division of physical-properties units. Unit A has a much lower impedance than units B and C (Fig. 19). The impedance in unit C decreases

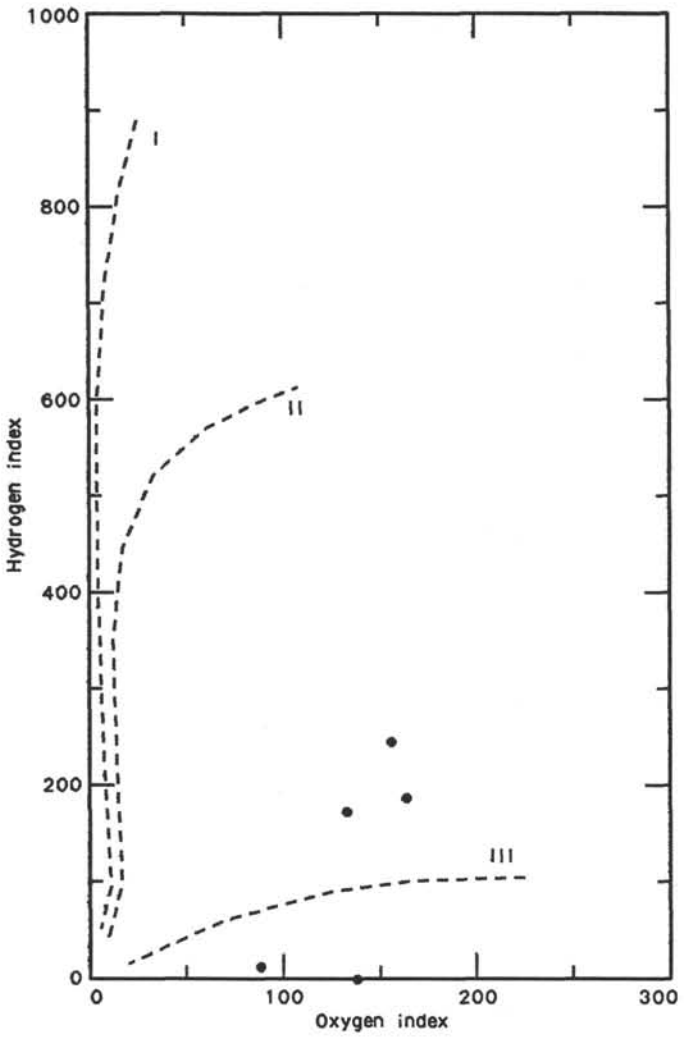

Figure 18. Hydrogen vs. oxygen indices for samples from Site 754. A good petroleum source rock shows high hydrogen and low oxygen indices at immature stages (type I or II source rocks). Terrestrial-derived organic matter from higher land plants is generally oxygen rich and relatively poor in hydrogen. The Neogene samples from Broken Ridge seem to contain inert, extremely degraded organic matter, and those from the Cretaceous possess a small potential for hydrocarbon generation.

slightly with depth, as does the bulk density, and returns to higher values in the lowermost part. Impedance contrasts at 132 and 316 mbsf are probable sources for acoustic reflectors. The detailed correlation of acoustic impedance and the seismic profile record is described in the "Seismic Stratigraphy" section.

Vane Shear Strength

Records of torque vs. vane rotation were obtained from the APC-recovered section in Hole 754A. The silty nature of the noncohesive calcareous sediments resulted in extremely low strength values (Table 9 and Fig. 21). A small increase in vane shear strength is observed with depth to 70 mbsf. The gradient of increasing shear strength with depth appears to change at 70 mbsf. The gradient change does not coincide, however, with the boundary between subunits A2 and A3.

Formation Factor

Formation factor was obtained by comparing electrical resistance of a probe in soft sediment against resistance of the same probe immersed in seawater. The results are listed in Table 9 and plotted in Figure 21. The observed variation of the formation factor correlates with the previously discussed division of subunits based on index properties. Formation factor is variable in subunits A1 and A2, with a value of 1.9 ± 0.3, and rather constant in subunit A3, with a value of about 2.0. A drastic decrease of the formation factor at 100 mbsf coincides with subunit A4, a boundary layer above the unconformity.

Thermal Conductivity

Thermal conductivity is reported in Table 12 and displayed in Figure 22. Variation in thermal conductivity with depth correlates with the division of units A and B. Conductivities in unit A are 1.4 ± 0.2 W/m°C, and those in unit B range from 1.6 to 2.2 W/m°C, with a tendency to increase with depth. The gradient in unit B is 0.4 W/m°C/100 m. The range in conductivity in unit A is small in comparison with that of unit B (±0.2 and ± 0.6 W/m°C, respectively).

Summary

Three units (A, B, and C) are identified on the basis of differences in index properties. The boundary between units A and B is coincident with the unconformity between lithologic Units I and II. The unit B/unit C boundary is close to the division of lithologic Subunits IIA/IIB and probably reflects the transition from chalk to limestone. The classification of these physical-properties units is coincident with the variation of thermal conductivity and compressional-wave velocity. Unit A is further divided into subunits A1, A2, A3, and A4. Velocity anisotropy of 9% between vertical and horizontal propagations and 3% between two different directions of horizontal propagation were measured in the consolidated chalks and limestones of lithologic Unit II.

Good agreements between laboratory and downhole-logging measurements corroborate these measurements ("Geophysical Well Logging" section, "Broken Ridge Summary" chapter).

GEOPHYSICAL WELL LOGGING

Two tool strings were run at this site: the geochemical string and a modified seismic stratigraphic string (LSS, DIT-E, NGT, CNL, GPIT, TCC, and AMS) (see "Explanatory Notes" chapter). Because of the presence of pebble/gravel layers from 120 to 153 mbsf, the logging plan was modified to provide maximum logging coverage at minimum risk to the tools. Thus, the geochemical tool string was run first because it is capable of logging through pipe. The seismic stratigraphic tool was run second. We planned to raise the pipe base 25 m on the second uphole recording of the seismic stratigraphic tool to allow access to the gravel interval while limiting exposure to the risk of gravel collapse to only several minutes. The only disadvantages to this plan were the loss of bulk density and photoelectric factor data and the biasing of the natural gamma data from the seismic stratigraphic tool by the irradiation of the formation by the geochemical string tool.

The geochemical string provided two uphole recordings: (1) 355–0 mbsf and (2) 184–0 mbsf (160–0 through pipe). The seismic stratigraphic tool provided one downhole and two uphole recordings: (1) 0–322 mbsf (0–160 through pipe), (2) 322–52 mbsf (160–52 through pipe), and (3) 321–186 mbsf.

The logging on the second uphole recording of the seismic stratigraphic tool did not proceed according to plan. The pipe base stuck in the gravel layer and could not be freed without endangering the logging tools in the hole. Logging was terminated because the gravel layer proved to be unstable, despite thorough hole conditioning.

Table 9. Index properties, vane shear strength, and formation factor of samples from Holes 754A and 754B.

Core, section, interval (cm)	Depth (mbsf)	Water content (%)	Porosity (%)	Density			Undrained shear strength (kPa)	Formation factor
				Wet bulk (g/cm^3)	Dry bulk (g/cm^3)	Grain (g/cm^3)		
121-754A-								
1H-2, 80	2.30	46.05	69.35	1.56	0.84	2.68	0.9	2.01
1H-4, 80	5.30	42.33	66.66	1.62	0.93	2.76	2.3	1.92
2H-2, 85	8.45	42.17	65.61	1.60	0.93	2.65	1.4	2.04
2H-4, 85	11.45	36.45	60.26	1.70	1.08	2.68	2.3	2.29
2H-6, 85	14.45	38.69	62.60	1.67	1.02	2.68	2.6	2.08
3H-2, 85	18.05	39.54	63.62	1.66	1.00	2.71	2.8	2.24
3H-4, 85	21.05	40.39	64.24	1.65	0.98	2.68	1.3	1.81
3H-6, 85	24.05	37.74	61.87	1.68	1.05	2.71	2.6	2.26
4H-2, 85	27.65	42.13	65.88	1.63	0.95	2.68	3.4	1.84
4H-4, 86	30.65	39.44	63.49	1.67	1.01	2.70	1.9	2.00
4H-6, 85	33.65	40.25	64.40	1.65	0.99	2.72	3.3	2.01
5H-2, 85	37.25	39.93	63.39	1.66	1.00	2.64	3.0	1.87
5H-4, 85	40.25	38.88	62.57	1.65	1.00	2.66	4.2	1.89
5H-6, 85	43.25	44.35	66.84	1.54	0.86	2.56	1.0	1.62
6H-2, 85	46.85			1.57			0.7	1.77
6H-4, 85	49.85	37.78	61.82	1.69	1.05	2.70	4.9	2.11
6H-6, 85	52.85	37.89	62.07	1.69	1.05	2.72	3.6	2.00
7H-2, 85	56.45			1.72			2.4	2.06
7H-4, 85	59.45			1.76			5.2	2.06
7H-6, 85	62.45			1.70			3.3	2.06
8H-2, 85	66.15	36.22	60.53	1.72	1.10	2.74	2.1	1.97
8H-4, 85	69.15	35.36	58.54	1.69	1.09	2.61	2.3	2.03
8H-6, 85	72.15			1.69			17.0	2.05
9H-2, 85	75.85	39.98	63.45	1.69	1.01	2.64	1.4	1.87
9H-4, 85	78,85	43.24	67.08	1.63	0.93	2.71	1.2	1.87
9H-6, 85	81.85	43.80	67.53	1.67	0.94	2.70	1.7	2.00
10H-2, 60	85.30						11.3	
10H-2, 80	85.50	46.92	70.64	1.63	0.86	2.75		1.86
10H-4, 80	88.50	49.40	72.95	1.69	0.86	2.79	5.4	1.94
10H-6, 80	91.50	38.33	62.50	1.72	1.06	2.71	13.4	2.02
11H-2, 80	95.20	34.09	58.43	1.80	1.19	2.75	7.0	2.00
11H-4, 85	98.25	39.91	64.30	1.71	1.03	2.74	6.7	2.03
11H-6, 80	101.20	45.25	68.88	1.65	0.90	2.71	6.7	1.74
12H-3, 80	106.40	47.07	70.22	1.58	0.84	2.68	1.9	1.37
12H-5, 80	109.40	39.69	63.21	1.70	1.02	2.64	5.8	1.41
13X-1, 120	113.50	44.98	69.35	1.61	0.88	2.80		
13X-2, 120	115.00	40.70	64.98	1.68	1.00	2.74		
13X-4, 25	117.05	37.30	61.78	1.90	1.19	2.75		
14X-1, 90	122.90	38.82	63.26	1.71	1.04	2.75		
14X-2, 90	124.40	40.13	63.81	1.71	1.02	2.66		
14X-4, 20	126.70	29.92	52.54	1.88	1.32	2.63		
121-754B-								
5R-1, 65	152.35	17.62	36.31	2.48	2.04	2.71		
5R-2, 12	153.32	28.45	50.28	2.42	1.73	2.58		
5R-3, 66	155.36	14.02	29.86	2.52	2.17	2.65		
121-754A-								
19N-1, 17	159.97	12.36	27.27	2.40	2.10	2.70		
20N-1, 82	163.42	12.78	28.56	2.36	2.06	2.77		
121-754B-								
6R-2, 85	163.65	20.40	39.83	2.51	2.00	2.62		
6R-3, 38	164.68	23.26	45.08	2.73	2.09	2.75		
121-754A-								
20N-2, 89	164.99	8.49	19.52	2.35	2.15	2.66		
20N-2, 120	165.30	22.54	42.79	2.09	1.62	2.61		
21N-1, 22	167.32	14.43	29.86	2.32	1.99	2.56		
21N-1, 134	168.44	14.48	31.15	2.31	1.98	2.71		
22N-1, 7	170.17	25.79	48.42	2.61	1.93	2.74		
23N-1, 64	171.74			2.29				
121-754B-								
7R-1, 81	171.81	48.42	71.41	2.22	1.15	2.69		
7R-3, 29	174.29	24.48	46.43	2.43	1.84	2.71		
7R-5, 25	177.25	18.79	38.27	2.49	2.03	2.72		
8R-1, 137	181.97	24.78	46.29	2.36	1.78	2.65		

Table 9 (continued).

Core, section, interval (cm)	Depth (mbsf)	Water content (%)	Porosity (%)	Density: Wet bulk (g/cm^3)	Density: Dry bulk (g/cm^3)	Density: Grain (g/cm^3)	Undrained shear strength (kPa)	Formation factor
121-754B- (Cont.)								
9R-2, 81	192.61	16.47	33.76	2.38	1.99	2.63		
9R-4, 81	195.61	24.27	45.42	2.55	1.93	2.64		
9R-6, 82	198.62	15.28	31.93	2.22	1.88	2.64		
10R-2, 82	202.32	13.28	28.77	2.26	1.96	2.68		
10R-4, 82	205.32	10.33	23.31	2.39	2.14	2.68		
11R-2, 81	211.91	9.49	21.33	2.36	2.14	2.63		
12R-1, 4	219.24	9.78	22.74	2.45	2.21	2.76		
13R-2, 92	230.28	13.05	27.91	2.24	1.95	2.62		
13R-4, 26	232.62	13.75	28.47	2.19	1.89	2.54		
13R-6, 61	235.97	11.90	25.93	2.33	2.05	2.63		
14R-3, 79	242.19	13.20	28.04	2.23	1.94	2.60		
14R-4, 38	243.28	20.94	40.31	2.09	1.65	2.59		
14R-6, 87	246.77	20.35	40.49	2.09	1.66	2.70		
15R-2, 92	250.62	10.09	22.45	2.41	2.16	2.62		
15R-4, 87	253.57	25.21	48.08	2.01	1.51	2.79		
15R-6, 113	256.83	10.14	23.07	2.38	2.14	2.70		
16R-1, 110	259.00	9.39	20.97	2.41	2.18	2.60		
16R-2, 59	259.99	7.58	17.70	2.50	2.31	2.67		
17R-2, 76	269.86	13.97	28.13	2.13	1.83	2.45		
18R-1, 62	277.92	12.46	26.77	2.23	1.95	2.61		
19R-1, 91	287.91	14.20	30.34	2.26	1.94	2.67		
20R-1, 44	297.14	15.30	27.51	2.07	1.76	2.13		
21R-1, 76	307.06	14.52	26.88	2.08	1.78	2.20		
22R-1, 21	316.21	17.39	34.27	2.10	1.73	2.51		
22R-1, 133	317.33	5.00	12.36	2.64	2.51	2.72		
24R-1, 145	336.75	0.58	1.48	2.85	2.83	2.63		
24R-2, 11	336.91	10.17	23.01	2.44	2.19	2.68		
25R-1, 18	345.18	9.44	21.93	2.45	2.22	2.74		

Logging Data

The quality of the data is good, especially in the open-hole interval. Natural gamma data from the geochemical string is used in this section. The data from the long-spacing sonic (LSS) tool is good, except for a small interval from 286 to 300 mbsf in which the borehole wall was extremely rough. Because of the tool geometries and differences in logged intervals, the logs presented in the figures have sections of unreliable data in their upper and lower parts. The range of reliable data is 165–338 mbsf for the geochemical string and 165–318 mbsf for the seismic stratigraphic string.

Interpretation

The transition from the chalks of lithologic Subunit IIA to the limestones of lithologic Subunit IIB (see "Lithostratigraphy and Sedimentology" section) appears as a slight increase in resistivity at 189 mbsf (Fig. 23). The logging data indicate a zone of high slowness, low resistivity, and a relatively high gamma response (largely because of an increase in potassium) from 227 to 260 mbsf (arrow 1, Fig. 23). An increase in aluminum and a sharp decrease in calcium yield (arrow 1, Fig. 24) are recorded in the same interval, which corresponds to a limestone with an ash content of 10%–25% found in Cores 121-754B-13R to 121-754B-15R. The presence of this low-velocity zone is important in the interpretation of the seismic stratigraphy (see "Seismic Stratigraphy" section), which is based in part on the synthetic seismogram generated from the logging data (Fig. 25). The lower part of Subunit IIB shows a change to higher sonic velocities (lower slowness) and more variable resistivities in the interval from 260 to 283 mbsf (arrow 2, Fig. 23). The high resistivity corresponds to an increase in limestone induration and is accompanied by a decrease in ash content.

The boundary between lithologic Subunits IIB and IIC is marked by an increase in resistivity and hole roughness, which disturbed the function of the sonic tool. These responses reflect the locations in Subunit IIC of the chert layers recovered in Cores 121-754B-19R to 121-754B-22R (particularly at 284–287 and 298–302 mbsf; Fig. 23). There is also an increase in silicon yield (Fig. 24). The usefulness of logging is obvious for this interval where core recovery averages 25%. The continuous nature of logging makes it possible to determine the correct positions of these chert layers. The Fe yield log (Fig. 24) highlights the gradual upward increase in ash content in the column from 280 mbsf.

Figure 25 is a synthetic seismogram generated from the velocity data (derived from the slowness data of the LSS tool), assuming a constant bulk density of 1.8 g/cm^3. This determination of the average density of the rocks in the upper part of the column will cause little error in the calculation of the synthetic seismogram, which is more sensitive to velocity changes than to density changes. The synthetic seismogram calculation involves a convolution of the impedance log with a zero-phase Ricker wavelet, for which the peak frequency of the wavelet was 60 Hz. A similar calculation using a 30-Hz wavelet provided nearly identical positioning of major reflectors, but lower resolution of the smaller ones.

Figure 26 shows the excellent agreement between the synthetic seismogram and the seismic data, which contain seismic energy in the 25–130-Hz frequency range (see "Seismic Stratigraphy" section). In addition to these log interpretations, data from the geophysical well logging at Site 754 were correlated with physical properties measured in the laboratory and with the magnetic susceptibility values (see "Broken Ridge Summary" chapter).

Summary

Geophysical well logging at Site 754 provided confirmation of lithostratigraphic boundaries, delineated the spatial relationships between strata in poorly recovered intervals, and detected

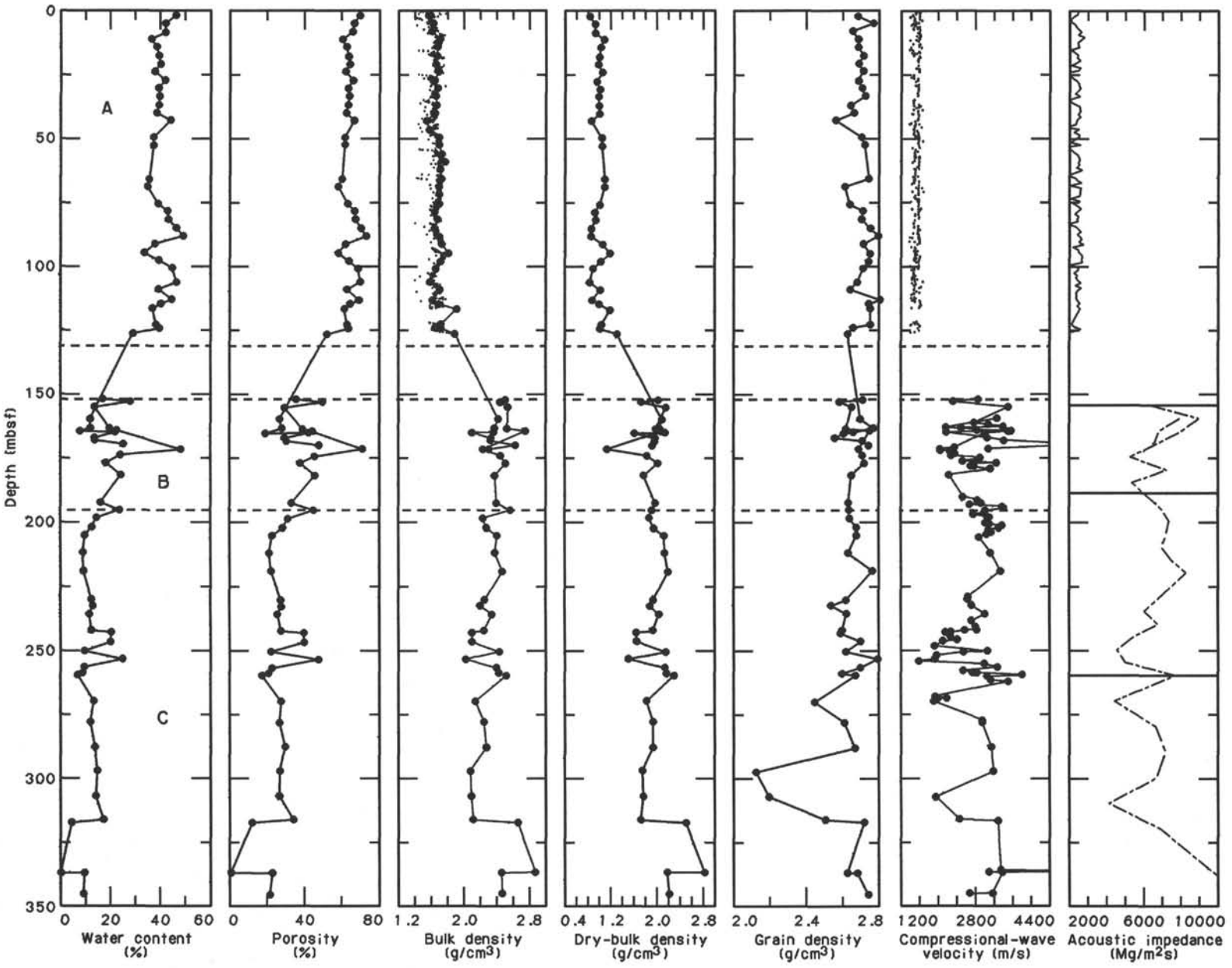

Figure 19. Water content, porosity, bulk density, dry-bulk density, grain density, compressional-wave velocity, and acoustic impedance of samples from Holes 754A and 754B. GRAPE densities (dots on bulk-density plot) and *P*-wave-logger velocities (dots) were collected in the upper 127 m of the section; however, these data are reliable to 112.3 mbsf. The black horizontal lines on the acoustic impedance plot indicate changes in acoustic impedance with depth that correlate with seismic reflectors. *A*, *B*, and *C* refer to the physical-properties units discussed in the text.

Table 10. Compressional-wave velocity of samples from Holes 754A and 754B.

Core, section, interval (cm)	Depth (mbsf)	Direction[a]	Compressional-wave velocity (m/s)
121-754A-			
13X-1, 120	113.50	C	1560.7
14X-1, 56	112.56	C	1760.5
14X-3, 82	125.82	C	1823.0
121-754B-			
5R-1, 65	152.35	A	2880.0
5R-2, 12	153.32	A	2340.2
5R-3, 66	155.36	A	3524.4
121-754A-			
19N-1, 17	159.97	A	3270.9
121-754B-			
6R-1, 29	161.59	B	3088.3
6R-1, 29	161.59	A	2788.7
6R-1, 98	162.28	B	3344.6
6R-1, 98	162.28	A	3081.9
6R-1, 98	162.28	C	3283.6
6R-2, 21	163.01	A	3422.9
6R-2, 21	163.01	B	3536.7
6R-2, 21	163.01	C	3585.8
121-754A-			
20N-1, 82	163.42	A	2191.4
121-754B-			
6R-2, 85	163.65	C	2827.9
6R-2, 85	163.65	B	2809.8
6R-2, 85	163.65	A	2518.6
6R-3, 23	104.53	A	2849.3
6R-3, 23	164.53	B	3141.0
6R-3, 38	164.68	A	3600.0
121-754A-			
20N-2, 89	164.99	A	3528.8
20N-2, 120	165.30	A	2191.9
121-754B-			
6R-3, 129	165.59	A	3018.1
6R-3, 129	165.59	B	3181.6
121-754A-			
21N-1, 22	167.32	A	3077.4
21N-1, 134	168.44	A	3433.1
22N-1, 7	170.17	A	5084.2
121-754B-			
7R-1, 29	171.29	C	2721.9
7R-1, 29	171.29	B	2802.1
7R-1, 29	171.29	A	2370.4
121-754A-			
23N-1, 64	171.74	A	3102.6
121-754B-			
7R-1, 81	171.81	A	2042.4
7R-1, 117	172.17	A	2074.3
7R-1, 117	172.17	C	2149.9
7R-1, 117	172.17	B	2164.5
7R-2, 28	172.78	A	2274.1
7R-2, 113	173.63	A	2383.1
7R-2, 113	173.63	C	2373.4
7R-2, 113	173.63	B	2779.3
7R-3, 31	174.31	A	2308.6
7R-3, 31	174.31	C	2643.6
7R-3, 31	174.31	B	2680.1

Table 10. (continued).

Core, section, interval (cm)	Depth (mbsf)	Direction[a]	Compressional-wave velocity (m/s)
121-754B- (Cont.)			
7R-3, 126	175.26	B	3324.7
7R-3, 126	175.26	A	2916.9
7R-4, 29	175.79	B	2919.6
7R-4, 29	175.79	A	2892.0
7R-4, 29	175.79	C	2508.0
7R-4, 107	176.57	A	2550.4
7R-4, 107	176.57	B	2920.8
7R-4, 107	176.57	C	2891.1
7R-5, 25	177.25	A	3267.8
7R-5, 35	117.35	C	3163.3
7R-5, 35	177.35	B	3127.2
7R-5, 35	177.35	A	2784.0
7R-5, 136	178.36	A	2787.9
7R-5, 136	178.36	C	3132.8
7R-5, 136	178.36	B	3162.8
7R-6, 4	178.54	A	2716.6
7R-6, 4	178.54	B	3135.4
7R-6, 4	178.54	C	3173.5
7R-6, 115	179.65	A	3140.0
7R-6, 115	179.65	C	3259.0
7R-6, 115	179.65	B	3437.8
8R-1, 139	181.99	A	2252.9
8R-1, 139	181.99	C	2622.4
8R-1, 139	181.99	B	2648.7
9R-1, 17	190.47	B	2980.7
9R-1, 17	190.47	C	2947.9
9R-1, 17	190.47	A	2553.6
9R-1, 134	191.64	C	3241.7
9R-1, 134	191.64	B	3211.6
9R-1, 134	191.64	A	2857.0
9R-2, 110	192.90	A	2942.5
9R-2, 110	192.90	B	3226.0
9R-2, 110	192.90	C	3244.3
9R-3, 17	193.47	A	2701.4
9R-3, 17	193.47	B	3097.7
9R-3, 17	193.47	C	3051.1
9R-3, 95	194.25	C	3526.2
9R-3, 95	194.25	A	3387.8
9R-3, 95	194.25	B	3555.4
9R-4, 21	195.01	A	3420.2
9R-4, 21	195.01	C	3465.5
9R-4, 21	195.01	B	3405.4
9R-4, 103	195.83	A	3042.2
9R-4, 103	195.83	C	3330.8
9R-4, 103	195.83	B	3371.9
9R-5, 32	196.62	C	3367.0
9R-5, 32	196.62	A	3013.9
9R-5, 32	196.62	B	3348.8
9R-5, 119	197.49	A	2766.6
9R-5, 119	197.49	B	3053.5
9R-5, 119	197.49	C	3103.4
9R-6, 37	198.17	C	3382.8
9R-6, 37	198.17	B	3426.1
9R-6, 37	198.17	A	3071.3
9R-6, 76	198.56	C	3401.3
9R-6, 76	198.56	B	3497.6
9R-6, 76	198.56	A	3116.9
10R-1, 56	200.56	B	3322.5
10R-1, 56	200.56	C	2941.9
10R-1, 56	200.56	A	3022.4
10R-1, 116	201.16	C	3131.7
10R-1, 116	201.16	B	3299.7
10R-1, 116	201.16	A	3124.8
10R-2, 33	201.83	C	3445.9
10R-2, 33	201.83	A	3386.2
10R-2, 33	201.83	B	3103.4
10R-2, 122	202.72	B	3347.3
10R-2, 122	202.72	A	3319.5
10R-2, 122	202.72	C	3230.2
10R-3, 34	203.34	B	3388.7
10R-3, 34	203.34	A	3093.1
10R-3, 34	203.34	C	3435.6
10R-3, 116	204.16	B	3328.2
10R-3, 116	204.16	A	3149.1

Table 10. (continued).

Core, section, interval (cm)	Depth (mbsf)	Direction[a]	Compressional-wave velocity (m/s)
121-754B- (Cont.)			
10R-3, 116	204.16	C	3234.7
10R-4, 43	204.93	A	3056.7
10R-4, 43	204.93	B	3401.3
10R-4, 43	204.93	C	3422.9
10R-4, 141	205.91	C	2356.3
10R-4, 141	205.91	B	3269.7
10R-4, 141	205.91	A	2894.0
11R-2, 106	212.16	A	3145.3
11R-2, 106	212.16	C	3604.0
12R-1, 4	219.24	A	3350.5
12R-1, 4	219.24	C	3154.6
13R-1, 42	229.32	C	2915.1
13R-1, 42	229.32	A	2659.7
13R-2, 96	230.32	C	2960.2
13R-2, 96	230.32	A	2653.6
13R-4, 28	232.64	A	2742.7
13R-4, 28	232.64	C	2311.9
13R-6, 63	235.99	A	3022.4
13R-6, 63	235.99	C	3287.0
14R-1, 19	238.69	C	2911.2
14R-1, 19	238.69	A	2731.7
14R-2, 119	241.09	A	2818.8
14R-2, 119	241.09	B	3133.5
14R-2, 119	241.09	C	3019.4
14R-3, 79	242.19	A	2839.0
14R-3, 106	242.46	A	2592.4
14R-3, 106	242.46	C	2860.2
14R-4, 34	243.24	A	2295.6
14R-4, 34	243.24	C	2595.5
14R-4, 38	243.28	A	2176.4
14R-5, 22	244.62	B	2567.9
14R-5, 22	244.62	A	2281.3
14R-6, 27	246.17	B	2603.8
14R-6, 27	246.17	A	2423.9
14R-6, 87	246.77	A	2124.5
15R-1, 39	248.59	A	1951.2
15R-1, 39	248.59	C	2247.7
15R-2, 92	250.62	A	3081.1
15R-2, 119	250.89	A	2565.2
15R-2, 119	250.89	B	2865.3
15R-3, 102	252.22	B	2287.7
15R-3, 102	252.22	A	1988.1
15R-4, 98	253.68	A	1955.7
15R-4, 98	253.68	B	2273.3
15R-5, 19	254.39	A	1608.8
15R-5, 19	254.39	B	2156.9
15R-5, 135	255.55	B	3201.5
15R-5, 135	255.55	A	3005.6
15R-6, 113	256.83	B	3413.0
15R-6, 113	256.83	A	3286.6
16R-1, 26	258.16	C	2910.7
16R-1, 26	258.16	B	3011.2
16R-1, 26	258.16	A	2562.4
16R-1, 108	258.98	C	3187.3
16R-1, 108	258.98	A	2760.6
16R-1, 108	258.98	B	3250.8
16R-1, 110	259.00	A	2852.3
16R-2, 38	259.78	C	3933.3
16R-2, 38	259.78	A	3814.8
16R-2, 38	259.78	B	3985.3
16R-2, 59	259.99	A	3815.1
16R-2, 117	260.57	A	3074.2
16R-2, 117	260.57	B	3404.4
16R-2, 117	260.57	C	3328.7
16R-3, 96	261.86	A	3151.4
16R-3, 96	261.86	C	3378.1
16R-3, 96	261.86	B	3314.4
16R-4, 2	262.42	B	3793.3
16R-4, 2	262.42	A	3522.0
16R-4, 2	262.42	C	3742.7
17R-1, 49	268.09	A	1964.9
17R-1, 49	268.09	C	2192.7
17R-1, 49	268.09	B	2160.8
17R-1, 144	269.04	B	2439.8
17R-1, 144	269.04	A	2208.5
17R-1, 144	269.04	C	2463.8

Table 10. (continued).

Core, section, interval (cm)	Depth (mbsf)	Direction[a]	Compressional-wave velocity (m/s)
121-754B- (Cont.)			
17R-2, 9	269.19	B	2175.2
17R-2, 9	269.19	A	2013.1
17R-2, 104	270.14	B	2169.5
17R-2, 104	270.14	C	2152.5
17R-2, 104	270.14	A	1927.0
18R-1, 19	277.49	C	3442.2
18R-1, 19	277.49	B	3467.9
18R-1, 19	277.49	A	2960.4
18R-1, 100	278.30	A	2953.7
18R-1, 100	278.30	B	3210.7
18R-1, 100	278.30	C	3213.9
19R-1, 93	287.93	C	3241.8
19R-1, 93	287.93	B	3355.0
19R-1, 93	287.93	A	3153.8
20R-1, 79	297.49	A	3212.5
20R-1, 79	297.49	B	3410.7
20R-1, 79	297.49	C	3391.2
21R-1, 122	307.52	A	1970.7
21R-1, 122	307.52	C	2036.7
21R-1, 122	307.52	B	2031.1
22R-1, 23	316.23	A	2479.9
22R-1, 23	316.23	C	2509.3
22R-1, 23	316.23	B	2637.7
22R-1, 86	316.86	A	3297.7
22R-1, 86	316.86	B	3449.8
22R-1, 86	316.86	C	3472.8
24R-1, 86	336.16	A	3360.3
24R-1, 86	336.16	B	3650.4
24R-1, 145	336.75		5563.7
24R-2, 11	336.91	A	3100.1
24R-2, 19	336.99	A	3394.7
24R-2, 19	336.99	C	3430.8
24R-2, 19	336.99	B	3505.7
25R-1, 18	345.18	A	3180.6
25R-1, 30	345.30	A	2692.2

[a] A = vertical propagation; B = propagation perpendicular to the split-core face; C = propagation parallel to the split-core face.

the presence of a low-velocity zone that has a significant effect on the seismic stratigraphy interpretation.

SEISMIC STRATIGRAPHY

Site 754

Site 754 is on the central part of the ridge, approximately 15 km north of the prominent southern scarp (Fig. 2). Site 754 was positioned to sample the oldest lithology above the prominent angular unconformity, in order to further constrain the time interval over which the erosional event occurred. The oldest unit overlying the angular unconformity occurs on the central part of the ridge in a subtle depression that dips slightly toward the west (Fig. 27). This unit onlaps the truncated and dipping limestone, chert, and chalk sequence, and thus the unit is progressively younger away from the center of the ridge. Another objective at Site 754 was to sample the seismic stratigraphic sequence boundary between the dipping and truncated limestones and cherts and the prograding downlapping wedge. RC2708 seismic line 20 shows the downlapping stratal patterns between the prograding downlapping wedge and the underlying limestones and cherts (Fig. 27).

Correlation Between Seismic Stratigraphy and Lithostratigraphy

Downhole sonic and density logs were recorded only below 150 mbsf in Hole 754B because of the hazardous hole condi-

Table 11. Anisotropy of compressional-wave velocity of samples from Hole 754B.

Core, section, interval (cm)	Depth (mbsf)	ANIS1[a] (%)	ANIS2[b] (%)
6R-1, 29	161.59	10.7	
6R-1, 98	162.28	7.5	−1.8
6R-2, 21	163.01	4.0	1.4
6R-2, 85	163.65	11.9	0.6
6R-3, 23	164.53	10.2	
6R-3, 129	165.59	5.4	
7R-1, 29	171.29	16.5	−2.9
7R-1, 117	172.17	4.0	−0.7
7R-2, 113	173.63	8.1	−14.6
7R-3, 31	174.31	15.3	−1.4
7R-3, 126	175.26	14.0	
7R-4, 29	175.79	−6.2	−14.1
7R-4, 107	176.57	13.9	−1.0
7R-5, 35	177.35	13.0	1.2
7R-5, 136	178.36	12.9	−0.9
7R-6, 4	178.54	16.1	1.2
7R-6, 115	179.65	6.6	−5.2
8R-1, 139	181.99	17.0	−1.0
9R-1, 17	190.47	16.1	−1.1
9R-1, 134	191.64	12.9	0.9
9R-2, 110	192.90	9.9	0.6
9R-3, 17	193.47	13.8	−1.5
9R-3, 95	194.25	4.5	−0.8
9R-4, 21	195.01	0.4	1.8
9R-4, 103	195.83	10.2	−1.2
9R-5, 32	196.62	11.4	0.5
9R-5, 119	197.49	11.3	1.6
9R-6, 37	198.17	10.8	−1.3
9R-6, 76	198.56	10.7	−2.8
10R-1, 56	200.56	3.6	−11.5
10R-1, 116	201.16	2.9	−5.1
10R-2, 33	201.83	−3.3	11.0
10R-2, 122	202.72	−0.9	−3.5
10R-3, 34	203.34	10.3	1.4
10R-3, 116	204.16	4.2	−2.8
10R-4, 43	204.93	11.6	0.6
10R-4, 141	205.91	−2.8	−27.9
11R-2, 106	212.16	14.6	
12R-1, 4	219.24	−5.8	
13R-1, 42	229.32	9.6	
13R-2, 96	230.32	11.6	
13R-4, 28	232.64	−15.7	
13R-6, 63	235.99	8.8	
14R-1, 19	238.69	6.6	
14R-2, 119	241.09	9.1	−3.6
14R-3, 106	242.46	10.3	
14R-4, 34	243.24	13.1	
14R-5, 22	244.62	12.6	
14R-6, 27	246.17	7.4	
15R-1, 39	248.59	15.2	
15R-2, 119	250.89	11.7	
15R-3, 102	252.22	15.1	
15R-4, 98	253.68	16.2	
15R-5, 19	254.39	34.1	
15R-5, 135	255.55	6.5	
15R-6, 113	256.83	3.8	
16R-1, 26	258.16	15.6	−3.3
16R-1, 108	258.98	16.6	−2.0
16R-2, 38	259.78	3.8	−1.3
16R-2, 117	260.57	9.5	−2.2
16R-3, 96	261.86	6.2	1.9
16R-4, 2	262.42	7.0	−1.3
17R-1, 49	268.09	10.8	1.5
17R-1, 144	269.04	11.0	1.0
17R-2, 9	269.19	8.1	
17R-2, 104	270.14	12.1	−0.8
18R-1, 19	277.49	16.7	−0.7
18R-1, 100	278.30	8.8	0.1
19R-1, 93	287.93	4.6	−3.4
20R-1, 79	297.49	5.9	−0.6
21R-1, 122	307.52	3.2	0.3
22R-1, 23	316.23	3.8	−4.9
22R-1, 86	316.86	5.0	0.7
24R-1, 86	336.16	8.6	
Maximum		34.1	11.0
Minimum		−15.7	−27.9
Average		8.9	−2.0
Absolute average		9.9	3.1

[a] ANIS1 = ([Vb + Vc]/2 − Va)/Va or ([Vb or Vc] − Va)/Va

[b] ANIS2 = (Vc − Vb)/Vb

tions resulting from a cherty gravel layer immediately above the prominent angular unconformity. Therefore, *P*-wave-logger and GRAPE density measurements on samples from Cores 121-754A-1H to 121-754A-14X (0–132 mbsf) were used to calculate the velocity and bulk density for this interval (Fig. 19), which corresponds to lithologic Unit I. The laboratory and downhole calculated velocities are in good agreement with the velocities derived from sonobuoy solutions (Figs. 19 and 28), except for a low-velocity zone at 230–260 mbsf. The low-velocity zone is detected in both the laboratory-measured compressional-wave velocity and the downhole sonic measurements. Low-velocity zones are extremely difficult to identify with sonobuoy data. Sonobuoy velocity solutions and laboratory compressional-wave measurements indicate average velocities of 1600 m/s for Unit I; the sonobuoy velocity solutions, laboratory compressional-wave measurements, and downhole sonic measurements indicate average velocities for lithologic Unit II of 3000 m/s, increasing to 3500 m/s toward the base of Hole 754B (260–336 mbsf). The approximate velocity for the low-velocity zone is 2100 m/s (Fig. 19).

Acoustic impedance is the product of velocity and bulk density. Seismic reflectors arise from changes in acoustic impedance with depth. Accordingly, downhole acoustic impedance calculations in conjunction with the seismic velocity allow correlation of the sampled lithostratigraphy at Site 754 with the seismic stratigraphy. Three major changes in acoustic impedance are noted at 152, 190, and 260 mbsf (Fig. 19).

Synthetic Seismogram

A synthetic seismogram for the interval from 150 to 300 mbsf was calculated from downhole sonic measurements and constant density (Figs. 25 and 26, "Geophysical Well Logging" section). The assumption of constant downhole density was necessary because no density log was run at Site 754. A zero-phase Ricker wavelet was convolved with the downhole acoustic impedance contrast to generate the synthetic seismogram.

Pelagic Cap

The horizontal pelagic cap, lithologic Unit I, rests unconformably on the dipping and truncated limestone, chert, and chalk sequence (Fig. 27). Unit I onlaps the truncated northward-dipping units and probably was deposited under the influence of both currents and relative sea-level changes. The depocenter for Unit I was sampled at Site 754. The following reflectors are observed within the horizontal cap:

1. A faint reflector is observed both in the high-resolution seismic record and the 3.5-kHz precision depth recorder (PDR) record at 0.055 s TWT bsf (Figs. 29 and 30). The reflector coincides with the base of an upper Miocene maximum in the mean grain size of the bulk sediment at 45 mbsf ("Lithostratigraphy and Sedimentology" section). The coarser grain size may indicate a winnowed layer; this reflector can be traced among Sites 754, 753, and 752.
2. The second reflector, at 0.096 s TWT bsf in both the high-resolution seismic and 3.5-kHz records (Figs. 29 and 30), coincides with an increase in the mean grain size of the bulk sediment within the middle Miocene (~15–16 Ma). The coarser grain size again may indicate a winnowed layer at 78 mbsf. The second reflector can also be traced between Sites 754, 753, and 752.
3. Another increase in grain size at 104 mbsf ("Lithostratigraphy and Sedimentology" section) corresponds to the third reflector observed in the 3.5-kHz PDR record at 0.128 s TWT bsf (Fig. 30). However, this reflector is not resolved on the high-resolution seismic profile (Fig. 29).
4. The fourth reflector, at 0.145 s TWT bsf on the high-resolution seismic record (Fig. 29) corresponds to a hiatus separating upper Oligocene nannofossil ooze (Zone CP19) from under-

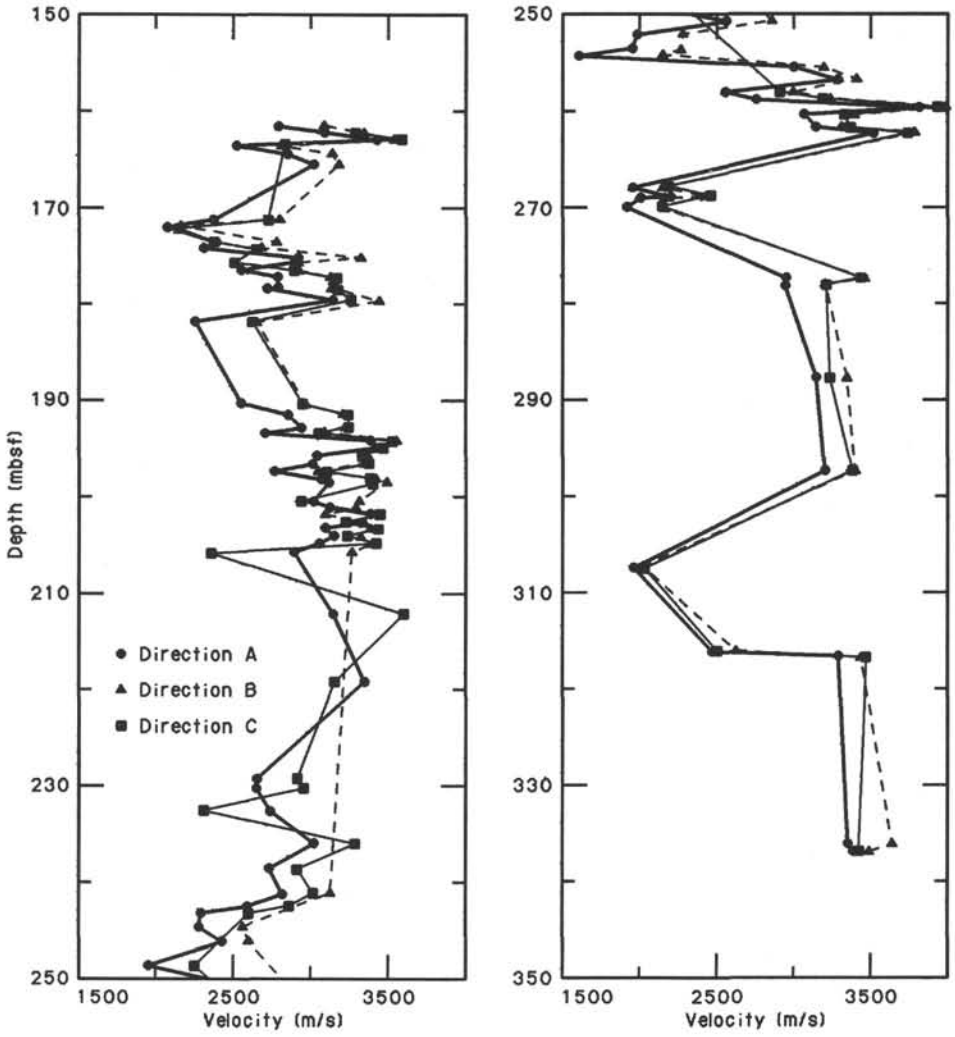

Figure 20. Anisotropy of compressional-wave velocities of samples from Hole 754B. Direction A is vertical propagation. Directions B and C are velocities of horizontal propagation; B is perpendicular to the split-core surface of the sample and C is parallel to it.

lying limestone pebbles and cobbles in an upper Eocene nannofossil ooze (118 mbsf).

5. The fifth reflector, at 0.185 s TWT bsf in the high-resolution seismic profile (Fig. 29), corresponds to an earlier erosional hiatus separating upper Eocene cherty gravel from the underlying dipping and truncated upper Maestrichtian calcareous chalk. A cherty gravel unit recovered in Cores 121-754A-17X through 121-754A-19N probably represents downhole contamination from a gravel layer above the prominent angular unconformity. There was no core recovery in Cores 121-754A-15X, 121-754A-16X, 121-754B-3R, and 121-754B-4R (~140–160 mbsf). This interval of no recovery may correspond to the stratigraphic position and thickness of the cherty gravel layer. The collapse of the drill hole at approximately 150 mbsf, which bound the drill string during removal, also suggests that a gravel layer occurs at that depth. This reflector corresponds to an increase in both the downhole and laboratory-derived acoustic impedance data at 150 mbsf (Figs. 19 and 26).

Dipping and Truncated Sequences

The dipping and truncated limestone, chert, and chalk sequence (the prograding and downlapping sequence of the seismic stratigraphy) underlying the angular unconformity thins toward the north (Fig. 27). The following reflectors are observed within this sequence:

1. A strong reflector (couplet) at 0.210 s TWT bsf in the high-resolution seismic profile (Fig. 29) corresponds to an acoustic impedance contrast at 190 mbsf in both the laboratory and downhole data (Figs. 19 and 25). Accordingly, the synthetic seismogram generated a couplet that is in good agreement with the observed seismic data (Figs. 25 and 26). A lithologic change from calcareous chalk to limestone between Cores 121-754B-8R and 121-754B-9R (~190 mbsf) coincides with this reflector.

2. Another strong reflector (couplet) at 0.255 s TWT bsf on the high-resolution seismic profile (Fig. 29) corresponds to a marked increase in both laboratory and downhole calculated acoustic impedance at 260 mbsf (Figs. 19 and 25). The couplet generated by the synthetic seismogram is in good agreement with the seismic data (Figs. 25 and 26). A change in lithology from limestone with ash to limestone with interspersed chert between Cores 121-754B-15R and 121-754B-16R (~258 mbsf) corresponds to this reflector. The ash-bearing limestones are noticeably less indurated than the ash-barren limestones. The limestones with ash (230–260 mbsf) also have a much lower velocity than the underlying ash-barren limestone intervals with interspersed chert (Fig. 19).

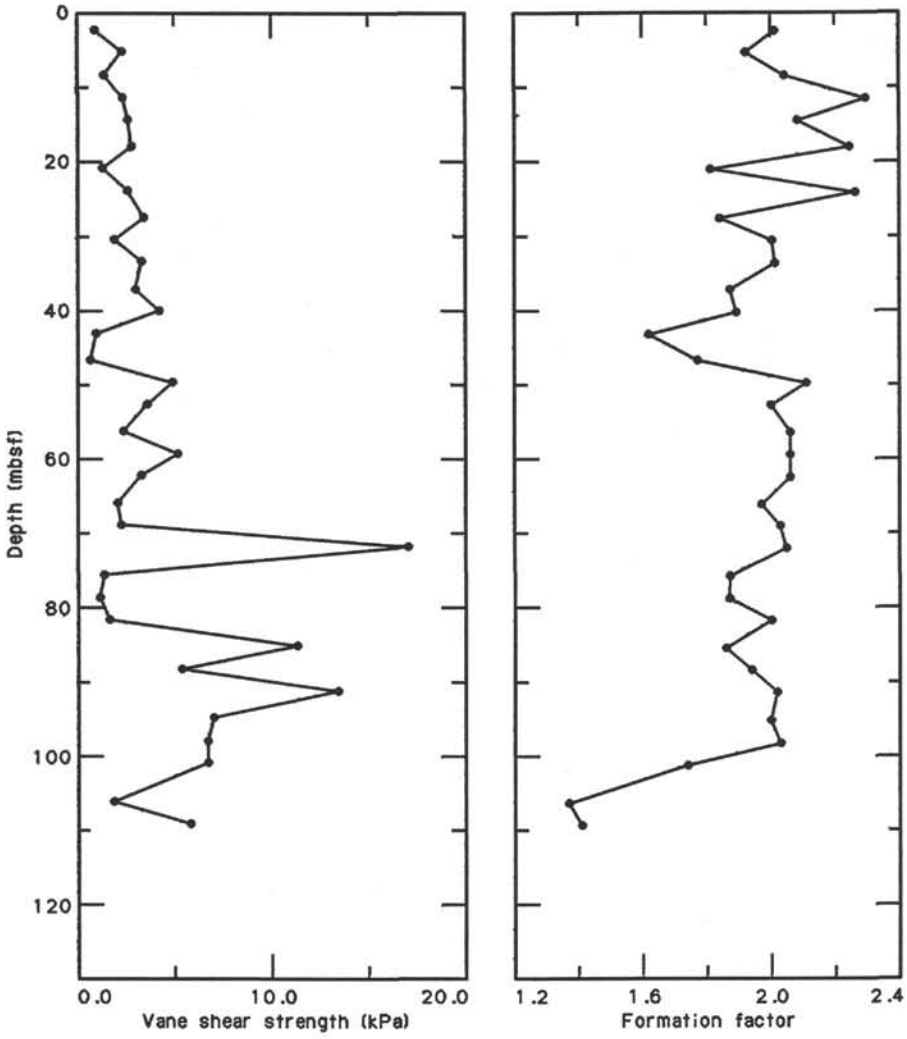

Figure 21. Vane shear strength and formation factor of sediments from Hole 754A.

REFERENCES

Banner, F. T., and Blow, W. H., 1965. Progress in the planktonic foraminiferal biostratigraphy of the Neogene. *Nature*, 208:1164–1166.

Bé, A.W.H., and Tolderlund, D. S., 1971. Distribution and ecology of living planktonic foraminifera in surface waters of the Atlantic and Indian oceans. *In* Funnell, B. M., and Riedel, W. R. (Eds.), *Micropaleontology of Oceans*: Cambridge (Cambridge Univ. Press), 105–149.

Berggren, W. A., 1973. The Pliocene time-scale calibration of planktonic foraminiferal and calcareous nannoplankton zones. *Nature*, 243:391–397.

Berggren, W. A., Kent, D. V., Flynn, J. J., and Van Couvering, J. A., 1985. Cenozoic geochronology. *Geol. Soc. Am. Bull.*, 96:1407–1418.

Blow, W. H., 1969. Late middle Eocene to Recent planktonic biostratigraphy. *In* Bronnimann, P., and Renz, H. H. (Eds.), *Proc. Int. Conf. Planktonic Microfossils, 1st, Geneva, 1967*, 1:199–421.

Bolli, H. M., and Saunders, J. B., 1985. Oligocene to Holocene low latitude planktic foraminifera. *In* Bolli, H. M., Saunders, J. B., and Perch-Nielsen, K. (Eds.), *Plankton Stratigraphy*: Cambridge (Cambridge Univ. Press), 155–262.

Boltovskoy, E., 1978. Late Cenozoic benthonic foraminifera of the Ninetyeast Ridge (Indian Ocean). *Mar. Geol.*, 26:139–175.

Bradshaw, J. S., 1959. Ecology of living planktonic foraminifera in the North and equatorial Pacific Ocean. *Contrib. Cushman Found. Foraminiferal Res.*, 10:25–64.

Caron, M., 1985. Cretaceous planktic foraminifera. *In* Bolli, H. M., Saunders, J. B., and Perch-Nielsen, K. (Eds.), *Plankton Stratigraphy*: Cambridge (Cambridge Univ. Press), 713–762.

Corliss, R. H., 1979. Recent deep-sea benthonic foraminiferal distributions in the southeast Indian Ocean: inferred bottom-water routes and ecological implications. *Mar. Geol.*, 31:115–138.

Herb, R., 1974. Cretaceous planktonic foraminifera from the eastern Indian Ocean. *In* Davies, T. A., Luyendyk, B. P., *Init. Repts. DSDP*, 26: Washington (U.S. Govt. Printing Office), 745–771.

Jenkins, D. G., 1960. Planktonic foraminifera from the Lakes Entrance oil shaft, Victoria, Australia. *Micropaleontology*, 6:345–371.

_____, 1967. Planktonic foraminiferal zones and new taxa from the lower Miocene to the Pleistocene of New Zealand. *N. Z. J. Geol. Geophys.*, 10:1064–1078.

_____, 1978. Neogene planktonic foraminifers from DSDP Leg 40 Sites 360 and 362 in the southeastern Atlantic. *In* Bolli, H. M., Ryan, W.B.F., et al., *Init. Repts. DSDP*, 40: Washington (U.S. Govt. Printing Office), 723–739.

_____, 1985. Southern mid-latitude Paleocene to Holocene planktic Foraminifera. *In* Bolli, H. M., Saunders, J. B., and Perch-Nielsen, K. (Eds.), *Plankton Stratigraphy*: Cambridge (Cambridge Univ. Press), 263–283.

Katz, B. J., 1982. Limitations of Rock-Eval pyrolysis for typing organic matter. *Org. Geochem.*, 4:195–197.

Kennett, J. P., 1973. Middle and late Cenozoic planktonic biostratigraphy of the southwest Pacific DSDP Leg 21. *In* Burns, R. E., An-

drews, J. E., et al., *Init. Repts. DSDP*, 21: Washington (U.S. Govt. Printing Office), 575–640.

Kennett, J. P., and Burns, R. E., 1972. Australian-Antarctic continental drift, paleocirculation changes and Oligocene deep erosion. *Nature*, 239:51–55.

Lawrence, J. R., 1973. Interstitial water studies, Leg 15: stable oxygen and carbon isotope variations in water, carbonates and silicates from the Venezuela Basin (Site 149) and the Aves Rise (Site 148). *In* Heezen, B. C., MacGregor, I. D., et al., *Init. Repts. DSDP*, 20: Washington (U.S. Govt. Printing Office), 891–899.

Morkhoven, F.P.C.M. van, Berggren, W. A., and Edward, A. S., 1986. Cenozoic cosmopolitan deep-water benthic foraminifera. *Bull. Cent. Rech. Expl. Prod. Elf-Aquitaine Mem.*, 11.

Müller, C., 1977. Distribution of calcareous nannoplankton in Oligocene to Holocene sediments of the Red Sea and the Indian Ocean reflecting paleoenvironment. *In* Heirtzler, J. R., Bolli, H. M., Davies, T. A., Saunders, J. B., and Sclater, J. G. (Eds.), *Indian Ocean Geology and Biostratigraphy*: Washington (Am. Geophys. Union), 295–371.

Okada, H., and Bukry, D., 1980. Supplementary modification and introduction of code numbers to the low-latitude coccolith biostratigraphic zonation (Bukry, 1973; 1975). *Mar. Micropaleontol.*, 5:321–325.

Peterson, L. C., 1984. Recent abyssal benthic foraminiferal biofacies of the eastern equatorial Indian Ocean. *Mar. Micropaleontol.*, 8:479–519.

Shipboard Scientific Party, 1989. Site 722. *In* Prell, W. L., Niitsuma, N., et al., *Proc. ODP, Init. Repts.*, 117: College Station, TX (Ocean Drilling Program), 255–317.

Sissingh, W., 1977. Biostratigraphy of Cretaceous calcareous nannoplankton. *Geol. Mijnbouw*, 57:433–440.

Srinivasan, M. S., and Kennett, J. P., 1981. Neogene planktonic foraminiferal biostratigraphy: equatorial to subantarctic, South Pacific. *Mar. Micropaleontol.*, 6:499–534.

Toumarkine, M., and Luterbacher, H., 1985. Paleocene and Eocene planktic foraminifera. *In* Bolli, H. M., Saunders, J. B., Perch-Nielsen, K. (Eds.), *Plankton Stratigraphy*: Cambridge (Cambridge Univ. Press), 87–154.

Vincent, E., 1977. Indian Ocean Neogene planktonic foraminiferal biostratigraphy and its paleoceanographic implications. *In* Heirtzler, J. R., Bolli, H. M., Davies, T. A., Saunders, J. B., and Sclater, J. G. (Eds.), *Indian Ocean Geology and Biostratigraphy*: Washington (Am. Geophys. Union), 469–584.

Woodruff, F., 1985. Changes in Miocene deep-sea benthic foraminiferal distribution in the Pacific Ocean: relationship to paleoceanography. *In* Kennett, J. (Ed.), *The Miocene Ocean: Paleoceanography and Biogeography*: Mem. Geol. Soc. Am., 163:131–176.

Ms 121A-108

Table 12. Thermal conductivity of samples from Holes 754A and 754B.

Core, section, interval (cm)	Depth (mbsf)	Thermal conductivity (W/m°C)
121-754A-		
1H-2, 70	2.20	1.370
1H-4, 70	5.20	1.600
3H-2, 70	17.90	1.265
3H-4, 70	20.90	1.359
3H-6, 70	23.90	1.549
4H-2, 70	27.50	2.286
4H-4, 70	30.50	1.421
4H-6, 70	33.50	1.393
5H-2, 70	37.10	1.159
5H-4, 70	40.10	1.171
5H-6, 70	43.10	1.201
6H-2, 70	46.70	1.313
6H-4, 70	49.70	1.381
6H-6, 70	52.70	1.495
7H-2, 70	56.30	1.432
7H-4, 70	59.30	1.451
7H-6, 70	62.30	1.283
8H-2, 80	66.10	1.439
8H-4, 80	69.10	1.352
8H-6, 80	72.10	1.464
9H-2, 80	75.80	1.153
9H-4, 80	78.80	1.244
9H-6, 80	81.80	1.455
10H-2, 80	85.50	1.018
10H-4, 80	88.50	1.426
10H-6, 80	91.50	1.374
11H-2, 80	95.20	1.559
11H-4, 80	98.20	1.369
11H-6, 80	101.20	1.330
12H-2, 80	104.90	1.341
12H-4, 80	107.90	1.579
12H-6, 80	110.90	1.351
13X-1, 70	113.00	1.513
13X-2, 70	114.50	1.405
13X-3, 70	116.00	1.530
14X-1, 70	122.70	1.333
14X-2, 70	124.20	1.315
14X-3, 70	125.70	1.365
121-754B-		
5R-1, 62	152.32	1.990
6R-1, 31	161.61	2.050
121-754A-		
20N-2, 92	165.02	2.210
21N-1, 24	167.34	2.150
23N-1, 66	171.76	1.990
121-754B-		
7R-1, 120	172.20	1.510
8R-1, 52	181.12	1.860
9R-1, 103	191.33	1.120
10R-3, 62	203.62	2.130
11R-1, 105	210.65	1.240
12R-1, 80	220.00	2.280
13R-6, 53	235.89	1.980
14R-5, 13	244.53	1.510
15R-6, 113	256.83	3.070
16R-2, 107	260.47	2.290
17R-2, 92	270.02	1.510
18R-1, 89	278.19	1.840
20R-1, 46	297.16	2.440
21R-1, 91	307.21	1.800
22R-1, 134	317.34	2.510
24R-2, 8	336.88	2.460
25R-1, 16	345.16	2.630

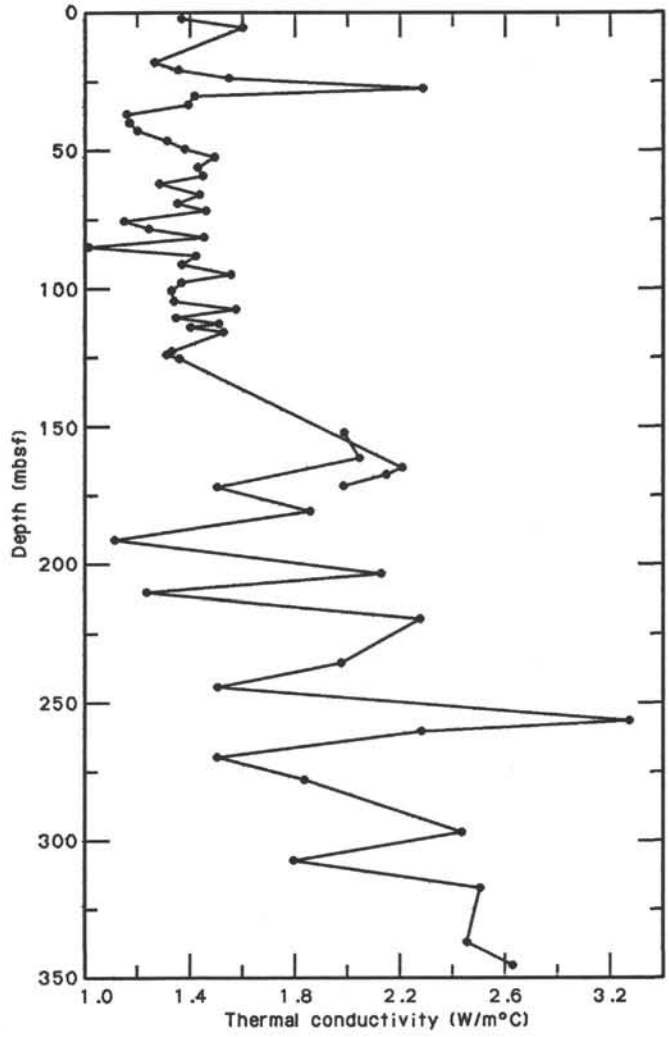

Figure 22. Thermal conductivity of samples from Holes 754A and 754B.

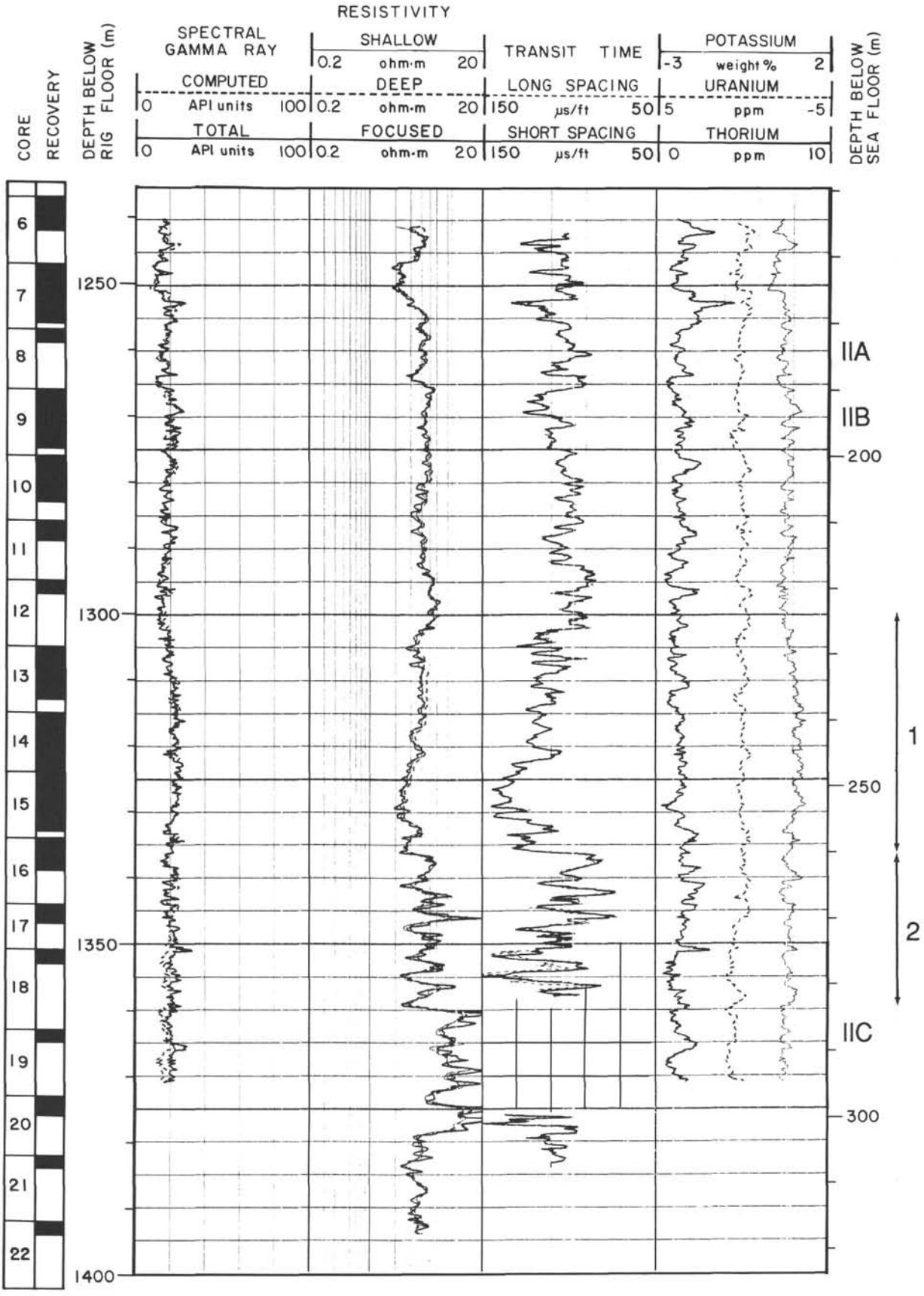

Figure 23. Computed and total spectral gamma ray, shallow, deep, and focused resistivity, long- and short-spacing transit time, and potassium, uranium, and thorium logs in Hole 754B, 165–317 mbsf. Numbered arrows are discussed in the text.

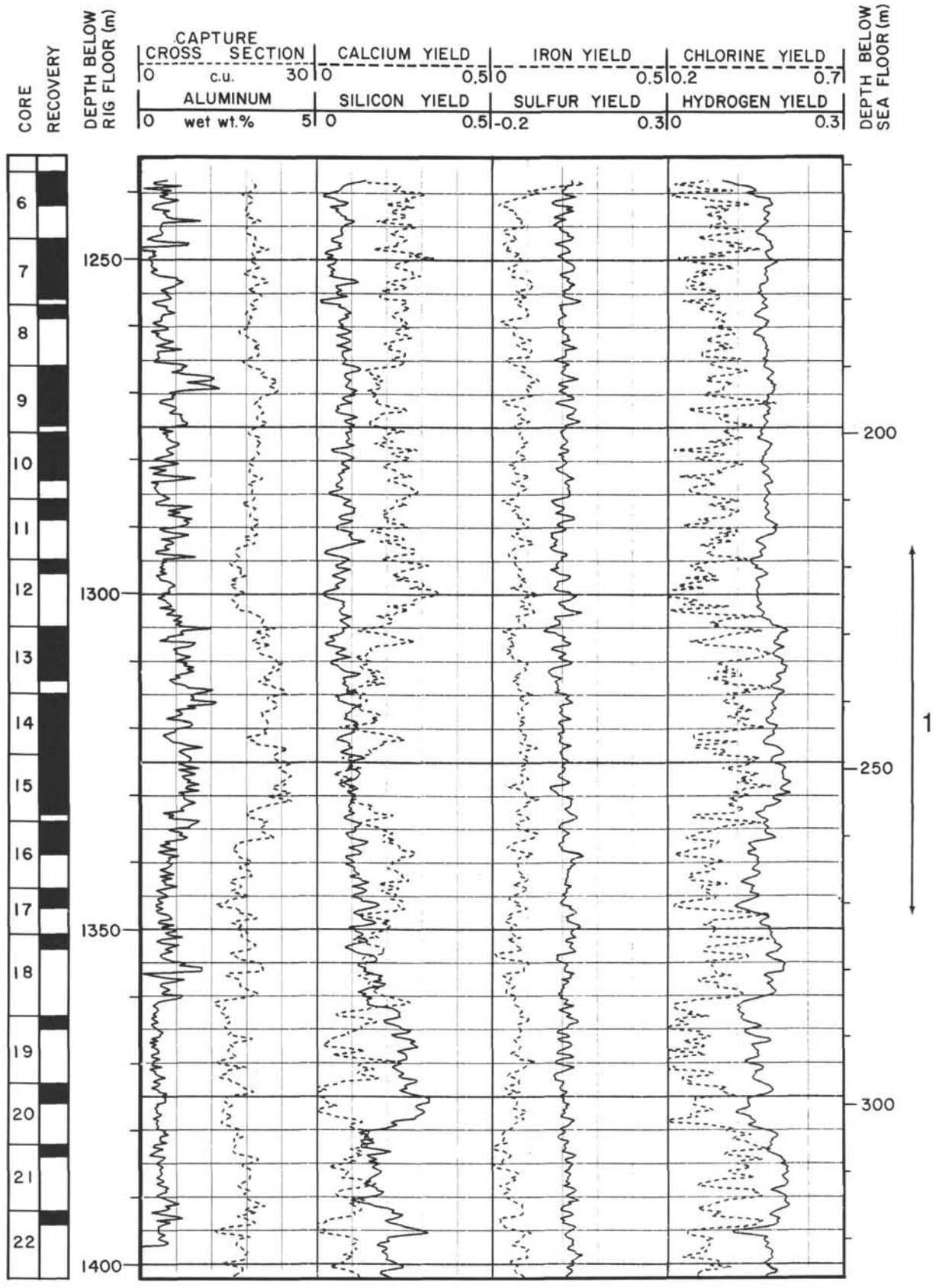

Figure 24. Capture cross section, aluminum, calcium yield, silicon yield, iron yield, sulfur yield, chlorine yield, and hydrogen yield logs in Hole 754B, 165–338 mbsf. Numbered arrow is discussed in the text.

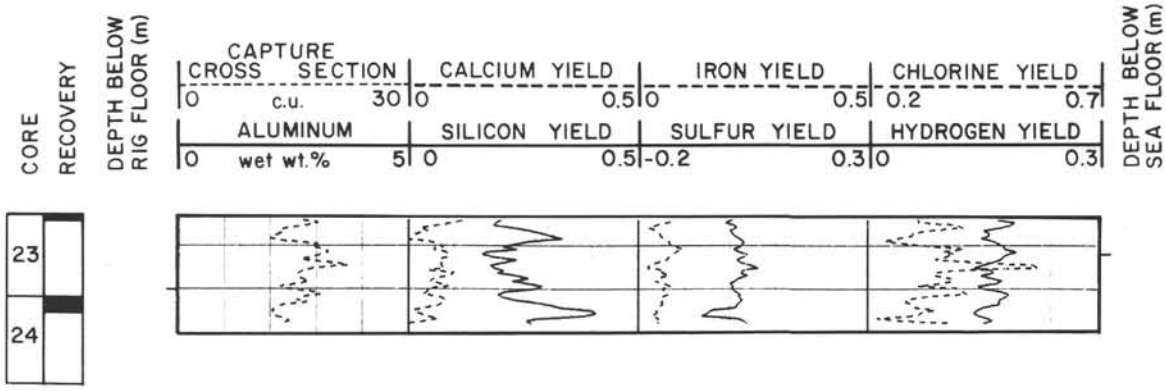

Figure 24 (continued).

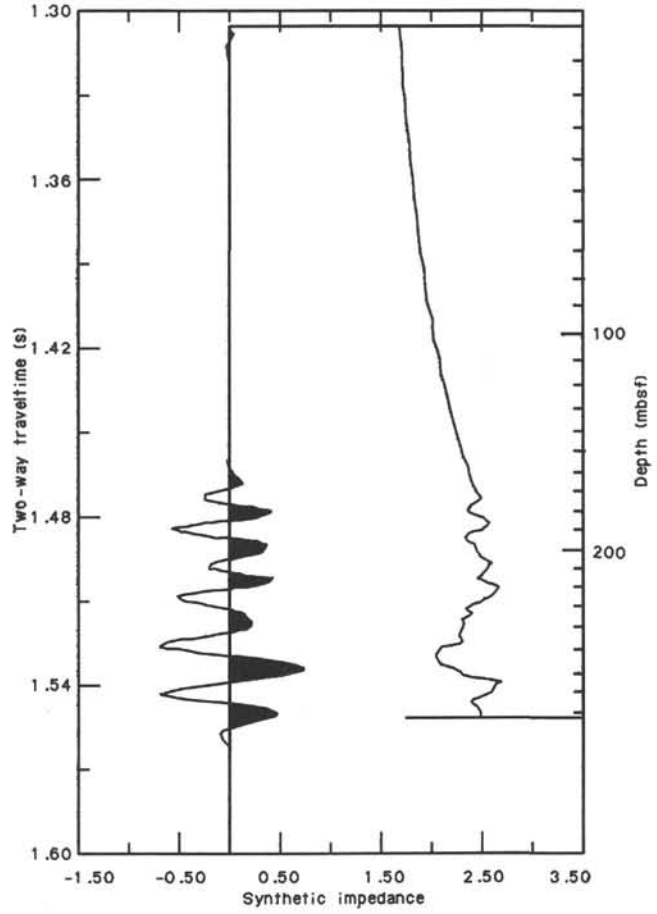

Figure 25. Synthetic seismogram from zero-phase Ricker wavelet at a peak frequency of 60 Hz and an assumed density of 1.8 g/cm^3, Hole 754B.

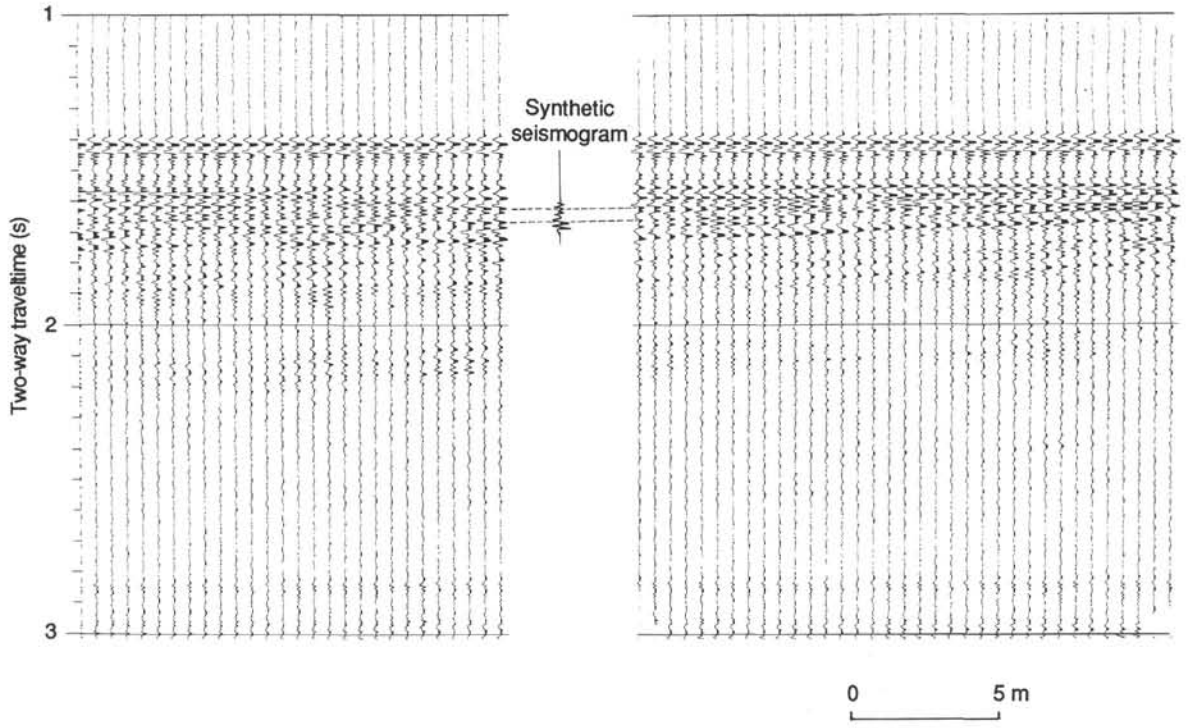

Figure 26. Comparison of synthetic seismogram (Fig. 25) with RC2708 seismic-reflection data. The seismic profile is filtered with a 10–125-Hz filter.

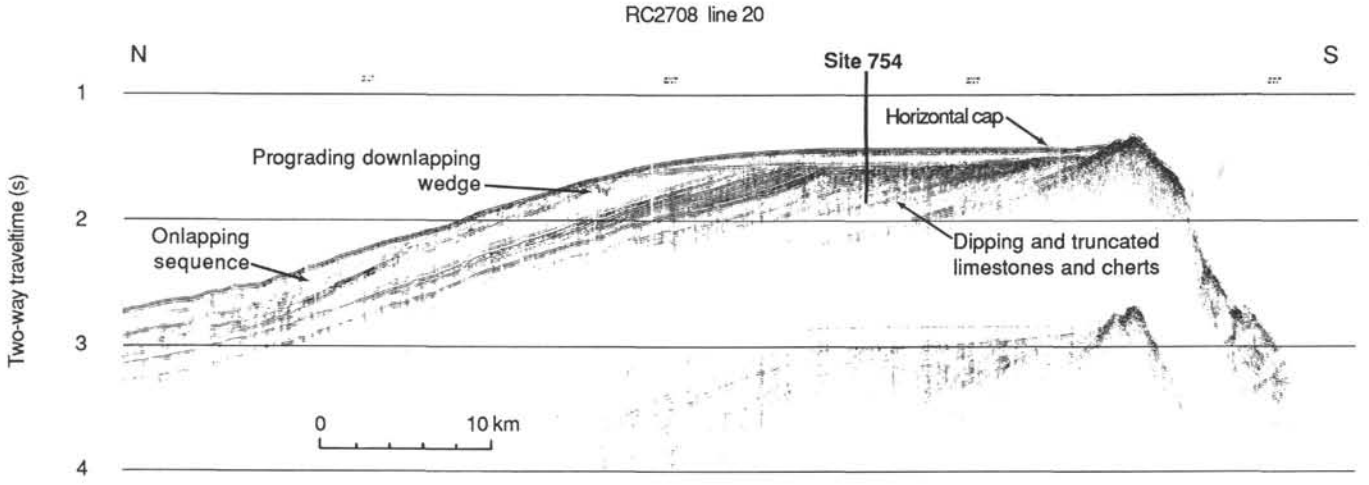

Figure 27. A single-channel seismic dip line across Broken Ridge, illustrating the stratigraphy on and surrounding the ridge. Site 754 penetrated the horizontal pelagic cap and bottomed in the prograding downlapping sequence.

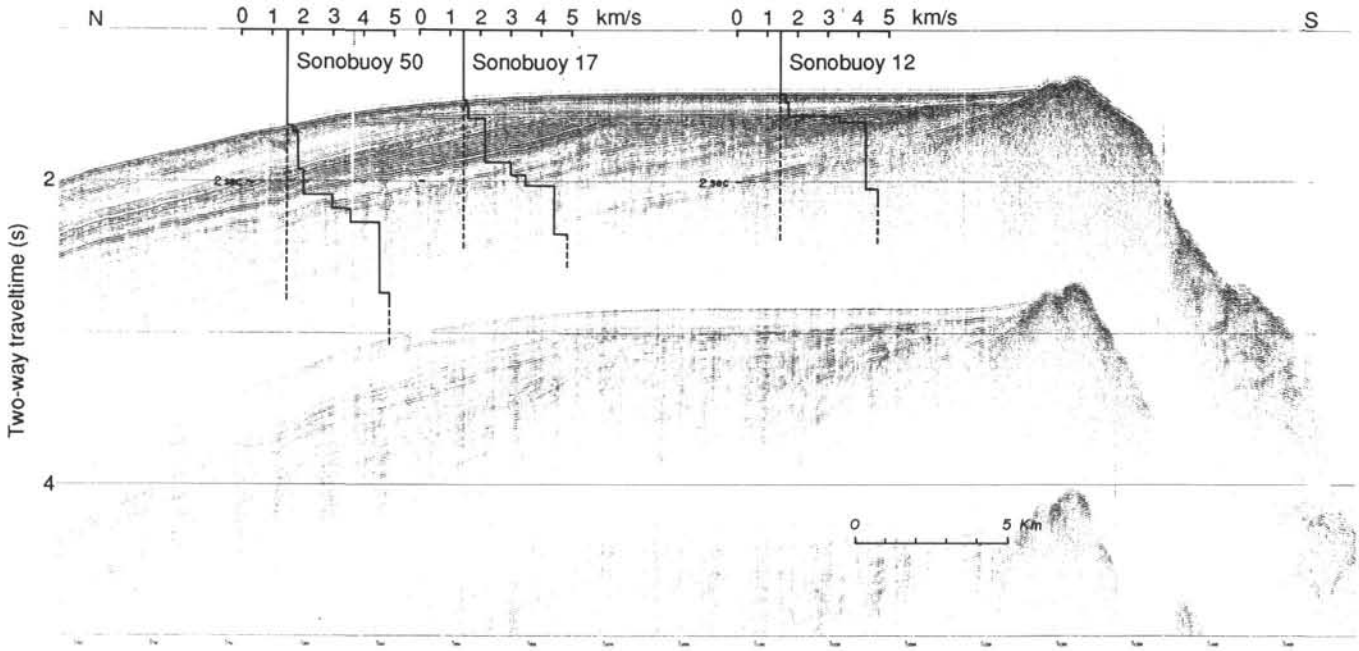

Figure 28. Sonobuoy velocity solutions from strike lines are projected onto the dip line, correcting for changes in water depth. The downsection velocity gradient, from 2200 to 4500 m/s, is also manifested downslope in response to the subcropping reflectors. There is good agreement between sonobuoy-derived velocities, laboratory-derived sonic velocities, and downhole velocity measurements from Site 754.

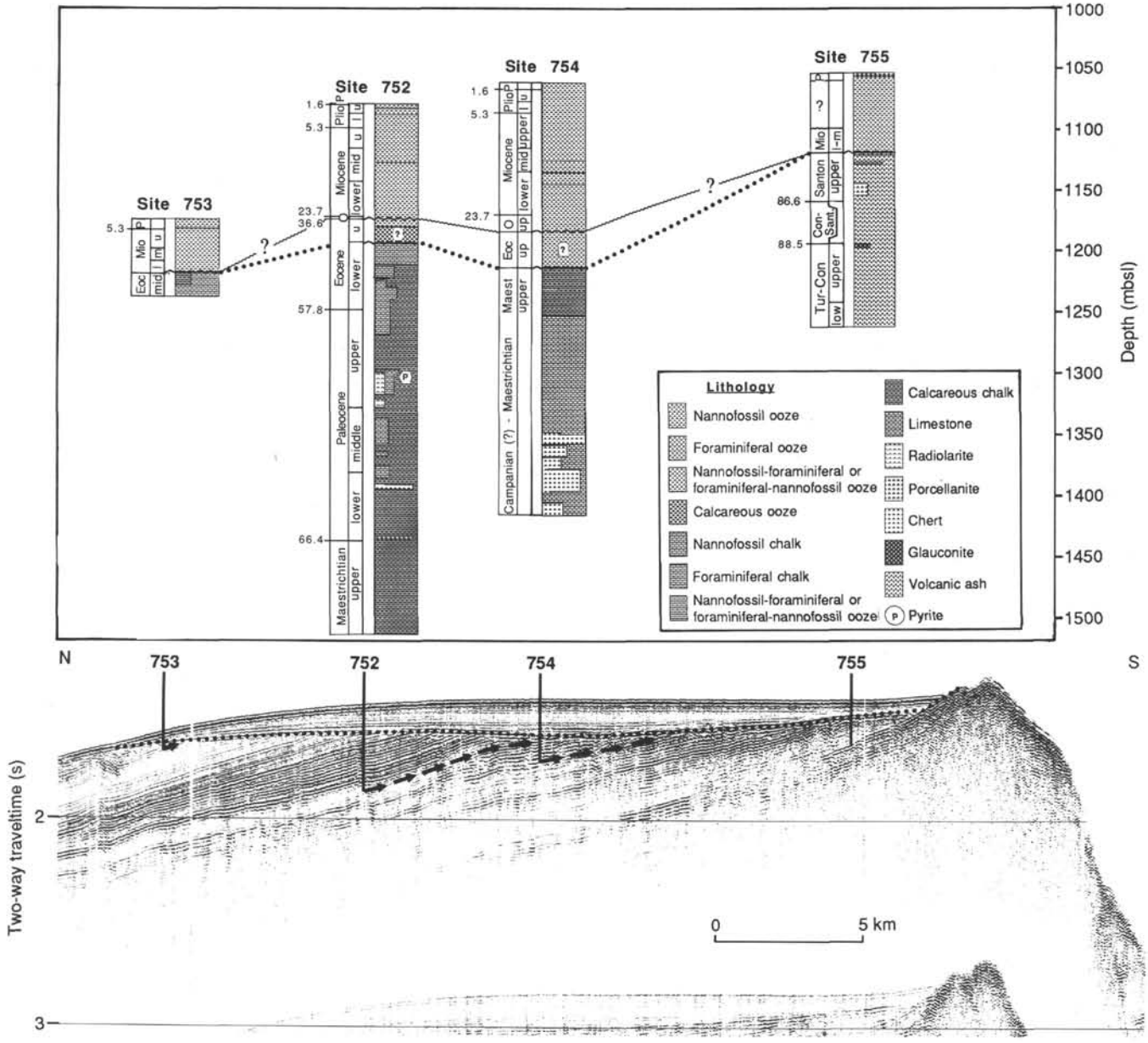

Figure 29. Correlation of seismic stratigraphy and lithostratigraphy sampled at Sites 752, 753, 754, and 755 on Broken Ridge. The arrows represent the upward continuation of the deepest horizon penetrated at Sites 752, 753, and 754 to the angular unconformity, illustrating the amount of stratigraphic section recovered and the stratigraphic overlap—if any—among the sites. The dotted line represents the middle Eocene hiatus and the wavy line denotes the Oligocene hiatus. The two hiatuses coalesce at Sites 753 and 755, but the question marks indicate that the position where they coalesce across Broken Ridge is not resolved.

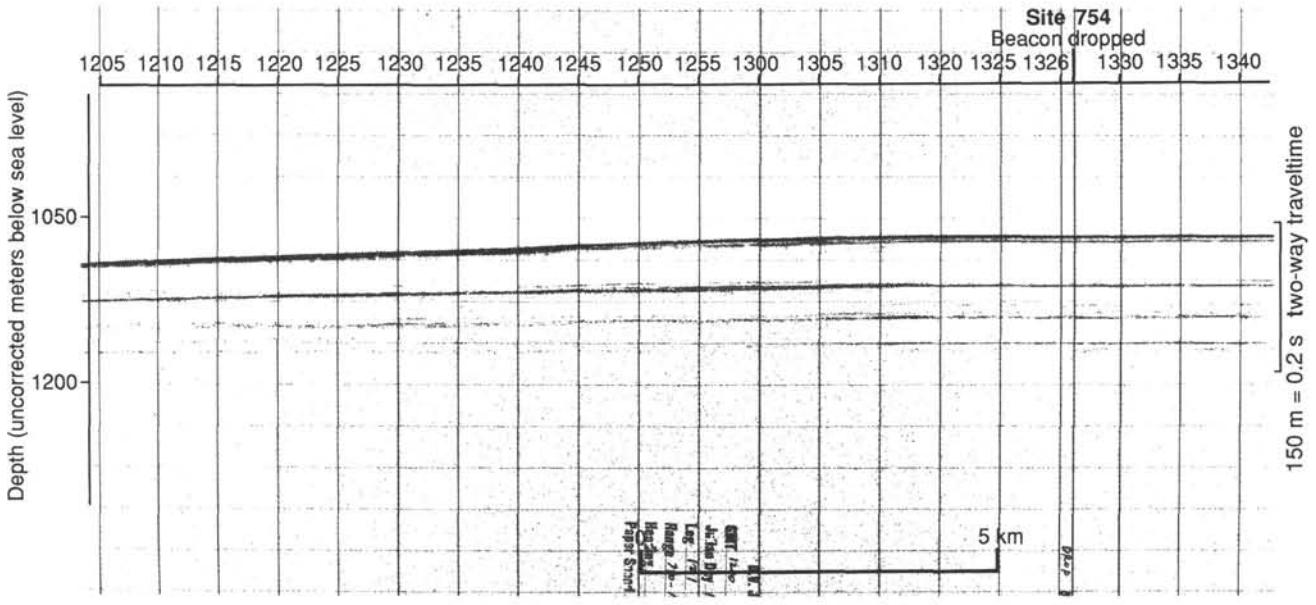

Figure 30. The 3.5-kHz PDR record over Site 754, corresponding to the water gun seismic section in Figure 29. The maximum acoustic penetration is approximately 100 mbsf because of the attenuation of the high-frequency signal. The 3.5-kHz profile augments the high-resolution seismic-reflection profile by providing a sonic character for shallow acoustic impedance contrasts that are at or below the vertical resolution of the water gun seismic system.